UNIVERSITÀ DEGLI STUDI DI ROMA “LA SAPIENZA”

FACOLTÀ DI SCIENZE MATEMATICHE FISICHE E NATURALI

TESI DI DOTTORATO IN SCIENZE CHIMICHE

XVIII CICLO

FUNCTIONALIZATION OF SILICON SURFACES FOR SENSOR APPLICATIONS

Relatore interno	Dottorando
Prof. G. Doddi	Fabrizio Cattaruzza

Relatore esterno
Dr. A. Flamini

A.A. 2004-2005

“There's Plenty of Room at the Bottom”

Richard P. Feynman

Preface

This PhD thesis is organized into two sections. In Section I, selected literature information, regarding the activation and functionalization in solution of unoxidized crystalline silicon surface, are outlined (CHAPTER 1-3). The specific research work, carried out by the author, is reported in Section II of the thesis. This section consists of three chapters. CHAPTER 4 is concerned with the preparation and characterization of carboxylic acid terminated monolayers on crystalline silicon surface. Such derivatized surfaces were then exploited for anchoring oligonucleotides and also magnetite nanoparticles, whose results are reported in CHAPTER 5 and 6, respectively.

Contents

SECTION I 1

INTRODUCTION

CHAPTER 1. 7

CRYSTALLINE SILICON

1.1. Flat Silicon

1.2 Porous Silicon 9

CHAPTER 2. 13

SILICON SURFACE PRECURSORS

2.1 Si–X (X=Cl, Br, I) Terminated Surfaces 14

2.2 Si–Hx -Terminated Surfaces

2.2.1 Si(111)–H surfaces 15

2.2.2 Si(100)–H surfaces 17

2.3 Stability of Hydrogen Terminated Surfaces 19

CHAPTER 3. 23

SILICON-CARBON BOND FORMATION

3.1. Thermal Functionalization

3.1.1. *Reactions Mediated by Metal Complexes* 29

3.1.2. Reactions of Alkyl/Aryl Carbanions

3.2. Photochemical Functionalization 30

3.2.1. UV Light

3.2.2. White Light 35

3.3. Electrochemical Functionalization 36

3.4. Functionalization of the Monolayer 39

SECTION II 45

CHAPTER 4. 47

A SURFACE COVERAGE DETERMINATION WITH A FLUORESCENCE PROBE IN SOLUTION

4.1 Introduction

4.2 Experimental 48

4.2.1 Amide Synthesis

4.2.2 Preparation Silicon Surface 51

4.3 Results 52

CHAPTER 5. 67

CONTROLLED LOADING OF OLIGODEOXYRIBONUCLEOTIDE MONOLAYERS ONTO UNOXYDISED CRYSTALLINE SILICON

5.1 Introduction

5.2 Experimental 68

5.2.1

5.2.2 73

5.3 RESULTS 74

CHAPTER 6.

MAGNETITE NANOPARTICLES ANCHORED TO CRYSTALLINE SILICON SURFACE

6.1 Introdution

6.2 Experimental

6.21 Material and Synthetic Procedures

6.22 Preparation of Magneite Nanoparticles

6.2.3 Anchoring of Magneite Nanoparticles on Silicon Surface

6.2.4 Physical Techniques

6.3 Reults

SECTION I

INTRODUCTION

The microelectronics revolution, started fifty years ago, has produced an industry that now is responsible for a market of nearly 1 trillion dollars in the world. Today, the devices based on silicon can be found in many ordinary objects from automobiles to home appliances. The rapidity with which microelectronic technologies have advanced is unprecedented, as, for example, the electronic component number on a single silicon chip which doubles every 18 months. The widespread availability of microelectronic controlled machines depends on these revolutionary progresses. Many of these advances have resulted from miniaturization of the building block of electronic devices; integrated circuits (ICs) on a chip now contain about 1 billion of transistors per square inch.[1] These advances had been foretold by a researcher of Intel, who published a semi logarithm diagram in 1965 (**Fig 0.1**).

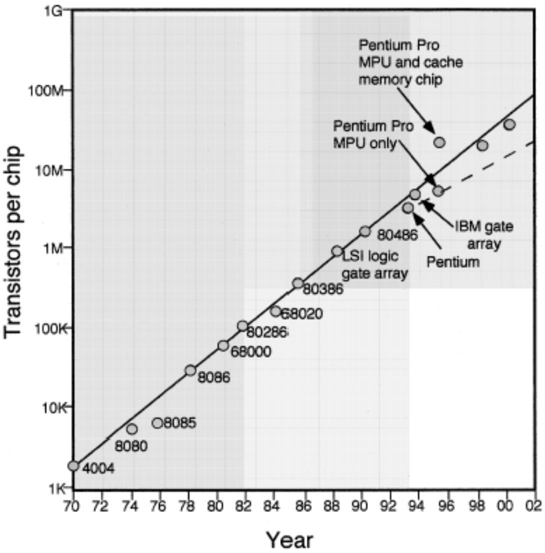

Fig. 0.1 Moore's diagram which shows the progress of miniaturization of transistor from 1970.

In the diagram the number of transistors per chip *vs* year is reported; this diagram is more famous simply as the Moore law. This dimension reduction has been accompanied by a substantial cost reduction, so that SIA (Semiconductor Industry Association) has foretold a cost decrease from 1735 to 217 microcent/transistor during the time interval 1999-2005, resulting in the end more expensive to print a character on a paper than to fabricate a transistor!!

In the new century the dimensions of electronic devices will be as small as the dimensions of a molecule. For example, it is predicted by an industry guideline, known as the Technology Roadmap for semiconductors,[2] that by the year 2014 lateral device dimension will reach 35 nm (350 Å) and vertical dimension will be even smaller. Accordingly, the dimension that microelectronic is projected to achieve in the future are few molecular layers. Consequently a lot of functions in a device could rely on the physical process between an interface of a layer of few molecules i.e. Si/SiO_2, Si/Metal and another surface exposed to the air.

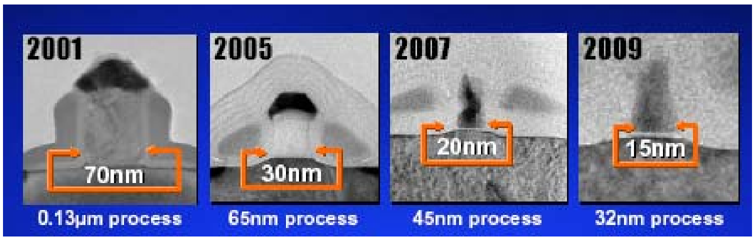

Fig. 0.2 Foretold of Technology Roadmap

Surface phenomena have always been a cornerstone of the microelectronic industry. Processes such as epitaxy,[3] chemical vapour deposition, etching, oxidation and passivation,[4] which are used routinely in the industry, involve chemical or physical processes occurring at the surface of semiconductor wafer. For this reason, research studies on the interfacial chemistry at semiconductor surface have seen a tremendous development in the last decade and promise to increase in the future,[5] although much is still to be understood about reactivity. It may seem initially surprising that today there are many topics to understand about silicon surface, because of the worldwide domination of silicon in ICs. In fact, there is a strong drive to control and tailor the characteristics of this material, not only to address future ICs[6] but also for a host of novel applications. As the size of devices on silicon chips decreases below 100 nm[7], the ratio of surface atoms/bulk becomes increasingly important, and thus an ideal manipulation of surfaces states is critical.[8] Much of the literature related to the surface chemistry of silicon is actually dealing with silicon oxide. The chemistry of the native oxide or the glasses is well developed and it is outside of the scope of this thesis. For many potential molecular electronic applications an interface Si/SiO_2 on silicon is not desirable because, unless grown under carefully controlled conditions, this interface has a high density of electronic defects and it represents an additional insulating barrier between organic layer and the bulk silicon in connection with electric transport properties.[9] Devices based on silicon chip are interesting in other than microelectronic applications, where control is required over the interfacial characteristics such as micoarray technology moving to the forefront of genomics, proteomics and sensing lab on chip,[10] TAS (Total Automated Systems),[11] and also MEMS and NEMS (Micro- and Nano-Electro-Mechanical Systems).[12]

The importance of atomic level surface chemistry is highlighted in the growing field of organic functionalization of semiconductors. Surface functionalization or organic modification is the process of depositing layers of organic molecules (i.e. those that contain carbon) at semiconductor surfaces. This area which traditionally has been dominated by physical scientists has increasingly been influenced by organic and bioorganic chemists. This convergence of surface science and organic chemistry is critical for the development of revolutionary concepts for the design of molecular scale devices and for the integration of solid state, inorganic structures with biologically active interfaces. **Fig. 0.3**

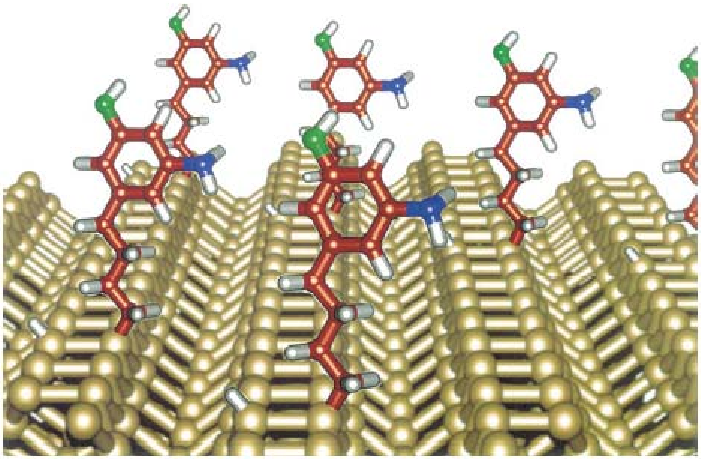

Fig. 0.3 A semi-conductor surface upon which organic molecules have been attached.

Organic molecules comprise more than 95% of all known chemical compounds. Carbon can form a myriad of molecules differing in shape, size and composition.[6] For example, the organic molecules attached to the surface in **Fig. 0.3** will exhibit certain properties based on the types and specific groupings of atoms in the molecules. As a result, organic materials offer great flexibility in designing and creating unique molecular properties, that can then be exploited to provide new capabilities in optical, electronic, and mechanical function as well as in chemical and biological activity.

Microelectronic technology provides an opportunity to create hybrid devices exploiting the best properties and features of both organic and inorganic materials. As an example, consider a chemical or biological sensor built with a mixed organic/semiconductor design. The vast resources of organic and organometallic chemistry can be tapped to permit access to a broad range of functionalities that can respond to different chemical or biological stimulus. A ‘‘sensing’’ response occurs if a species of interest (the molecule-target) binds to the end group of the molecule-probe anchored on the semiconductor surface, causing transduction of signal within the organic layer. If this signal can be coupled into the silicon substrate, then all of the capabilities of silicon-based microelectronic circuitry (such as signal amplification, processing and storage) become available. The end product is a chip-based chemical or biological sensor. Hybrid organic/semiconductor materials also are being explored for use in molecular electronics and computing and for imparting biocompatibility to semiconductor devices for implantation. Organic materials are also finding use in more conventional microelectronic processing, such as for new-generation dielectric materials for metal interconnect isolation, or for surface passivation and protection. Fortunately, the surfaces of most semiconductors of interest for microelectronics have characteristics that enable organic molecules to be attached by a number of different chemical reactions. This provides not only an element of rational design of interfaces, but presents opportunities for systematic physical organic studies of the kinetics and mechanisms of reactions. Clearly, potential applications in hybrid molecular-semiconductor devices or chemical-biosensors require a detailed understanding of the interface between semiconductor surface and organic materials. In the case of silicon, this is described in the following chapters.

---

[1] (a) S.A. Campbell, *The Science and Engineering of Microelectronic Fabrication*, Oxford, New York, 1996 (b) C.Y. Chang, S.M. Sze (Eds.), ULSI Technology, McGraw-Hill, New York, 1996.

[2] International Technology Roadmap for Semiconductors, Semiconductor Industry Association, 1999.

[3] See, for example: (a) J.R. Arthur, *Surf. Sci.* **2002**, *500*, 189; (b) P. Finnie, Y. Homma, *Surf. Sci.* **2002**, *500*, 437.

[4] (a) M.K. Weldon, K.T. Queeney, J. Eng Jr., K. Raghavachari, Y.J. Chabal, *Surf. Sci.* **2002**, *500*, 859. (b)J.W. Hill, D.K. Kolb, Chemistry for Changing Times, Prentice Hall, Englewood Cliffs, NJ, 1995. (c)J.T. Yates Jr., *Science* **1998**, *279*, 335. (d)J.M. Buriak, Organometallic chemistry on silicon surfaces: formation of functional monolayers bound through Si–C bonds, *Chem. Commun.* **1999**, *12*, 1051. (e)R.A. Wolkow, Controlled molecular adsorption on silicon: laying a foundation for molecular devices, *Ann. Rev. Phys. Chem.* **1999**, *50*, 413.

[5] (a) H. N. Waltenburg, J. T Yates, *Chem. Rev.* **1995**, *95*, 1589. (b) R. J. Hamers, Y. Wang, *Chem. Rev.* **1996**, *96*, 1261.

[6] The National Technology Roadmap for Semiconductors; Semiconductor Industry Association (SIA): San Jose, CA, 1997.

[7] H. Hasegawa, H. Fujikura, H. Okada, *MRS Bull.* **1999**, *24*, 25.

[8] M. J. Sailor, E. J. Lee, *Adv. Mater.* **1997**, *9*, 783.

[9] S. M. Sze, The Physics of Semiconductor Devices, 2nd ed.; Wiley: New York, 1981.

[10] (a) K. J. Albert, N. S. Lewis, C. L Schauer,. G. A. Sotzing, S. E. Stitzel, T. P. Vaid, D. R. Walt, *Chem. Rev.* **2000,** *100*, 2595. (b) W. M.Freeman, D. J. Robertson, K. E. Vrana*,* *Biotechniques* **2000**, *29*, 1042. (c) K. M. Hansen, H. F. Ji, G. H. Wu, R Datar, R. Cote, A. Majumdar, T. Thundat, *Anal. Chem*. **2001**, *73*, 1567. (d) F. Zee, J. W. Judy, *Sensor Actuators B* **2001**, *72*, 120. (e) K.Birkinshaw, *Int. Rev. Phys. Chem*. **1996**, *15*, 13.

[11] (a) J. C. T. Eijkel, A. Prak, S. Cowen, D. H. Craston, A. Manz, *J. Chromatogr. A* **1998**, *815*, 265. (b) J. Drott, K. Lindstrom, L. Rosengren, T. Laurell, *J. Micromech. Microeng*. **1997**, *7*, 14. (c) B. H.Weigl, P. Yager, *Science* **1999**, *283*, 346.

[12] R. Maboudian, *Surf. Sci. Rep.* **1998**, *30*, 209.

CHAPTER 1

CRYSTALLINE SILICON

1.1 Flat Silicon

Due to their wide use in microelectronic applications, single-crystal silicon wafers of high purity (at better than 99.999999999%) are commercially available and relatively inexpensive. Its electronic properties (Energy gap at 300 K is 1.12 eV) can be tuned dramatically by substituting only a small fraction of silicon atoms in the lattice with another element in a process called ‘‘doping’’. Depending upon the desired electronic properties, silicon wafers are doped in a controlled fashion with electron-donor (P, As, Sb: n-type) or –acceptor (B: p-type) impurities to render the intrinsic material more highly conducting. Silicon is a covalent solid that crystallizes into a diamond cubic lattice structure, illustrated in **Fig. 1.1**. In a covalent solid, bonding is produced by overlap of the highly directional electronic orbitals of the atoms.

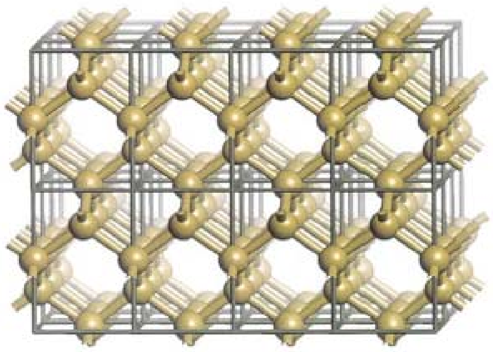

Fig. 1.1 The diamond cubic lattice is the crystal structure found for diamond, silicon and germanium. Each atom is bonded to four neighbouring atoms in a tetrahedral geometry.

In the bulk solid, the diamond cubic lattice allows silicon atoms to achieve this tetrahedral configuration. At the surface of the material, however, the bulk is truncated, so the stable bulk tetrahedral bonding is disturbed. The reactivity of the silicon surface is controlled in part by the unsatisfied bonding orbitals, called dangling bonds, which remain upon truncating the bulk. A surface silicon atom that is bonded to only two other silicon atoms instead of four, as shown at the top surface of the crystal illustrated in **Fig. 1.1** for example, would have two dangling bonds. Dangling bonds contain single electrons, whereas normal covalent bonds contain two spin-paired electrons. At the surface, atoms can readjust to minimize the total free energy of the system and eliminate the dangling bonds. This process, associated with the loss of coordination of the silicon atoms, is referred to as surface ‘‘reconstruction’’. The energy minimization is a trade-off between energy gained by forming new local bonds (to eliminate the dangling bonds) with energy lost because of bond strain that results from this new configuration.[1] The influence of the electronic and crystallographic structure of the reconstructed surfaces on the reactivity and selectivity of organics is a subject of ongoing interest and also is beyond the scope of this thesis.

The crystallographic faces of silicon that are most important industrially are the Si(100) and the Si(111) surfaces, although other Si(hkl) orientations are known.[2] The numbers in parentheses refer to a crystallographic notation known as Miller indices, which designate the particular orientation at which the bulk is terminated. The top surface in **Fig. 1.1**, e.g., has the (100) orientation. Both the (100) and (111) surfaces undergo extensive reconstructions, i.e. their surface atomic geometry differs significantly from that of the bulk. Moreover, the two surfaces have markedly different surface structures. [1d, 1e]

The Si(100) surface reconstructs into a (2x1) structure, where (2x1) designates the new periodicity of the surface atoms. The Si(100)- 2x1 surface, illustrated in **Fig. 1.2(a)**, consists of pairs of silicon atoms in adjacent rows that have bonded to each other, thereby reducing the number of dangling bonds. These pairs of silicon atoms are called dimers.

Si(111), on the other hand, reconstructs into a complex (7x7) structure that contains 49 surface atoms in the new unit cell.

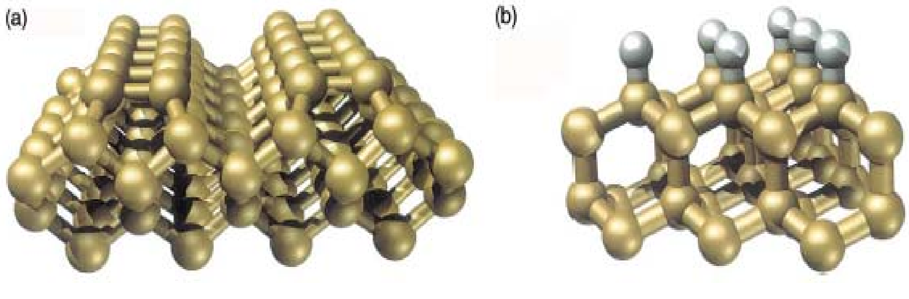

Fig. 1.2. Two surfaces of silicon that are important in organic functionalization chemistry. (a) The clean Si(100)- 2x1 surface. (b) The hydride-terminated Si(111) surface.

Also after reconstruction both surfaces Si(100)- 2x1 and Si(111)-7x7 are highly reactive.

A silicon surface can be contaminated from species metallic, organic and ceramic. For example a silicon wafer can present a typically concentration of 10^{11}-10^{12} cm^{-2} atoms of Fe, Ni, Cu, and Zn.[12, 13]

Both surfaces are typically cleaned and prepared in an ultrahigh vacuum environment (p= 10^{-10} Torr) by bombarding the surface with argon ions to sputter away surface layers and/or heating to temperatures near 900 °C. The resulting surfaces are not stable in air, as they quickly oxidize to form a SiO_2 layer. Hence, experiments on the clean Si(100)-2x1 and Si(111)-7x7 surfaces must be performed in vacuum, and the organic reactants for functionalization are introduced in vapour form into the vacuum chamber. A recent review appeared recently in literature on this topic.[3] On the other hand, silicon surfaces can be rendered relatively stable in air (i.e. relatively resistant to oxidation) by coating the surface with hydrogen.

1.2 Porous Silicon

In 1990, Canham made the important discovery that nanocrystalline porous silicon can emit visible light through photoluminescence at room temperature.[4] Porous silicon samples emitting orange-red light under photo- and electroluminescence conditions are shown in **Fig. 1.3**.

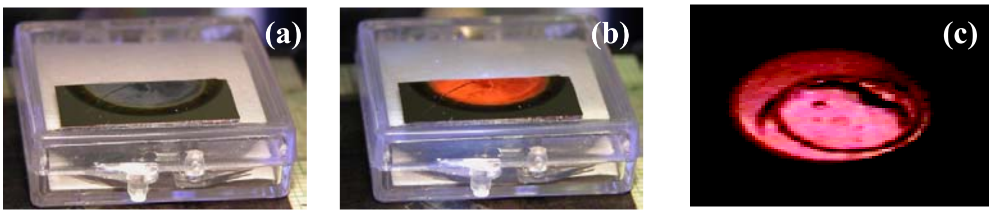

Fig. 1.3 (a) Porous silicon ; (b) Photoluminescence; (c) Electroluminescence

This discovery was quickly followed up by electro- and chemi-luminescence studies in a subsequent explosion of interest.[5] Porous silicon has a highly complex nanoscale architecture made up of 1-dimensional crystalline nanowires and 0-dimensional nanocrystallites;[6] an SEM image is shown in **Fig. 1.4**

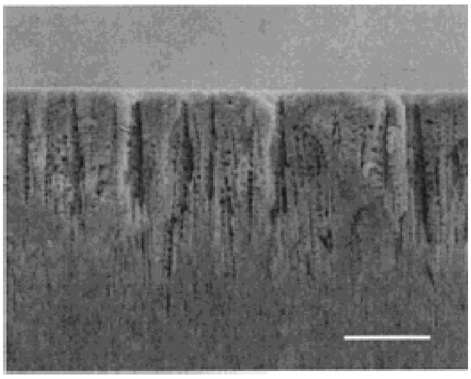

Fig. 1.4 Cross-sectional scanning electron micrograph (SEM) image of a porous silicon sample. Scale bar is 10 μm.

The major barrier preventing commercial applications of porous silicon is the instability of its native interface, a metastable Si-H termination, and thus, surface chemistry has proven to be a crucial element for the technological success of this material.[7] The photoluminescence of porous silicon depends strongly upon the surface passivation.[8] The precision of organic chemistry promises to allow for fine-tuning of these important interfacial effects, leading ultimately toward an understanding of the role of surface states on semiconducting nanoparticles in general. The nature of the surface bond, sterics, conjugation, and electronics of organic substituents can all be modulated at will and should provide the following: (i) stable porous silicon surfaces, (ii) modifiable surface characteristics, and (iii) potential to interface with organic conductor/ semiconductors/LEDs and biologically relevant molecules for an array of applications, such as sensing,[9] photonics,[10] and other analytical uses.[11] From a technological standpoint, light-emitting porous silicon is especially attractive because it could be readily integrated with existing silicon-based integrated circuit (IC) manufacturing processes. Moreover, porous silicon is an especially attractive testing ground for surface chemistry due to its high surface area which renders analysis relatively straightforward through conventional transmission spectroscopies: Fourier transform infrared (FTIR) or diffuse reflectance infrared (DRIFT). As a result, routine characterization of this material is practical and facile for most chemists.

---

[1] (a) K. Birkinshaw, *Int. Rev. Phys. Chem.* **1996**, *15*, 13. (b) J. C. T.Eijkel, A. Prak, S. Cowen, D. H. Craston, A. Manz, *J. Chromatogr. A* **1998**, *815*, 265. (c) J. Drott, K. Lindstrom, L. Rosengren, T. Laurell, *J. Micromech. Microeng.* **1997**, *7*, 14. (d) B. H. Weigl, P. Yager, *Science* **1999**, *283*, 346. (e) R. Maboudian, *Surf. Sci. Rep.* **1998**, *30*, 209.

2 (a)H. N. Waltenburg, J. T Yates, *Chem. Rev.* **1995**, *95*, 1589. (b) R. J. Hamers, Y. Wang, *Chem. Rev.* **1996**, *96*, 1261.(c) D. Q. Hu, C. D. MacPherson, K. T. Leung, *Surf. Sci.* **1992**, *273*, 21. (d) C. D. MacPherson, D. Q. Hu, M. Doan, K. T. Leung, *Surf. Sci.* **1994**, *310*, 231.

3 S.F. Bent *Surf. Sci.* **2002**,*500*, 879.

4 L. T. Canham, *Appl. Phys. Lett.* **1990**, *57*, 1046.

5 (a) A. Halimaoui, C. Oules, G. Bomchil, A. Bsiesy, F. Gaspard, R. Herino, M. Ligeon, F. Muller, *Appl. Phys. Lett.* **1991**, *59*, 304. (b) P. McCord, S. L. Yau, A. J.Bard, *Science* **1992**, *257*, 68. (c) M. P. Stewart, J. M. Buriak, *Adv. Mater.* **2000**, *12*, 859.

6 (a) A. G. Cullis, L. T. Canham, P. D. J. Calcott, *J. Appl. Phys.* **1997**, *82*, 909. (b) M. J. Sailor, E. J. Lee, *Adv. Mater.* **1997**, *9*, 783.

[7] J. H. Song, M. J. Sailor, *Comments Inorg. Chem.* **1999**, *21*, 69.

[8] (a) Lauerhaas, J. M.; Sailor, M. J. Science **1993**, *261*, 1567.(b) Song, J. H.; Sailor, M. J. *J. Am. Chem. Soc*. **1998**, *120*, 2376.(c) Allen, M. J.; Buriak, J. M. *J. Lumin.* **1999**, *80*, 29.

[9] (a) Sailor, M. J. *In Properties of Porous Silicon*; Canham, L. T., Ed.; INSPEC: London, **1997**; 364. (b) Lin, V. S.-Y.; Motesharei, K.; Dancil, K.-P. S.; Sailor, M. J.; M. R. Ghadiri, *Science* **1997**, *278*, 840. (c) A.Janshoff, K.-P. S. Dancil, C. Steinem, D. P. Greiner, V. S.-Y. Lin, C. Gurtner, K. Motesharei, M. J. Sailor, M.R. Ghadiri, *J. Am. Chem. Soc.* **1998**, *120*, 12108. (d) S. E. Letant, M. J. Sailor, *Adv. Mater.* **2001**, *13*, 335. (e) S. E. Letant, S.;Content, T. T. Tan, F. Zenhausern, M. J. Sailor, *Sensor Actuators B* **2000**, *69*, 193.

[10] (a) M. Thönissen, M. Krüger, G. Lerondel, R. Romestain, *In Properties of Porous Silicon*; Canham, L. T., Ed.; INSPEC: London, **1997**; 349. (b) M.Van Belle, *Photonics Spectra* **1998**, *32*, *10*, 57.

[11] J. Wei, J. M. Buriak, G. Siuzdak, *Nature* **1999**, *399*, 243.

CHAPTER 2

SILICON SURFACES PRECURSORS

The surfaces of silicon have several different chemical handles through which functionalization may be carried out. The typical bond dissociation energies of various reactive groups on both surfaces and in molecular compounds are listed in **Table 2.1**. Caution must be taken in using these values to predict reactivity.

element	self	H	C	O	F	Cl	Br	I
C	292-360	416		336	485	327	285	213
Si	210-250 (bulk) 310-340 (disilane) 105-126 (disilene)	323	369	368	582	391	310	234

Table **2.1** Typical Bond Energies for Various Related Silicon Groups (kJ mol^{-1})

For instance, the Si-F bond is one of the strongest known between any two elements of the periodic table and yet is highly polarized in the direction $^{\delta+}$Si-F$^{\delta-}$; this enables facile substitution at the Si center upon nucleophilic attack and hence this bond is kinetically very labile. As can be seen, the weakest bonds on the silicon surfaces are the Si-Si bonds, but if the surface is substituted with other groups, they may be less reactive due to steric hindrance. The different surfaces prepared and utilized for Si-C bond formation are described here. Wet chemical reactions require a metastable surface to successfully carry out surface chemistry. The surface precursors must be stable enough to be handled at atmospheric pressure in the presence of solvent vapors, inert gas impurities, and other contaminants and yet they must be reactive enough towards selected chemicals. Two silicon surface precursors, showing these properties due to their bipolar character, are Si-H and Si-X (X: Cl, Br, I). The Si-H-terminated surface is relatively stable in air for short periods; in contrast, the Si-X-derivatized surface is much more reactive with respect to hydrolysis and Si-OH formation and can generally be handled only under inert atmosphere.

2.1 Si–X (X=Cl, Br, I) Terminated Surfaces

Halogenation of silicon surfaces through wet chemistry is very easy. In general, these surfaces are quite reactive and thus they should be handled under an inert atmosphere.

Si-X terminations on flat single-crystal silicon, *e.g.* Si(111)-X surfaces, have been prepared by treating the corresponding hydride-terminated silicon surfaces with halogenation agents (*i.e.* PCl_5, N-bromosuccinimide, heating using benzoyl peroxide as a radical initiator in solution,[1] or under UV irradiation[2] from an Hg-lamp with lines at 254, 312, and 364 nm). Also, the molecular halides (Cl_2, Br_2, I_2) can be used to convert the Si(111)-H surface to Si(111)-X,[2] either photochemically (near UV at 350 nm for 15 s -10 min, or in the visible region with a 300 W tungsten lamp for 2 min) or thermally (80 °C for 10 min).

2.2. Si–Hx -Terminated Surfaces

The hydride-terminated surfaces are reasonably stable and can be prepared and manipulated in air as well as in a number of organic solvents. Thus, high quality materials are available without the need of expensive vacuum systems. Other advantages offered by this surface are their excellent chemical homogeneity (>99% H termination) and strong FTIR vibrational modes (Si-H stretching, ν=2100 cm^{-1}), which can provide information as to surface flatness and makeup **Fig. 2.1**.

Longterm use of an Si-H-terminated surface for many applications is precluded due to its propensity to oxidize, but it can be easily handled in air for tens of minutes without measurable degradation.

The hydrogen termination is carried out in wet chemistry by etching in aqueous fluoride following different procedures depending on the specific surface. For simplicity, we will describe two particular silicon surfaces (on which essentially all of the studies in the literature have been carried out). The first is the Si(111) surface, from which a real atomically flat surface may be obtained, the second is the Si(100) surface which is quite rough, but all the same is the surface upon which commercial microelectronic devices are fabricated.

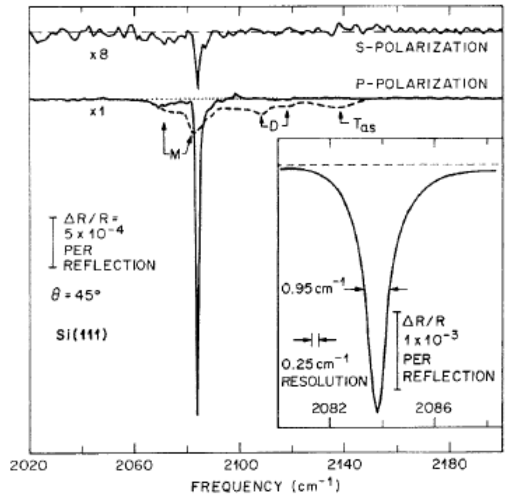

Fig. 2.1 ATR-FTIR spectra of the hydride-terminated Si(111) surface, prepared through the 40% NH4F (aq) etching procedure, taken with both s- and p-polarized IR light. The sharpness of the ν(Si-H) vibration at 2083.7 cm-1 clearly indicates the high degree of chemical homogeneity of this

2.2.1 Si(111)–H Surfaces

In 1990 Chabal and his coworkers described a simple wet chemical method for the preparation of atomically flat hydrogen terminated Si(111) (henceforth referred to as Si(111)–H).[3] They found that the HF etching of Si(111) at pH 8–9 (*i.e.* ammonium fluoride) resulted in the formation of Si(111)–H in which the Si–H bond is oriented normal to the surface. The observation of a single narrow line at 2083.7 cm^{-1} (the Si–H stretch) with p-polarized infrared light (*i.e.* the electric field component is perpendicular to the surface) and the absence of this vibration with s-polarized infrared light (*i.e.* the electric field component is in the plane of the surface) provided unambiguous proof of the orientation of the Si–H bond (**Fig. 2.2**).

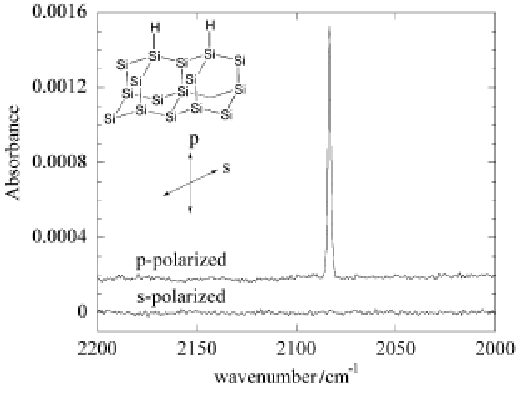

Fig. 2.2 Internal reflection spectra of Si(111)–H in p- and s-polarization.

The procedure was later modified by Wade and Chidsey[4] who showed that dissolved oxygen initiated pitting of the surface since the open circuit potential (*i.e.* the effective oxidation potential) of the Si(111) surface in ammonium fluoride was sufficiently low to generate superoxide, $O_2^{-\cdot}$. The superoxide ion then reacts with an Si(111)–H bond on a terrace to initiate the formation of an etch pit. The procedure was further modified by Allongue *et al.* who showed that surface pitting could be further suppressed by using one-side polished silicon wafers or by abrading part of the polished surface.[5] They suggested that the rough surface provides cathodic protection by acting as a sacrificial anode.The surfaces prepared in this way are reasonably stable and atomically flat on the tens of microns scale and are of very high quality, both structurally and electronically.

The mechanism of the ammonium fluoride etching of Si(111) has been the subject of detailed investigation. Chabal and coworkers [4,6] and later Behm and his coworkers[7] noted that etching with HF at low pH led to rougher surfaces than etching at high pH (*i.e.* ammonium fluoride). This work led to the widely accepted step-flow mechanism which accounts for the smoothing of the Si(111)–H surface. This mechanism, which has been refined by Allongue *et al.*[6,8] and by Hines and coworkers,[9] is initiated by a rate limiting oxidative addition of hydroxide on a silicon atom at a step edge followed by displacement of the hydroxide by fluoride ion. This leads, eventually to the removal of silicon from the surface (etching) in the form of SiF_3OH and the capping of the surface silicon atoms by hydrogen.

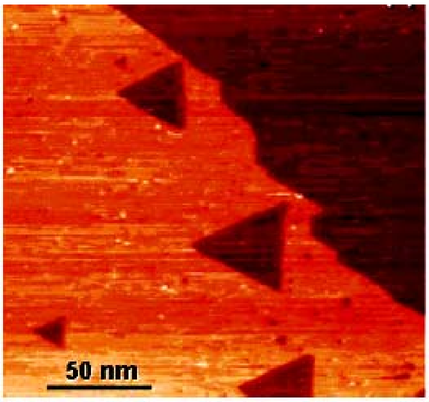

Fig. 2.3 STM images of H-terminated 200 nm x 200 nm images, taken at 77 K, show large flat terraces separated in height by single atomic steps.

The eventual smoothing of the surface leading to well defined steps and terraces (**Fig. 2.3**) is a consequence of the relative rates of reaction of hydroxide with different surface sites. The relevant reactions are shown in eqns. (1) and (2).

$$(Si)_3Si–H + H_2O \longrightarrow (Si)_3Si–OH + H_2 \qquad (1)$$

$$(Si)_3Si–OH + 3HF \rightarrow (Si)_3SiH + SiF_3OH \qquad (2)$$

Using a deuterium labeled surface, Luo and Chidsey[10] determined the rate of step-flow etching to be 4.2 nm s^{-1} in Ar sparged ammonium fluoride at 25 °C, or about 10 rows of silicon atoms per second. The rate was measured by the zero order disappearance of the Si–D stretching using FTIR and the average terrace width which was measured by STM.

2.2.2 Si(100)–H surfaces

Recently, Sakaue[11] proposed a wet treatment using the hot NH_4F aqueous solution to prepare an atomically smooth Si(100) wafer surface with a step/terrace periodic structure. The surface is mainly terminated by a dihydride structure with a missing atomic low relaxation structure.

The oxide layer on the Si surface was removed by immersing in a 1%HF solution and then in a 40% NH4F aqueous solution at approximately 76 °C, which is hereafter referred to as the hot NH4F treatment. Quantitative estimates of the surface roughness were conducted by calculating the mean square height (Rms).The hot NH_4F has Rms of 0.14 nm, which is an extremely low value compared to the HF-treated surface (Rms of 0.45 nm) and confirms that the maximum surface roughness is only 1 or 2 atomic layers.

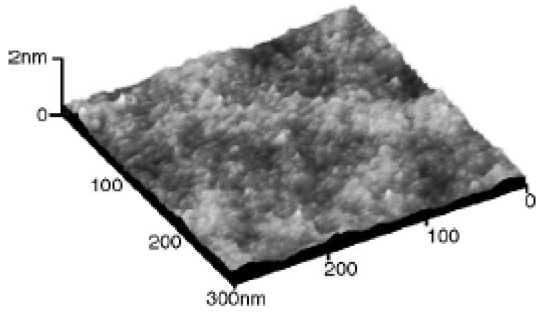

Fig. 2.4 AFM 3D topography images of the surfaces etched by hot NH_4F solution .

Fig 2.5 shows FTIR-ATR spectra of the HF-treated and the hot NH_4F-treated Si(100) surface. The spectrum of the HF-treated surface has a dominant peak at 2112 cm^{-1}

due to the asymmetric stretching vibration mode of SiH_2, a medium peak at 2140 cm^{-1} due to the stretching vibration mode of SiH_3 and a small peak at 2080 cm^{-1}. Since the HF-treated spectrum is sharper, which had a broad peak in the region between 2100 and 2160 cm^{-1}, this HF-treated Si(100) surface has a slightly higher regularity.

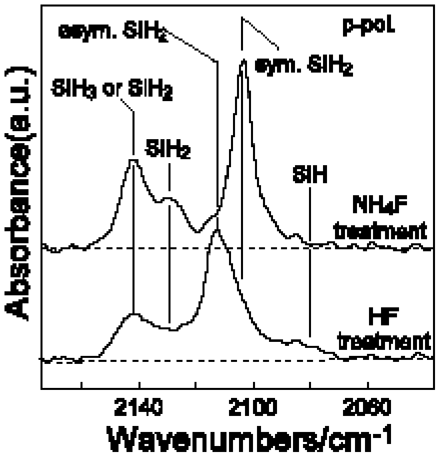

Fig. 2.5 FTIR-ATR spectra of the HF-etched and the hot NH_4F etched Si(100) surface.

The IR spectrum of the hot NH_4F treated Si(100) surface shows a dominant peak due to the symmetric stretching vibration mode of SiH_2 at 2104 cm^{-1} and a medium peak at the same wavenumber as the HF-treated surface spectrum. In the hot NH_4F-treated surface spectrum, the asymmetric stretching vibration mode peak, which is the main peak in the HF-treated surface spectrum, is negligible. Generally, a polarization change of symmetric vibration is vertical and that of asymmetric vibration is parallel on an ideal smooth Si(100) surface. When a p-polarized IR light is used for ATR measurement, more sensitive vibration is a symmetric vibration on a smooth surface. Therefore, the hot NH_4F-treated surface implies an atomically smooth surface, because of the dominant peak of the symmetric stretching vibration of SiH_2 under p-polarized IR light. Moreover, the SiH stretching vibration mode peak completely vanished in the hot NH_4F-treated surface spectrum, revealing that the hot NH_4F-treated surface does not have the SiH chemical structure. Following these authors, also STM results suggest that the hot NH_4F-treated Si(100) surface has di-hydride terminated chemical structure with a missing atomic row, as shown in **Fig. 2.6**.

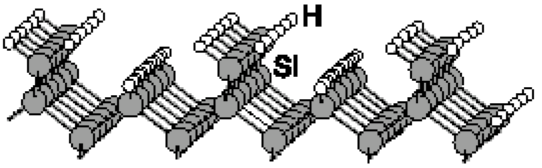

Fig. 2.6 Chemical structure model of the hot NH_4F-treated Si(100)surface.

In conclusion, this material is supposed to have three different layers: the uppermost atomic layer was SiH_2, the second layer had SiH_2 as Si(100) rinsed in ultrapure water, while the third layer was a mono-hydride atomic layer. The difference between the two structures is that the former does not have atomic defects in second layer and neither a mono-hydride third atomic layer. The authors cannot explain these differences and stated that further studies were under way to clarify them.[11]

2.3 Stability of hydrogen terminated surfaces

The hydrogen terminated silicon surfaces are actually quite stable and can be handled in air for several minutes before measurable oxidation of the surface occurs. Infrared studies[12] have shown that the half-life of the Si–H stretching in air is humidity dependent. The mechanism of the oxidation by water is shown in **Fig. 2.7**. In this reaction, water is believed to react with the surface by the donation of an electron to form a pentacoordinated silicon which subsequently loses dihydrogen to form an Si–OH group.

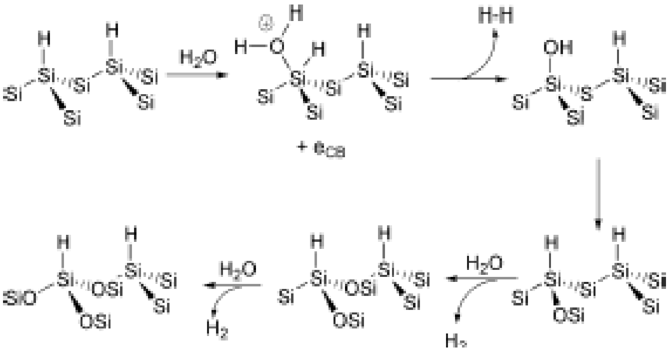

Fig. 2.7 Mechanism of oxidation of Si(111)H by water

The OH then inserts into an Si–Si back bond to regenerate a surface Si–H bond. The reaction proceeds until all of the back bonds are oxidized. Interestingly, the $(SiO)_3Si$–H species is kinetically stable and is the predominant species on the surface after standing for several hours in humid air. The evidence for this is the observation of the growth of an

IR absorption at 2250 cm^{-1} at the expense of the $(Si)_3Si$–H stretch at 2084 cm^{-1}.[12] The implication is that the reaction of water with the $(SiO)_3SiH$ species is kinetically limited, although a clear explanation of why this should be was not offered.

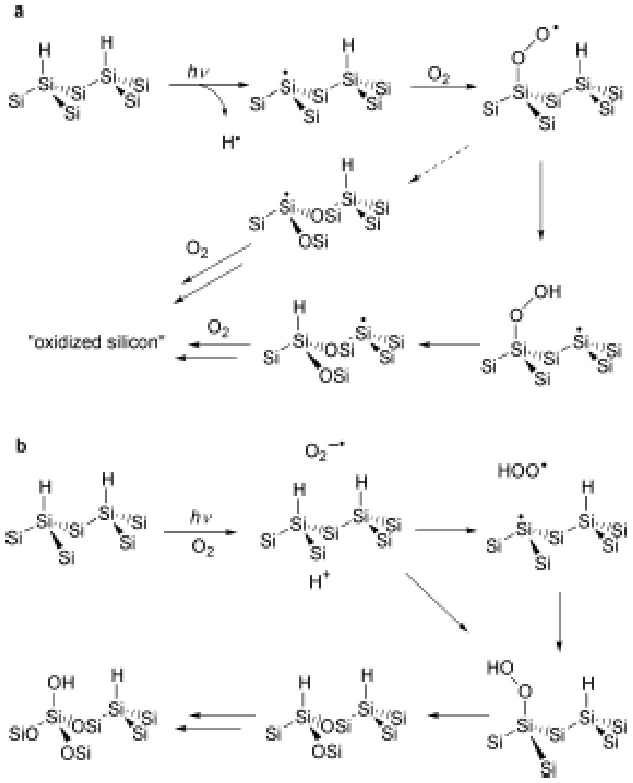

Fig. 2.8 Two of the possible mechanisms for the photooxidation of Si(111)–H.

The Si–H surface has been shown to oxidize under photochemical conditions (λ = 254 nm) in a reaction which presumably involves dioxygen. There are several possible mechanisms for this reaction. Chidsey proposed a mechanism in which irradiation of the surface produces silyl radicals (dangling bonds) on the surface which then react with dioxygen in a surface chain process (**Fig. 2.8a**). While this mechanism is plausible, Chatgilialoglu and coworkers[13] found that silylperoxyl radicals undergo a double insertion reaction to insert its oxygens into Si–Si back bonds of silane polymers (**Fig. 2.8a**, dotted arrow). Also, another mechanism should be considered, as follows. It is difficult to rule out the formation of superoxide, since 254 nm is close to the photoemission threshold of silicon (**Fig. 2.8b**). Moreover, superoxide was shown by Chidsey to initiate etch pit formation during the aqueous etching of Si(111).[4] The same initiation process in air may lead to surface oxidation. Whatever the mechanism at work, it is noteworthy that, unlike the oxidation by water, photooxidation leads to a predominantly hydroxylated silicon surface.[14][21]

---

[1] Bansal, A.; Li, X.; Lauermann, I.; Lewis, N. S.; Yi, S. I.; Weinberg, W. H. *J. Am. Chem. Soc.* **1996**, *118*, 7225.

[2] (a) He, J.; Patitsas, S. N.; Preston, K. F.; Wolkow, R. A.; Wayner, D. D. M. *Chem. Phys. Lett.* **1998**, *286*, 508. (b) Zhu, X.-Y.; Boiadjiev, V.; Mulder, J. A.; Hsung, R. P.; Major, R. C. *Langmuir* **2000**, *16,* 6766. (c) Luo, H.; Chidsey, C. E. D.; Chabal, Y. *Mater. Res. Soc. Proc.* **1997**, *477*, 415.

[3] G. S. Higashi, Y. J. Chabal, G. W. Trucks and K. Raghavachari,*Appl. Phys. Lett.*, **1990**, *12*, 656.

[4] C. P. Wade and C. E. D. Chidsey, *Appl. Phys. Lett.*, 1998, **71**, 1679.

[5] P. Allongue, C. Henry de Villeneuve, S. Morin, R. Boukherroub and D. D. M. Wayner, *Electrochim. Acta*, **2000**, *45*, 4591.

[6] P. Jakob and Y. J. Chabal, *J. Chem. Phys.*, **1991**, *95*, 2897.

[7] H. E. Hessel, A. Feltz, M. Reiter, U. Memmert and R. J. Behm, *Chem. Phys. Lett.,* **1991**, ***186,*** 275.

[8] (a) P. Allongue and J. Kasparian, *Microsc. Microanal. Microstruct.*, **1994**, *5*, 257. (b) P. Allongue, V. Kieling and H. Gerischer, *Electrochim. Acta*, **1995**,*40*, 1353.

[9] (a) Y.-C. Huang, J. Flidr, T. A. Newton and M. A. Hines, *Phys. Rev. Lett.*, **1998**, *80*, 4462. (b) J. Flidr, Y.-C. Huang and M. A. Hines, *J. Chem. Phys.*, **1999**, *111*, 6970. (c) Y. C. Huang, J. Flidr, T. A. Newton and M. A. Hines, *J. Chem. Phys.*, **1998**, *109*, 5025.

[10] H. Luo and C. E. D. Chidsey, *Appl. Phys. Lett.*, **1998**, *72*, 477.

[11] H. Sakaue, Y. Taniguchi, Y. Okamura, S. Shingubara, T. Takahagi; *Appl. Surf. Scie.* **2004**, *234*, 439 and reference cited therein

[12] T. Miura, M. Niwano, D. Shoji and N. Miyamoto, *J. Appl. Phys.*, **1996**, *79*, 4373.

[13] C. Chatgilialoglu, A. Guerrini, M. Lucarini, G. F. Pedulli, P. Corrozza, G. Da Roit, V. Borzatta, V. Licchini, *Organometallics*, **1998**, *17*, 2169.

[14] J. C.T. Wojtyk, R. Boukherroub, D. D. M. Wayner, *J. Am. Chem. Soc.*, **2001**, *123*, 1535.

CHAPTER 3

WET CHEMICAL APPROACHES TO SI-C BOND FORMATION

The Si-C bond is both thermodynamically and kinetically stable, due to the high bond strength and low polarity of the bond.[1] The procedures for the formation of silicon-carbon bond on these semiconducting surfaces are divided in “wet chemical” or “benchtop chemistry” and “ultrahigh vacuum (UHV)” routes. Specifically, wet chemical routes are a subject of this thesis. In the last 10 years a lot of this kind of approaches have arisen in the literature. These approaches can be classifies in three kind: thermal, photochemical and electrochemical.

3.1 Thermal Functionalization

Thermal functionalization involves insertion of an unsaturated bond into a silicon-hydride group (hydrosilylation). Alkyne and alkene hydrosilylation on Si-H-terminated surfaces yield alkenyl and alkyl termination, respectively, as shown in **Fig. 3.1**.

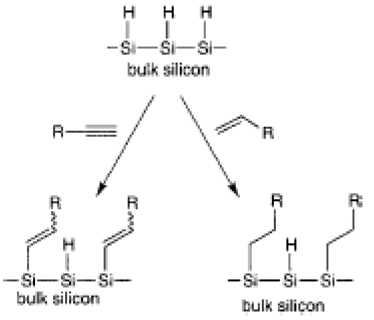

Fig. 3.1 Scheme of hydrosilylation chemistry. Hydrosilylation involves the insertion of an unsaturated bond, here an alkyne or an alkene, into an Si-H bond, resulting in Si-C bond formation and formation of alkenyl or alkyl groups, respectively.

The first example of hydrosilylation of nonoxidized hydride-passivated silicon was carried out in 1993 on flat crystal Si(111)-H surfaces whit alkenes.[2] This reaction, carried out in the presence of a diacyl peroxide radical initiator, provided high-quality alkyl monolayers in 1 h at 100 °C. Monolayers prepared from octadecene, yielding octadecyl groups on the surface, are densely packed and tilted approximately 30° from the surface normal direction. As a result of the good coverage provided by the film, the silicon surfaces demonstrate excellent stability and withstand extended boiling in aerated chloroform, water, acid (2.5 M H_2SO_4 in 90% dioxane, v/v), and base (10% aqueous 1 M NH_4OH) and are resistant to fluoride (immersion in 48% aqueous HF). Under ambient conditions in air, little oxidation of the silicon surface is observed, indicating the usefulness of this approach for technological applications. A radical mechanism was proposed for monolayer formation under these conditions, as shown in **Fig. 3.2**. The initiator, the diacyl peroxide, undergoes homolytic cleavage to form two acyloxy radicals which decompose to carbon dioxide and an alkyl radical. The alkyl radical can then abstract H• from a surface Si-H group to produce a silicon radical. Because silyl radicals are known to react extremely rapidly with olefins, formation of a silicon carbon bond is the next probable step.[3] The carbon-based radical can then abstract a hydrogen atom either from a neighboring Si-H group or from the allylic position of an unreacted olefin.

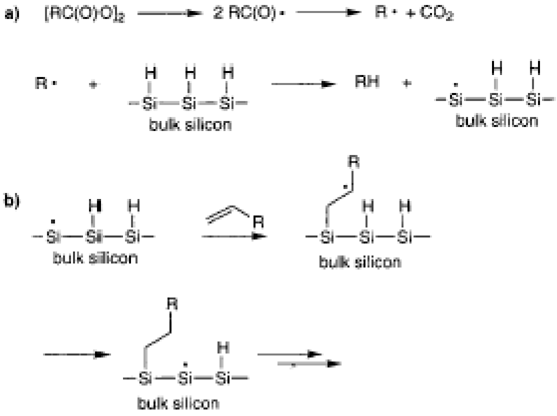

Fig. 3.2 Mechanism for radical-based hydrosilylation. (a) Initation reaction in the presence of diacylperoxide, resulting in R• radicals. The R• can then abstract a hydrogen atom from the surface, forming a highly reactive silicon radical. (b) Reaction of the surface silicon radical with the alkene substrate and formation of the Si-C bond.

Further functionalization of the surface is possible using the ω-Cl-terminated olefin. As an example, 11-chloroundec-1-ene, produced good-quality mono-layers with chloride termination. Differently, the use of the bromide-terminated olefin, 11-bromoundec-1-ene, however, produced a poorly organized monolayer, perhaps due to the incompatibility of the Br with the radical nature of the reaction.

Chidsey and coworkers[2] during their investigations of diacylperoxide initiated olefin hydrosilylation on Si(111) surfaces indicated that the reaction could occur in the absence of diacylperoxide initiator at higher temperatures (≥150 °C), almost certainly through homolytic Si-H cleavage, Si-H $\rightarrow$ Si• + H•. This yields the silicon surface-based radical (dangling bond) which can then react via the mechanism outlined in **Fig. 3.2b**.[4] Aliphatic monolayers produced on hydride-terminated Si(111) and Si(100) through the thermal hydrosilylation of alkenes are stable up to 615 K under vacuum, which indicates that organic monolayers on silicon are thermally resistant.[5] Hydride-terminated Si(100) was shown to react in a similar fashion.[6] Different olefins (12-18 carbon atoms) produced closely packed monolayer after 2 h at 200°C, as judged by X-ray reflectivity, ATR infrared spectroscopy, and contact angle measurements. Examples of surface terminations accessible through the thermal hydrosilylation route are shown in **Fig. 3.3**.

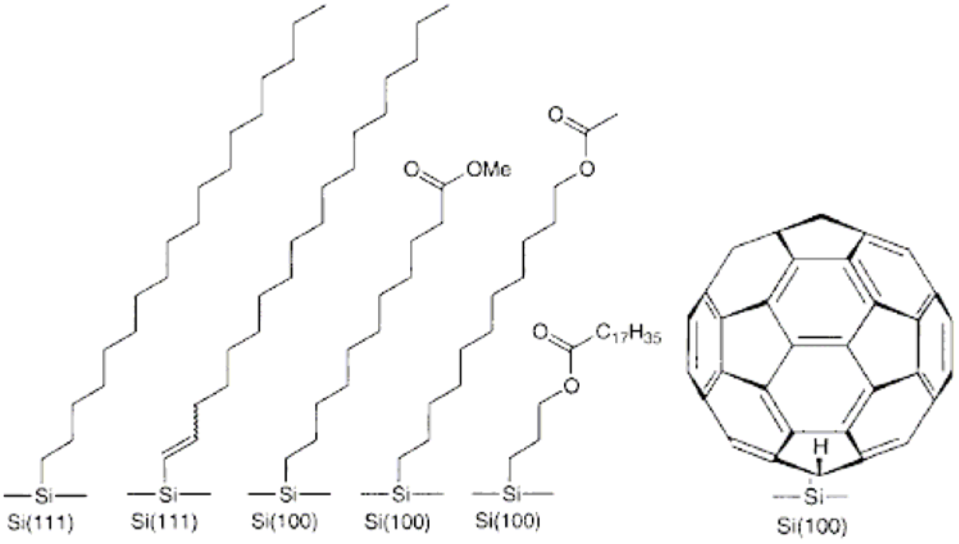

Fig. 3.3

A major limitation of the thermal hydrosilylation approach is the large excess of alkene required.[7] Particular substrates which are not commercially available and thus need to be synthesized are potential limitations. To get through this restriction, a range of alkenes dissolved in inert, high-boiling hydrocarbons were examined. 1-Hexadecene (10%) in solvents such as n-decane, anisole, toluene, xylene, cumene, tert-butylbenzene, and mesitylene was compared with the results obtained with neat 1-hexadecene by contct angle measurements. Surprisingly, a solution concentration as low as 2.5% of 1-hexadecene in mesitylene can be compared with neat 1-hexadecene (from contact angle measurement $\Theta \approx 109°$ with water).

The apparent advantage of mesitylene, as opposed to the other high-boiling solvents tried, is that this molecule does not result in pinhole defects in the monolayer as a result of its large size, as opposed to n-hexadecane which intercalates into the forming monolayer. This work is very useful because it reveals that even dilute solutions of alkene (2.5%) in mesitylene, a 10-fold reduction in absolute quantity, can result in ordered monolayers via thermal functionalization. In conclusion, neat alkene is not required. Because the bulk spectroscopic techniques measure only macroscopic properties of the organic monolayers, molecular modeling of Si(111) alkyl-terminated surfaces, the product of alkene hydrosilylation, was carried out to try to extract molecular- and atomic-level information.[8] The modified surface was described as a repeating box using the polymer consistent force field (PCFF). The PCFF-optimized structures are shown in **Fig. 3.4**.

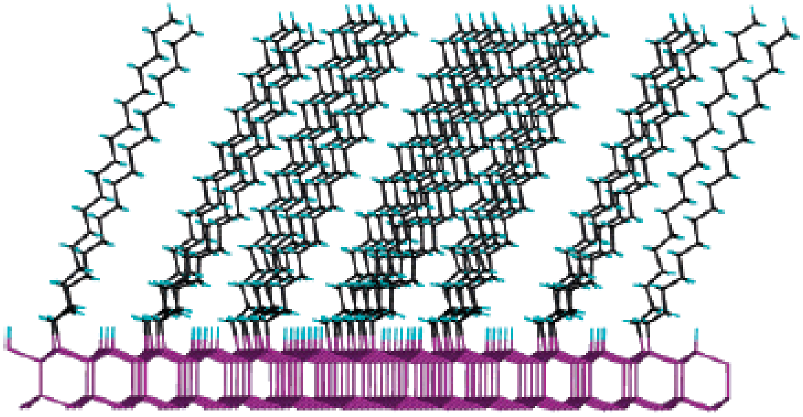

Fig. 3.4 PCCF-optimized structure of the alkyl monolayer formed on Si(111)-H The side view clearly shows the tilt of the alkyl groups at this level of surface substitution (~50%).

Different percent coverages result in monolayers that do not fit the experimental evidence. For instance, lower substitution values of 33.3% result in highly disordered monolayers in which the alkyl chains attempt to compensate for the extra space by tilting 60° from the surface normal direction and bending, twisting, or adopting banana-like configurations, behavior not substantiated by the ATR-FTIR spectroscopy and X-ray reflectivity data. Substitution of 100% of the surface hydrides with alkyl chains results in a tilt angle of ~1°, serious deformations of the surface Si-C bonds, and substantial interpenetration of the van der Waals volumes, a highly unfavorable situation. The authors conclude that about 50-55% of the surface hydrides on an Si(111)-H surface are replaced during thermal hydrosilylation, as this appears to be the optimal substitution percentage based on their theoretical calculations. These results substantiate the suggestions made by Chidsey and co-workers, that the alkyl chains on the Si(111) structure cannot pack with complete substitution of the apical Si-H functionalities (1x1 structure); an average pattern more similar to a 2x1 substitution motif is more likely, which is equivalent to ~50% substitution.[1]

Thermal hydrosilylation has been utilized to graft C60 to a hydride-terminated Si(100) surface, as shown in **Fig. 3.3**. [9] Cyclic voltammetry of these C60-modified surfaces indicates that the surfaces are quite stable and C-60 is almost certainly chemically bonded; cycling several times does not result in a decay in current density, as observed with a hydride-terminated silicon sample. On the basis of integration of the cyclic voltammograms, the surface coverage is about 10% that of a full monolayer, based on what would be expected for a close-packed monolayer. The authors conclude that such surfaces may be of interest for photovoltaic and sensor applications.

Chidsey mentioned earlier that alkyne hydrosilylation on Si(111)-H surfaces was successful, in the presence of a diacylperoxide radical initiator at 100 °C, and an infrared active vibration at 1600.8 cm^{-1} was observed by FTIR.[10] This stretching frequency correlates perfectly with a monosilicon-substituted double bond, and thus, an alkenyl-derivatized surface was formed under these conditions, shown schematically in **Fig. 3.1**. On hydride-terminated Si(100) surfaces, however, formation of alkenyl monolayers is not observed by ATR-FTIR.[11] Very stable and ordered organic layers are formed at 165 °C for 2 h with high contact angles (with water, (Θ_a)= 108°-110°) and tilt angles of ~30°-35° from the surface normal direction, suggesting that the monolayers are very similar to those formed from alkene hydrosilylation. The lack of an observable SiC=C stretch, clearly seen on the Si(111) surface and on porous silicon, however, points toward bis-silylation, therefore reducing the bond order of the C≡C triple bond to a C-C single bond. In contrast to the alkene hydrosilylation monolayers, the X-ray reflectivity data of the alkyne-reacted surface required introduction of an intermediate layer between the organic monolayer and the bulk silicon substrate. The calculated electron density of this layer is higher than that of both the alkyl layer and the bulk silicon, which indicates a high density of electronegative atoms at this interfacial region. SiO_2 is discounted because the electron density of silicon dioxide is comparable to that of Si and thus cannot account for this increase. Instead, a bis-silylated alkyne is proposed in which a carbon atom is bonded to two silicon atoms, as shown in **Fig. 3.5**.

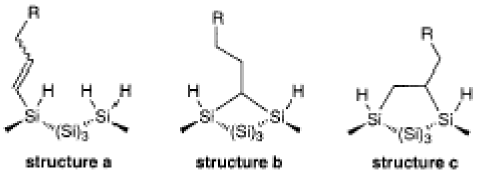

Fig. 3.5 Three proposed possible products of alkyne hydrosilylation on hydride-terminated Si(100). Structure a is the monohydrosilylation product, and structures b and c are the 1,1- and 1,2-bridged bis-hydrosilylation products.

Two possible bis-silylated structures are possible, a methine-bound carbon (1,1-bridge, structure b) and an ethylene chain (1,2-bridge, structure c), in contrast to the usual hydrosilylation product, structure a. To provide insight into the two possible binding configurations, the 1,1- and 1,2-bridge, quantum mechanical B3LYP/6-31G(d) calculations on a 32- atom cluster were carried out.[11] An alkenyl (monohydrosilylated) surface was also examined for comparative purposes. The 1,1-bridged species has the lowest energy, 4.7 and 7.3 kcal mol^{-1} lower than the two possible 1,2-bridging configurations. It is also 20 kcal mol^{-1} lower in energy than the alkenyl surface. The authors conclude that not only is the 1,1-bridge structurally feasible, but it is actually energetically the most favorable structure. They do note, however, that because of the high-temperature reaction conditions and surface roughness of the Si- (100) hydride-terminated surface, both the 1,1- and 1,2-bridged species may be present. Perhaps detailed spectroscopic studies (FTIR) could differentiate between these two possibilities.

However, there is some discrepancy as to the surface termination produced upon alkyne hydrosilylation on hydride-terminated porous silicon. Initial reports suggested that alkyne hydrosilylation does not produce surface-bound vinyl groups based upon transmission FTIR data[12], presumably because it undergoes two consecutive hydrosilylations (bis-silylation), forming a 1,1- or 1,2-bridged species. Other work has indicated that the surface-bonded alkenyl group, presumably an intermediate, can be observed at shorter (1-2 h) reflux times at higher temperatures (>150 °C).[13] Further work is required to better understand this reaction on porous silicon.

3.1.1 Reaction Mediated by Metal Complexes

Hydrosilylation of alkenes, promoted by Lewis acids or transition metals, is well known in the molecular organosilane literature. Buriak and coworkers[14] showed that the surface of hydrogen terminated porous silicon could effectively be hydrosilylated in a reaction with $EtAlCl_2$ as the catalyst at room temperature. The mechanism of this reaction is shown in **Fig. 3.6**. Although it is possible to catalyse the reaction of an alkene on the Si(111)–H surface,[15] the requirement to bring the catalyst in close proximity to the surface raises concerns about steric effects. These Si(111)–R surfaces were shown to have only about 80 percent of the maximum coverage achieved using the photo-chemical approach.

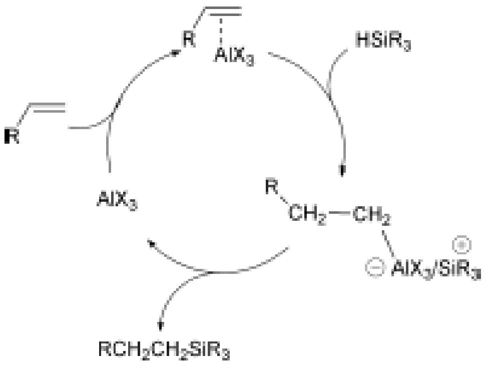

Fig. 3.6 Mechanism of the Lewis acid catalysed reaction of alkenes with the Si(111)–H surface.

3.1.2 Reactions of Alkyl/Aryl Carbanions

The addition of organolithium and Grignard reagents to porous silicon was investigated either under electrochemical conditions[16] or without an electronic bias[17] and was found to proceed efficiently at room temperature.

The first approach to functionalize flat single crystal silicon with carbanions involved a two-step halogenation/alkylation route.[18] Halogenation of a hydride-terminated flat Si(111) is explained below. Transmetalation of Si(111)-X surface with an alkyllithium or Grignard reagent at 80 °C for 30 min to 8 days yields LiX or MgXCl and an alkyl group bound to the silicon surface through an Si-C linkage, as shown in **Fig. 3.7**.

The resulting surfaces with long alkyl termination are more resistant to oxidation under ambient conditions and to boiling in aerated chloroform and water. Thermal desorption and XPS experiments indicate that ≡Si-OR linkages are not formed which provides support for the expected Si-C bond formation event.

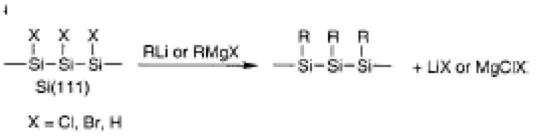

Fig. 3.7 Outline of the reaction of carbanions (organolithium and Grignard reagents) to flat halide- and hydride-terminated Si(111) surfaces.

The effects of the two-step halogenation/alkylation reaction on recombination velocities on the Si(111) surface were measured using a contactless rf conductivity apparatus, and it was found that alkyl termination can stabilize the electronic properties of the bulk silicon.[19] Freshly etched Si(111)-H in strong acid has a very slow recombination velocity, <20 cm s^{-1}, but with 30 min of exposure to air, it increases dramatically. An octyl-terminated surface, prepared by reacting the chloro-terminated surface with octyl Grignard, also has a slow recombination velocity, <25 cm^{-1}, and this value remains basically unchanged after 4 weeks. Recent work has shown that hydride-terminated Si(100) surfaces may be alkylated directly (without halogenation pretreatment) with butyl-, hexyl-, phenyl- and 5-(N-pyrrolyl)pentyllithium reagents in THF at room temperature.[30] The Si(111)-H surface has also been shown to be alkylated directly with decylmagnesium bromide after 16 h exposure in diethyl ether with slight heating.[28] ATR-FTIR reveals that no Si-H remains on the Si(111)-H surface, suggesting that the reaction proceeds via silicon- hydride cleavage. The surfaces prepared *via* this route are very stable to a range of treatments, including sonication and boiling in chloroform, boiling in water, and extended exposure to fluoride and hydroxide.

3.2 Photochemical functionalization

3.2.1 UV

It is known in the literature that UV irradiation can promote hydrosilylation of unsaturated compounds[20] due to homolytic cleavage of Si-H bonds, as is the case with thermal induction. UV photoinduction, however, takes place at room temperature and thus provides a way to avoid thermal input that could be harmful to delicate or small features on a silicon chip. Minimal input of thermal energy would be preferable in any IC manufacturing process (thermal budget). Irradiation of a hydride-terminated Si(111) surface with UV light (185 and 253.7 nm) in the presence of an aliphatic alkene like 1-

pentene or 1-octadecene brings about hydrosilylation in 2 h at room temperature, as shown in **Fig. 3.8**.[21]

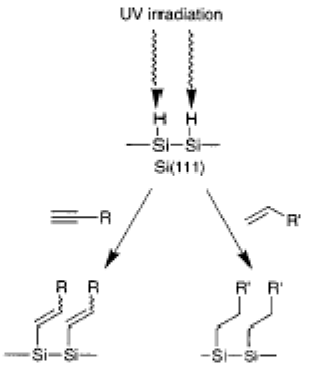

Fig. 3.8. Schematic for UV-mediated alkene hydrosilylation on Si(111)-H.

A range of alkenes and alkynes were successfully tried, including 1-octene, 1-octadecene, 1-octyne, styrene, and phenylacetylene. Alkenes yield alkyl monolayers and the alkynes yield alkenyl monolayers; examples of surfaces prepared are shown in **Fig. 3.9**.

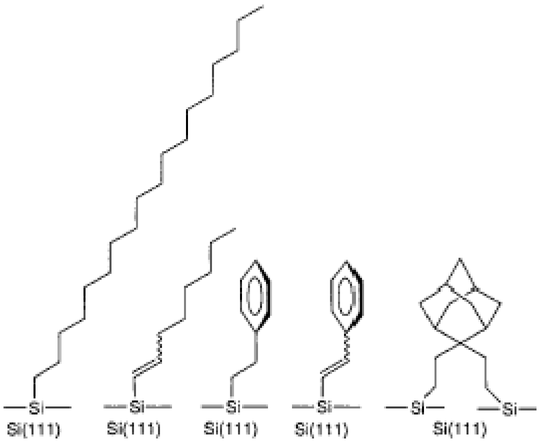

Fig. 3.9 Some surfaces produced through UVmediated hydrosilylation on Si(111)-H.

The XPS spectrum of an Si(111)-H surface irradiated with an Hg lamp (254 nm) in the presence of 1-octene leads to a coverage of 0.44 eight-carbon adsorbates per surface silicon atom, about one alkyl group per two silicons, as proposed to be ideal based on molecular modeling.[6-8] The thickness of this monolayer was measured by ellipsometry to be 9 Å, as predicted. Hydrosilylation of 1-octadecene, forming an octadecyl surface, showed an asymmetric methylene stretch at 2917 cm^{-1} which indicates a highly ordered film. Alkyne hydrosilylation leads to alkenyl-terminated surfaces, as indicated by the observed absorbance in the ATR-FTIR spectrum for 1-octyne at 1601 cm^{-1}, corresponding to a monosilicon-substituted vinyl group. XPS analysis also substantiates this conclusion as a slightly higher energy component of the carbon signal is seen, which is absent for the 1-octene reacted surface. The maximum coverage by alkenes and alkynes is obtained in about 1 h of UV irradiation with the Hg lamp. It was later shown that irradiation of an Si(111)-H surface with longer wavelengths, up to 385 nm, could be used to promote alkene hydrosilylation, but irradiation had to be prolonged for 20-24 h, with an accompanying increase in temperature to 50 °C.[22]

The mechanism proposed is radical based, with homolytic Si-H bond cleavage initiating the reaction to form a silicon radical (dangling bond),[23] similar to that shown in **Fig. 3.2b**.[15d] Because silicon radicals are known to react very rapidly with unsaturated carbon-carbon bonds,[2,24] Si-C bond formation is expected to be a facile step. Abstraction of a neighboring hydrogen completes the hydrosilylation. On the basis of the bond strengths, it appears that a minimum of 3.5 eV UV ($\lambda < 350$ nm) is required to efficiently perform Si-H bond homolysis[15d] (dissociation bond energy of ≡Si-H bond ~3.5 eV). In fact, irradiation of the Si(111)-H surface in air results in fast and efficient loss of hydrides, as observed by ATR-FTIR, only at wavelengths shorter than 350 nm, again pointing to the threshold near this wavelength for Si-H bond activation on this surface. The radicals are almost certainly surface-based radicals since polymerization of styrene and phenylacetylene, two readily polymerizable substrates under radical conditions, is not observed.

The use of this UV irradiation method invites photopatterning, which was undertaken to induce hydrosilylation in spatially defined areas on a flat silicon surface.[25] Using the observation that irradiation of an Si(111)-H surface in air with 254 nm results in loss of hydrides and concomitant oxide formation,[15d] irradiation through a commercially available gold grid with 10 μm wires results in micrometerscale oxide features on the surface. The unexposed areas, however, remain Si-H terminated and can undergo further chemistry. Immersion of this oxide/ Si-H-patterned surface in deoxygenated 1-decene and irradiation of this entire surface at 300 nm for 3 h induces hydrosilylation and results in an oxide/ alkyl pattern. AFM and CCD optical images of these patterned surfaces are shown in **Fig. 3.10**. The SAES spectrum clearly shows the alternation of carbon and oxygen as one moves laterally across the pattern. Through this very simple method hydrophobic and hydrophilic domains can be created, which can, as the authors suggest, be extended to DNA and protein microarray synthesis. Very recently, the electronic properties and electrontransfer characteristics of the UV hydrosilylated Si(111)-H monolayer surfaces were examined.[26]

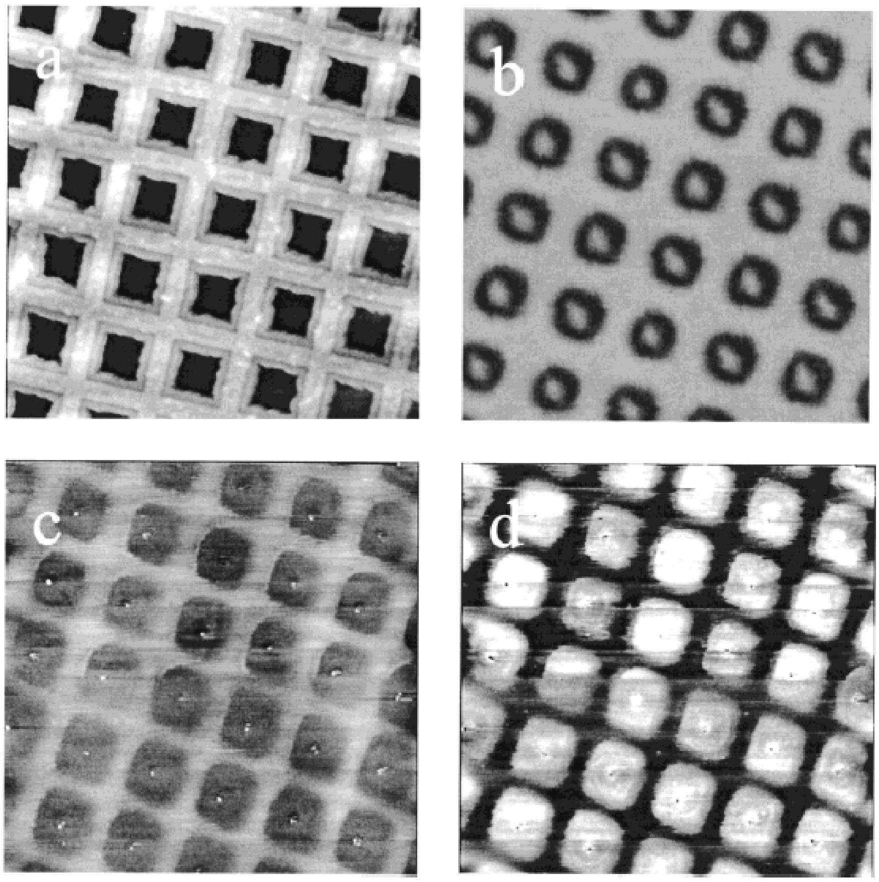

Fig. 3.10 140 μm x 140 μm images of (a) an AFM tapping mode image of the gold wire grid, (b) CCD optical image of the Si(111) surface following patterning and exposure to water vapor, (c) AFM height image of the patterned surface, and(d) AFM image taken in frictional force mode.

As an example, two different monolayers were investigated, alkyl and fluoro, which were contrasted with an alkoxymonolayer formed by reaction of an alcohol with the Si(111)-H surface. The obtained results were consistent with the different carbon content per surface silicon atom of the various monolayers: alkyl monolayer has the highest number of organic adsorbates per surface silicon atom (0.43), compared to the fluorinated alkyl (0.27) and alkoxy (0.21) monolayers.

Electrochemical techniques have been also used to characterize organic monolayers anchored on silicon surface. For istance, cyclic voltammetric experiments were carried out on Si(111) surfaces as working electrode, using aqueous 3 mM potassium ferrocyanide, 3 mM potassium ferricyanide, 0.1M potassium chloride, and a platinum reference electrode. As shown in **Fig. 3.11**, an Si(111)-H surface has a diffusion-limited peak at ~ -0.7 V, corresponding to the reversible reduction $[Fe(CN)_6]^{-3}$ + 1e- → $[Fe(CN)_6]^{-4}$, whereas the octyl-terminated surface shows significant blocking of the current. Interestingly, the octyl-terminated silicon electrode can be cycled several times (**Fig. 3.11b**), whereas the Si(111)-H surface current decreases significantly. Clearly, the hydride-terminated surface is oxidized under these conditions, forming an SiO_2 barrier.

The blocking behavior of the octyl surface is most effectively and reproducibly observed using THF as the solvent and the decamethylferrocene/decamethylferrocenium as the electroactive couple.

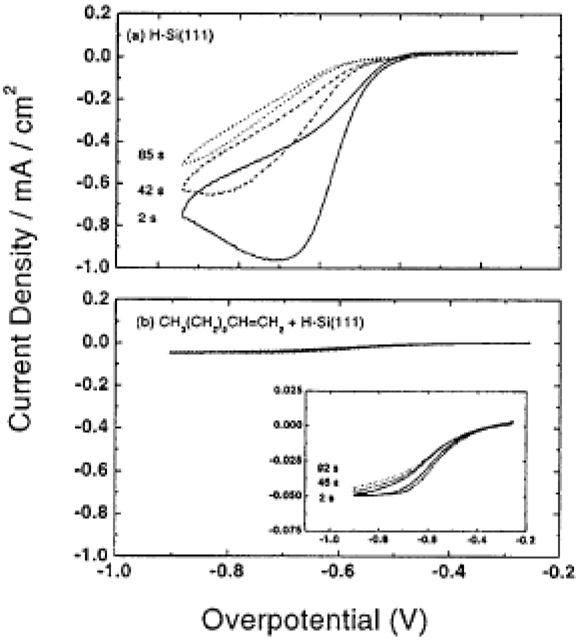

Fig. 3.11 Three successive cyclic voltammograms using a $K_3Fe(CN)_6/K_4Fe(CN)_6/KCl$ (aq) electrolyte of (a) an S-(111)-H electrode and (b) an octyl-terminated Si(111) electrode.

A study of the dependence of the electron transfer on the monolayer thickness was undertaken and revealed a direct correlation, suggesting no significant contribution from electron transfer through pinhole defects.[21] UV-induced hydrosilylation has also been utilized on Si(111)-H surfaces to prepare functionalized surfaces for chemical vapor deposition (CVD) of diamond.[27] Hydrosilylation of 2,2-vinyladamantane results in an adamantyl-coated monolayer bonded through Si-C bonds (**Fig. 3.8**). CVD of carbon produced a respectable diamond film.

3.2.2 White Light

It is well know that a simple white-light (22-44mW/cm^2) source can induce hydrosilylation of alkenes and alkynes on Si-H-terminated photoluminescent porous silicon surfaces at room temperature in minutes.[28]

Recently[29] Sudhölter *et al.* obtained a well-defined and highly stable organic monolayers on silicon surfaces, easily prepared by irradiating a hydrogen-terminated silicon wafer with visible light at room temperature in the presence of a 1-alkene or 1-alkyne. Using a combination of water contact angles, X-ray reflectivity, X-ray photoelectron spectroscopy, atomic force microscopy, and infrared reflection-absorption spectroscopy (IRRAS), it was shown that high-quality mono-layers can be obtained in this manner. The reaction is rather flexible with regard to the wavelength of irradiation (from 371 to more than 650 nm) and light source, and thus any light absorption can be avoided by the agent that needs to be attached. These extremely mild conditions are compatible with a very large variety of biologically active moieties that can be covalently linked to the reactive alkene or alkyne functionality. A chain mechanism for this reaction was tentatively proposed. **Fig. 3.12**

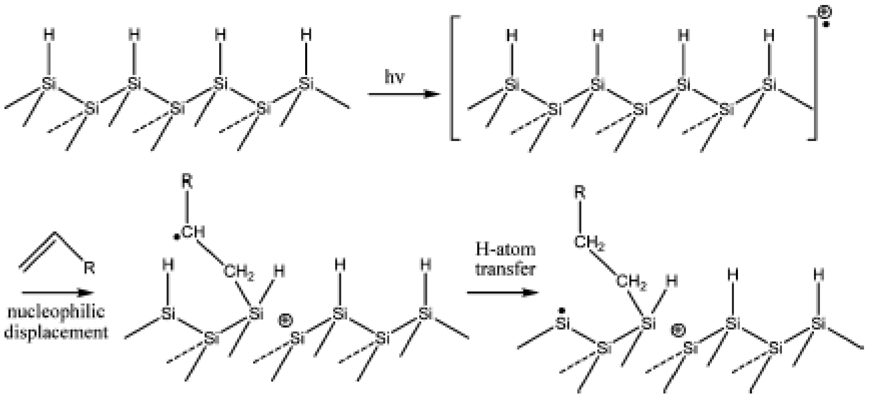

Fig. 3.12

This mechanism can also rationalize the differences in efficiency between Si(100) and Si(111). Since the Si(111) is more flat as compared to Si(100), the chain formation on the former surface will be hampered due to larger steps between the terraces. As a result the monolayer formation on Si(111) is more efficient.

Due to the formation of delocalized radical cations at the silicon surface (electrons temporarily being moved to the bulk) upon excitation thereof, this surface is susceptible to nucleophilic attack. Such a reaction may result in a Si-Si bond cleavage in a concerted manner, as in Si-Si-containing radical cations the Si-Si bond is not very strong, while the resulting Si-centered cation at the surface is highly stabilized by the neighboring Si atoms. As a result we obtain the structure at the bottom left in **Fig.3.12**, with a β-CH radical site. This radical can pick up a H atom, and leave a Si radical at the surface that is available for the attachment of a second alkene. The authors investigated, finally, the influence of the nature and degree of doping, the variation of the irradiation wavelength, and the type of silicon surface [Si-(100) *vs* Si(111)]. They could conclude that the efficiency of the photochemical monolayer formation on n-type Si(100) is higher than on p-type Si(100). It could also be stated that covalent attachment follows the rate order: high doped n > low doped n > low doped p > high doped p.

3.3 Electrochemical functionalization

Electrochemistry has also been used to produce close-packed phenyl monolayers on hydride-terminated flat n-type Si(111) surfaces, starting from aromatic diazonium salts, as shown in **Fig. 3.13**.[30]

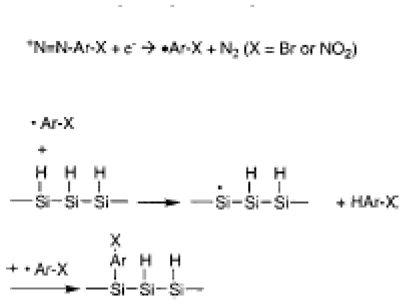

Fig. 3.13 Mechanism for electrochemical diazonium reduction and formation of R¥ radicals. The radicals can then abstract a surface hydride, leading to formation of a surface silicon radical which can then combine with another R¥, forming the Si-C bond.

Application of a negative potential of about 1 V to a dilute HF solution containing a 4-nitro or bromobenzene diazonium salt results in production of an aryl radical and dinitrogen. The aryl radical can then abstract a surface hydride to form silicon radicals, which can react with another aryl radical to form the silicon-carbon bond. The covalent nature of the phenyl bonding to the surface is demonstrated by the stability of the surfaces to aqueous 40% HF solutions as shown by XPS and Rutherford backscattering (RBS) measurements. Because this reaction utilizes the electrode nature of the semiconducting silicon, no clear reaction parallels can be found for soluble, molecular silanes. One important advantage of this approach is that the process is cathodic, thus making the surface electron rich during the reaction, which renders it less susceptible to nucleophilic attack by water, suppressing oxidation.

Diverse alkyl iodides or bromides, commercially available, can be electrochemically reduced *in situ*, leading to Si-C bond formation on hydride-terminated porous silicon.[31] Solutions (0.2-0.4 M) of the alkyl halide and 0.2 M $LiBF_4$ (electrolyte) in dry, deoxygenated acetonitrile or acetonitrile/ THF mixtures, upon application of a cathodic current of 10 mA cm^{-2} for 2 min at room temperature, result in efficient coverage.

The same chemistry appears to work on flat hydride-terminated silicon as the resulting surfaces become much more corrosion resistant upon exposure to base.

The proposed mechanism may involve reduction of the alkyl halide to the alkyl radical and halide anion, followed by abstraction of a surface H• by the alkyl radical, forming a surface silicon radical (dangling bond). At this point, three possible things could happen: (i) R•could react directly with Si•, forming the Si-C bond, (ii) reduction of the Si• with an electron to form Si^- could react in a nucleophilic fashion with RX, leading to Si-R bond formation and release of X^-, or (iii) in situ reduction of R• to R^-, the carbanion, which could attack weak Si-Si bonds.

Alkynes can also be grafted to Si-H-terminated porous silicon samples under negative bias (cathodic electrografting, or CEG), as outlined in **Fig. 3.14a**.[32] The alkyne is bonded through an Si-C bond directly and in contrast to hydrosilylation is not reduced. Examples of surface terminations prepared by this method are shown in **Fig. 3.14b**.

The surface-bonded alkyne C≡C vibration can be observed by transmission FTIR at 2179 cm^{-1} for a pentynyl- or octynylderivatized surface; the C≡C stretch of the molecular analogue 1-trimethylsilyldodec-1-yne appears at 2176 cm^{-1}. To definitively prove the alkynyl nature of this vibration, the pentynyl surface was subjected to hydroboration reaction conditions. These studies prove that alkynes are grafted on the surface carrying their triple bond. The cathodic electrografting approach allows for many of the synthesized organic molecular wires to be grafted directly to a silicon device for testing and characterization.

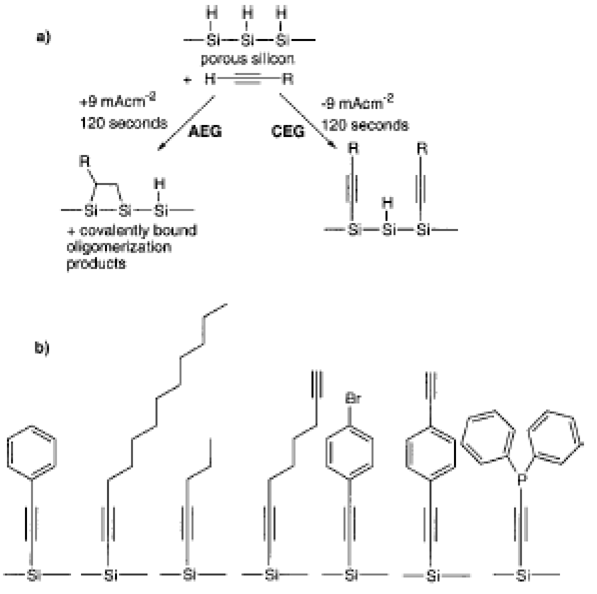

Fig. 3.14 (a) Outline of cathodic (CEG) and anodic (AEG) electrografting on hydride-terminated porous silicon. (b) Examples of surface terminations produced *via* CEG.

Positive bias (anodic electrografting, or AEG) was also tried and found to lead to Si-C bond formation but with total reduction of the bond order of the alkyne to aliphatic groups as judged by the lack of C≡C and C=C stretching modes in the transmission FTIR. The proposed mechanisms for both CEG and AEG are shown in **Fig. 3.15**.[33] CEG may involve a concerted reaction between a silicon-hydride, whose hydridic nature is even more pronounced under the effect of the negative bias, and an alkyne C-H, leading to ½H_2.

On the other hand, formation of a surface-bound silyl anion could deprotonate an alkyne, leading to a carbanion which has been shown to attack the weak Si-Si bonds on the surface, forming the Si-C bond. Indeed, carrying out the reaction in the presence of HCl in ether shuts down the reaction, possibly due to protonation of the silyl anion. AEG may be the result of a cationic hydrosilylation mechanism, previously postulated for molecular silanes and alkynes under electrochemical conditions.[34] Bis-silylation or cationic polymerization[35] appears to be occurring with the vinyl intermediate since no unsaturation is observed by transmission FTIR.

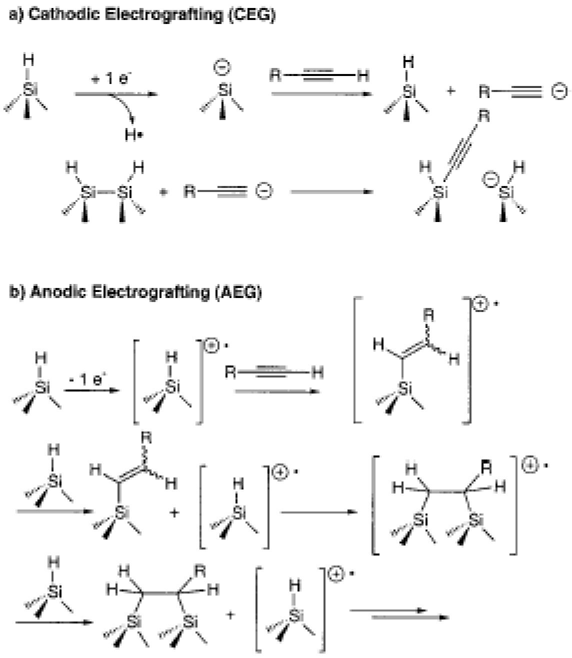
a) Cathodic Electrografting (CEG)
+ 1 e⁻
H•
b) Anodic Electrografting (AEG)
- 1 e⁻

Fig. 3.15 Proposed mechanisms for (a) CEG and (b) AEG Si-C bond formation on hydride-terminated porous silicon.

3.4 Functionalization of Monolayer

The ability to incorporate more complex organic or bioorganic structures at the interface implies to tailor the chemical functionality of the surface in order to meet predeterminated physical or chemical requirements. Chidsey and coworkers addressed this problem using a two step process in which the Si(100) surface is first chlorosulfonated by a photoinitiated free radical reaction followed by sulfonamide formation by reaction of the sulfonyl chloride with an amine[36] or by reaction with photogenerated singlet carbenes.[37] Using this approach it was possible to functionalize the surface with a diverse range of amines including those containing DNA and dendrimers. In both last reactions, the resulting yield was difficult to control as it depends on a number of factors including the concentration of reagents and the intensity and spectrum of the light source. This route may be suitable for the incorporation of biocomponents (DNA or proteins) onto these surfaces for the construction of integrated biosensors and microarrays, allowing at the same time to control the distance (at least average distance) between reactive centers in order to reduce steric interference while optimizing the sensitivity of a device.[38] Sieval *et al.*[5] carried out more traditional solid phase synthetis on modified surfaces. Thermal reaction of alkenes terminated with ester groups reacted with the Si(100)– H to form an ester terminated surface which could be hydrolyzed to form a carboxylic acid modified surface or reduced with $LiAlH_4$ to form an alcohol modified surface. The carboxylic acid surface could be re-esterified by refluxing the surface in an acidified solution of a different alcohol. While this demonstrated the possibility of carrying out sequential chemical transformations on the surface, a poor IR signal to noise ratio in the carbonyl region made it difficult to assess the overall chemical yields and, perhaps more importantly, the reaction conditions were too harsh to be compatible with most biological materials, if one would use these surfaces for biological applications. Boukherroub and Wayner further elaborated this approach to the functionalization of the covalently bonded alkyl monolayers by showing that reactions commonly used in solid phase synthesis could be adapted to the silicon surface chemistry.[39] The photochemical reaction of ethyl undecylenate with Si(111)–H provided a surface whose chemical properties were manipulated using standard chemical and solid phase chemical procedures. The surface density of the reactive esters could be controlled simply by diluting the ester with an n-alkene. Strother and coworkers[40] modified silicon surfaces with DNA using two different chemical approaches. In one approach they hydrolyzed a monolayer of Si(111)–$(CH_2)_{10}C(O)OCH_2$-CF_3 (prepared from the photoinitiated reaction of the corresponding alkene with Si(111)–H) to the undecylenate ion. This served as a substrate for the attachment of DNA by means of an electrostatically adsorbed layer of polylysine and the attachment of thiol-modified DNA using a heterobifunctional cross-linker (**Fig. 3.15**).

The second method made use of a similar linking procedure but an amino terminated alkyl chain was formed on the silicon surface by the reaction of t-Boc-protected 10-aminodec-1-ene followed by hydrolysis. The density of DNA binding sites on the surface could be controlled using the same method reported by Boukherroub and Wayner.[39] All of the surface chemistry described at this point results in the formation of monolayer films on the silicon surface, typically less than 2 nm in thickness. Besides being chemically robust, these monolayers provide excellent electronic passivation for the silicon surfaces, which may have electrical defect densities of less than one per 50000 surface atoms (seemingly as good as the defect density found in the best semiconductor devices).[41] Lewis and coworkers recently described a method using ring opening metathesis polymerization which allows a polymer film of uniform thickness to be grown from an Si(111) surface modified by the reaction of Si(111)–Cl with allyl magnesium bromide.[42] Activation with a ruthenium complex allows to grow 5 µm thick films. These polymer films may find applications in the fabrication of hybrid organic-silicon molecular or optical devices.

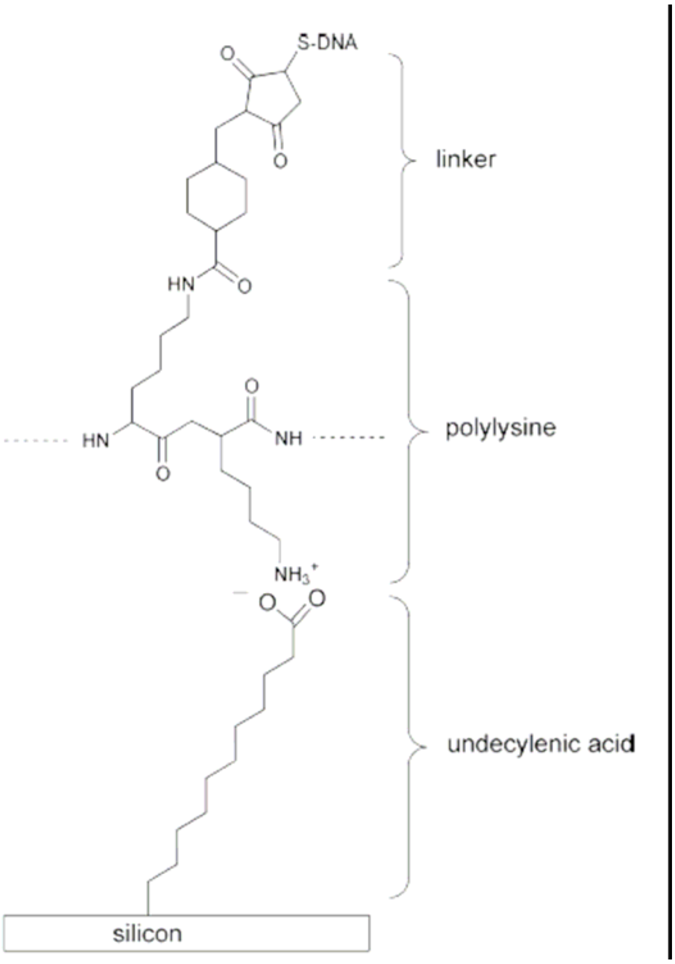

Fig. 3.15 Attachment of DNA to modified Si(111) surfaces.

---

[1] (a) M. A. Brook, *Silicon in Organic, Organometallic, and Polymer Chemistry*; Wiley: New York, 2000. (b) Patai, S., Rappoport, Z., *The Chemistry of Organic Silicon Compounds*; Eds.; John Wiley and Sons: New York, 1989.

[2] (a) Linford, M. R.; Chidsey, C.E.D. *J. Am. Chem. Soc.* **1993**, *115*, 12631. (b) Linford, M. R.; Fenter, P.; Eisenberger, P. M.; Chidsey, C. E. D. *J. Am. Chem. Soc.* **1995**, *117*, 3145.

[3] Chatgilialoglu, C. *Acc. Chem. Res.* **1992**, *25*, 188.

[4] Labinger, J. A. In *Comprehensive Organic Synthesis*; Trost, B.M., Fleming, I., Eds.; Pergamon: New York, 1991; Vol. 8, p 699.

[5] Sung, M. M.; Kluth, J.; Yauw, O. W.; Maboudian, R. *Langmuir* **1997**, *13*, 6164.

[6] Sieval, A. B.; Demirel, A. L.; Nissink, J. W. M.; Linford, M. R.; van der Maas, J. H.; de Jeu, W. H.; Zuilhof, H.; Sudhölter, E. J. *R. Langmuir* **1998**, *14,* 1759.

[7] Sieval, A. B.; Vleeming, V.; Zuilhof, H.; Sudhölter, E. J. *Langmuir* **1999**, *15,* 8288.

---

[8] (a) Sieval, A. B.; van den Hout, B.; Zuilhof, H.; Sudhölter, E. J. *Langmuir* **2000,** *16,* 2987. (b)Sieval, A. B.; van den Hout, B.; Zuilhof, H.; Sudhölter, E. J. R. *Langmuir* **2001**, *17*, 2172.

[9] Feng, W.; Miller, B. *Langmuir* **1999**, *15*, 3152.

[10] In footnote 33 of the cited paper in ref. 2, the authors note that the surface hydrosilylation of hexadecyne produces a small peak at 1600.8 cm^{-1} which they state suggests a surface-bound vinyl group.

[11] Sieval, A. B.; Opitz, R.; Maas, H. P. A.; Schoeman, M. G.; Meijer, G.; Vergeldt, F. J.; Zuilhof, H.; Sudhölter, E. J. R. *Langmuir* **2000**, *16*, 10359.

[12] Bateman, J. E.; Eagling, R. D.; Worrall, D. R.; Horrocks, B. R.; Houlton, A. *Angew. Chem., Int. Ed. Engl.* **1998**, *37*, 2683.

[13] Buriak, J. M.; Stewart, M. P.; Allen, M. *J. Mater. Res. Soc. Symp. Proc*. **1998**, 536, 173

[14] (a) Stewart and J. M. Buriak, *Adv. Mater.*, 2000, **12**, 859.(b) J. M. Buriak and M. J. Allen, *J. Am. Chem. Soc.*, 1998, **120**, 1339.

[15] R. Boukherroub, F. Bensebaa, S. Morin and D. D. M. Wayner, *Langmuir*, **1999**, *15*, 3831.

[16] (a) Viellard, C.; Warntjes, M.; Ozanam, F.; Chazalviel, J.-N. *Proc. Electrochem. Soc.* **1996**, *95*, 250. Ozanam, F.; Vieillard, C.; Warntjes, M.; Dubois, T.; Pauly, M.; Chazalviel, J. N. *Can. J. Chem. Eng.* **1998**, *76*, 1020. (c) Fidelis, A.; Ozanam, F.; Chazalviel, J.-N. *Surf. Sci.* **2000**, *444*, L7.

[17] (a) Song, J. H.; Sailor, M. J. *J. Am. Chem. Soc.* **1998**, *120*, 2376. (b) Song, J. H.; Sailor, M. J. *Inorg. Chem.* **1999**, *38*, 1503. (c) Kim, N. Y.; Laibinis, P. E. *J. Am. Chem. Soc.* **1999**, *121*, 7162. (d) Kim, N. Y.; Laibinis, P. E. *J. Am. Chem. Soc.* **1998**, *120*, 4516.

[18] Bansal, A.; Li, X.; Lauermann, I.; Lewis, N. S.; Yi, S. I.; Weinberg, W. H. *J. Am. Chem. Soc.* **1996**, *118*, 7225.

[19] Royea, W. J.; Juang, A.; Lewis, N. S. *Appl. Phys. Lett.* **2000**, *77*, 1988.

[20] Fleming, I. In *Comprehensive Organic Chemistry*; Jones, N., Ed.; Pergamon: New York, 1979; Vol. 3, p 568.

[21] (a) Terry, J.; Linford, M. R.; Wigren, C.; Cao, R.; Pianetta, P.; Chidsey, C. E. D. *Appl. Phys. Lett.* **1997**, *71*, 1056. (b) Terry, J.; Mo, R.; Wigren, C.; Cao, R.; Mount, G.; Pianetta, P.; Linford, M. R.; Chidsey, C. E. D. *Nucl. Instrum. Methods Phys. Res., Sect. B* **1997**, *133*, 94.(c) Terry, J.; Linford, M. R.; Wigren, C.; Cao, R.; Pianetta, P.; Chidsey, C. E. D. *J. Appl. Phys.* **1999**, *85*, 213. (d) Cicero, R. L.; Linford, M. R.; Chidsey, C. E. D. *Langmuir* **2000**, *16*, 5688.

[22] Effenberger F.; Götz, G.; Bidlingmaier, B.; Wezstein, M. *Angew. Chem., Int. Ed. Engl.* **1998***, 37,* 2462.

[23] Burkhard, C. A.; Krieble, R. H. *J. Am. Chem. Soc.* **1947**, *69*, 2687.

[24] Kanabus-Kaminska, J. M.; Hawari, J. A.; Griller, D.; Chatgil-ialoglu, C. *J. Am. Chem. Soc.* **1987**, *109*, 5267.

[25] Wojtyk, J. T. C.; Tomietto, M.; Boukherroub, R.; Wayner, D. D. *M. J. Am. Chem. Soc.* **2001***, 123,* 1535.

[26] (a) Barrelet, C. J.; Robinson, D. B.; Cheng, J.; Hunt, T. P.; Quate, C. F.; Chidsey, C. E. D. *Langmuir* **2001**, *17*, 3460. (b) Cheng, J.; Robinson, D. B.; Cicero, R. L.; Eberspacher, T.; Barrelet, C. J.; Chidsey, C. E. D. *J. Phys. Chem. B* **2001**, *105*, 10900.

[27] Leroy, E.; Ku¨ttel, O. M.; Schlapbach, L.; Giraud, L.; Jenny, T. *Appl. Phys. Lett.* **1998**, *73,* 1050.

---

[28] (a)Stewart, M. P.; Buriak, J. M. *Angew. Chem., Int. Ed. Engl.* **1998**, *23*, 3257. (b)Stewart, M. P.; Buriak, J. M. *J. Am. Chem. Soc.* **2001**, *123*, 7821.

[29] Sun, Q.-Y.; de Smet, L. C. P.; van Lagen, M B.; Giesbers, M.; van Engelenburg, J.; Thüne, P. C.; de Wolf, F. A.; Zuilhof, H.; Sudhölter, E. J. R. *J. Am. Chem. Soc*. **2005**, *127*, 2514

[30] Henry de Villeneuve, C.; Pinson, J.; Bernard, M. C.; Allongue, P. *J. Phys. Chem. B* **1997**, *101*, 2415.

[31] Gurtner, C.; Wun, A. W.; Sailor, M. J. *Angew. Chem., Int. Ed.* **1999**, *38*, 1966.

[32] Robins, E. G.; Stewart, M. P.; Buriak, J. M. *J. Chem. Soc., Chem. Commun.* **1999**, 2479.

[33] Yang, C. S.; Kauzlarich, S. M.; Wang, Y. C. *Chem. Mater.* **1999**,*11,* 3666.

[34] (a) Jouikov, V. V. *Russ. Chem. Rev.* **1997**, *66*, 509. (b) Jouikov, V.; Salaheev, G. *Electrochim. Acta* **1996**, *41*, 2623. (c) Kunai, A.;Ohnishi, O.; Sakurai, T.; Ishikawa, M. *Chem. Lett.* **1995**, 1051.

[35] *Cationic Polymerization*; Faust, R., Shaffer, T. D., Eds.; American Chemical Society: Washington, DC, 1997; Vol. 665.

[36] R. L. Cicero, P. Wagner, M. R. Linford, C. J. Hawker, R. M. Waymouth and C. E. D. Chidsey, *Polym. Prepr.*(Am. Chem. Soc., Div. Polym. Chem.), 1997, 38, 904

[37] P. Wagner, S. Nock, J. A. Spudich, W. D. Volkmuth, S. Chu, R. L. Cicero, C. P. Wade, M. R. Linford and C. E. D. Chidsey, *J. Struct. Biol.,* **1997**, *119*, 189.

[38] E. Southern, K. Mir and M. Shchepinov, *Nature Genetics*, **1999**, *21*, 5.

[39] R. Boukherroub and D. D. M. Wayner, *J. Am. Chem. Soc.*, **1999***, 121*, 11513.

[40] (a) T. Strother, W. Cai, X. Zhao, R. J. Hamers and L. M. Smith, *J. Am. Chem. Soc.,* **2000**, *122*, 1205. (b) T. Strother, R. J. Hamers and L. M. Smith, *Nucleic Acids Res.*, **2000**, *28*, 3535.

[41] W. J. Royea, D. J. Michalak and N. S. Lewis, *Appl. Phys. Lett.*, **2000**, *77*, 1988.

[42] A. Huang, O. R. Scherman, R. H. Grubbs and N. S. Lewis, *Langmuir*, **2001**, *17*, 1321.

Section II

As shall be detailed in this section, the research work carried out throughout this PhD thesis has been focused on the preparation, characterization and subsequent, further derivatization of carboxylic acid terminated monolayer, immobilized on crystalline unoxidized silicon surface through a covalent Si-C bond. To make this, the 10-undecynoic acid **1** has been anchored on Si(100). For many reasons, also outlined above (see section I), these functionalized surfaces are of particular interest. There is perhaps no material that is more important for modern technology than silicon (i), the Si-C bond is a robust linkage (ii), silicon surface is quite stable in an acidic environment (iii), the chemistry of the –COOH group is rich and versatile (iv).

In summary, first the concentration of the free –COOH group on the silicon surface has been first measured by the application of an analytical procedure, which has been elaborated to this end, based on fluorescence measurements in solution. Then, the free –COOH group has been utilized for anchoring a variety of other entities on this surface, providing access to the hetero-supramolecular chemistry on silicon. These entities are oligonucleotides and magnetite nanoparticles. The results from all these investigations are reported in the following chapters of the thesis.

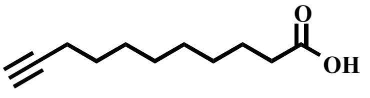

1

Fig.II.1 10-undecynoic acid **1**

CHAPTER 4

A SURFACE COVERAGE DETERMINATION WITH A FLUORESCENCE PROBE IN SOLUTION.

4.1 Introduction

As reported in the literature by many authors, the surface coverage determination of the monolayer concentration on a flat silicon surface is a difficult goal, due to the little amount of the material to be measured. Even when attempts have been made to this end, this concentration has been estimated by comparing the XPS,[1] ATR,[2] water contact angle[3] measurements with the analogous data relative to other correlated but different surfaces (SiO_2, Au).

Our contribution to this matter consists of the elaboration of an analytical procedure, based on a fluorescence measurement in solution, for determining the Si surface coverage by an α,ω-bifunctional molecule such as 10-undecynoic acid **1**, 6-heptynoic acid methyl ester **2** and 12-bromododecanoic acid **3**.

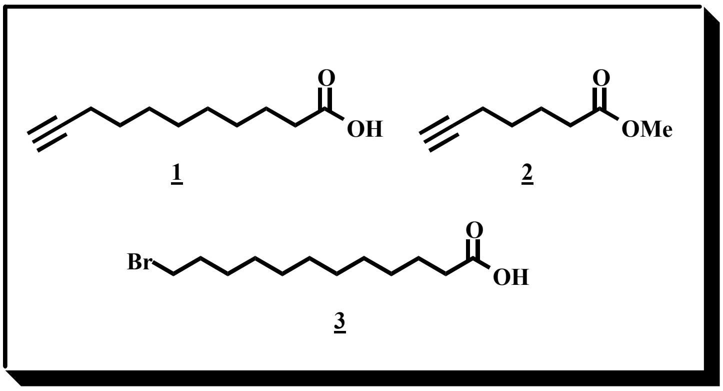

Fig.4.1 Structure of 10-undecynoic acid **1**, 6-heptynoic acid methyl ester **2** and 12-bromododecanoic acid **3**.

These molecules have been selected since they can be attached to a solid support through several different routes and they are very similar to other molecules used for the same purpose, like ω-undecenoic acid,[3] ethyl undecenoate,[2] 10-aminodec-1-ene.[4] Also, the corresponding amides **4a** have been synthesised with 7-amino-4-methylcoumarin **5** from **1**. Si surfaces have been derivatized in several different ways. The amides have been anchored on the surfaces by a one-step procedure utilising the preformed species **4a** or by a two step procedure carrying out the amidation reaction with **5a** in the heterogeneous phase on the surfaces previously derivatized with **1**, **2** or **3**. The analogous **4b** amide derived from 7-amino-4-trifluoromethylcoumarin **5b** have been also prepared, the related monolayers deposited on Si surface and investigated through XPS measurements. The results from all these experiments have allowed to shed some light on the points raised above. Moreover, the samples have been also characterised by atomic force microscopy (AFM),[5] which is a very useful technique for the investigation of the morphology of surfaces, yielding three-dimensional real space information[6] and revealing surface defects at a very high resolution.

4.2 Experimental

X-Ray photoelectron spectroscopy (XPS) studies were performed on the carboxylic acid **1** or the methyl ester derivative **2** monolayers, deposited on Si by using different functionalization procedures, and on the fluorinated **4b** amide monolayer, thermally deposited on Si. The following calculation was used in order to evaluate the percent amount of fluorine compound remained on the samples after hydrolysis:

$$\frac{\text{F/Si (after hydrolysis)}}{\text{F/Si (as prepared)}} \times 100$$

4.2.1 Amide synthesis

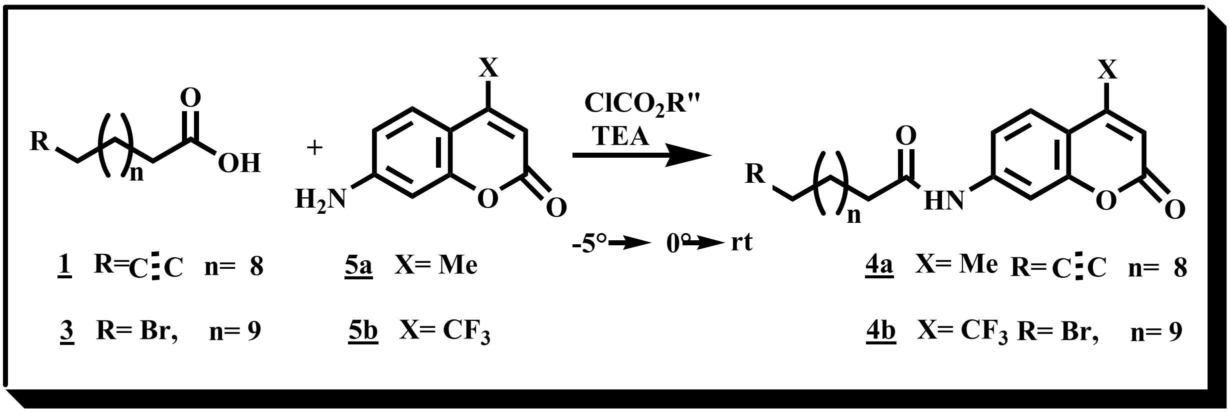

Fig.4.2 General procedure for amide synthesis

The amidation reaction was performed following the mixed anhydride method.[7] In a solution of the carboxylic acid (**1** or **3**, 5.5 mmol) and triethylamine (TEA, 5.5 mmol) in tetrahydrofuran (THF) (5 cm^3) an equimolar amount of isobutylchloroformiate is dissolved at low temperature (-5 °C). After stirring for 5 min, a solution of coumarin **5** (5.5 mmol) in N, N-dimethyl-formamide (DMF) (12 cm^3) is added. The reaction mixture is heated to 0 °C, left at this temperature for 1 h, then heated to room temperature and left at this temperature overnight. This mixture is concentrated under a stream of air. The residue is dissolved in CH_2Cl_2 (10 cm^3). The resulting clear solution is washed with a water solution of HCl (2 M, 20 x 3 cm^3) and then of $KHCO_3$ (20% w/w, 20 x 3 cm^3), dried over Na_2SO_4, filtered and evaporated to dryness on a rotary evaporator. In the case of amides **4a**, the residue is transferred to a fritted glass filter, washed with ethyl acetate and dried in a vacuum desiccator (25 °C, 24 h) over $CaCl_2$. In the case of the corresponding trifluoromethylamides **4b**, the residue is purified by column chromatography on silica gel with hexane/Et_2O (2/1 v/v) as eluent. The eluted fraction is evaporated on a rotary evaporator. The residue is crystallised from a heptane/CH_2Cl_2 mixture (1/1 v/v).

Analytical data of the new compounds

Undec-10-ynoic acid (4-methylcoumarin-7-yl)-amide **4a** – White microcrystalline powder, yield 38%, mp 167-169 °C. Analysis found: C 74.07, H 7.54, N 4.17; $C_{21}H_{25}NO_3$ requires: C 74.31, H 7.42, N 4.13; δ_H 7.81 (1 H, d, J 1.84, Ph), 7.64 (1 H, s, Ph), 7.57 (1 H, d, J 1.84, Ph), 6.23 (1 H, s, CHC=C), 2.46 (2 H, t, J 6.8, CH_2CO), 2.45 (3 H, s, CH_3), 2.21 (2 H, dt, J 2.4-6.8, $CH{\equiv}CCH_2$), 1.96 (1 H, t, J 2.4, CH≡C), 1.3-1.8 (12 H, m br, CH_2); ν_{max} 3295 (s, H-N), 3256 (s, H-C≡C) 2925 and 2850 (s, H-CH_2), 1687 (vs, br, CO); the assignment of the band at 3295 and 3256 cm^{-1} to the H-N and H-C≡C stretching vibration, respectively, is based on the deuteration of the amide group (H-N → D-N, recrystallizing **4** from THF/D_2O), after which the band at 3295 cm^{-1} disappears and a new band appears at 2435 cm^{-1} (s, D-N).

12-Bromo-dodecanoic acid (4-methylcoumarin-7-yl)-amide **8** – White microcrystalline powder, yield 32%, mp 161-163 °C. Analysis found: C 63.24, H 7.35, N 3.31; $C_{22}H_{30}BrNO_3$ requires: C 63.13, H 7.17, N 3.35; δ_H 7.80 (1H, d, J 2.03, Ph), 7.66 (1H, dd, J 2.03-8.82, Ph), 7.52 (1H, dd, J 2.03-8.82, Ph), 6.24 (1H, s, CHC=C), 3.43 (2.0 H, t, J 6.8, CH_2Br), 2.45 (3H, s, CH_3), 2.44 (2H, t, J 6.8, CH_2CO), 1.3-1.9 (18H, m br, CH_2); ν_{max} 3298 (s, br, H-N), 2926 and 2853 (s, H-C), 1687 (vs, br, CO).

Undec-10-ynoic acid (4-trifluoromethylcoumarin-7-yl)-amide **4b** - Yellow microcrystalline powder, yield 24%, mp 114-115 °C. Analysis found: C 63.42, H 5.85, N 3.61; $C_{21}H_{22}F_3NO_3$ requires: C 64.10, H 5.60, N 3.60; δ_H 7.79 (d, J 2.03, Ph), 7.66 (dd, J 2.03-8.82, Ph), 7.52 (dd, J 2.03-8.82, Ph), 6.69 (1 H, s, CHC=C), 2.42 (2 H, t, J 7.46, CH_2CO), 2.28 (2 H, dt, J 2.38-7.12, $CH{\equiv}CCH_2$), 1.93 (1 H, t, J 2.38, $CH{\equiv}C$), 1.3-1.8 (12 H, m br, CH_2); ν_{max} 3355 (s, H-N), 3286 (s, $H{-}C{\equiv}C$), 2929 and 2855 (s, $H{-}CH_2$), 1706 (vs, br, CO), 1145 (s, C-F). As in the case of **4**, the assignment of H-N and $H{-}C{\equiv}C$ stretching vibration is based on the deuteration experiment, from which it results that H-N stretching shifts to 2478 cm^{-1} (s, D-N).

Hepten-7-ynoic acid methyl ester **2** $HC{\equiv}C(CH_2)_4COOCH_3$ The methyl ester of 6-heptynoic acid **7** was prepared and purified as described in the literature for the synthesis of 10-undecylenic acid methyl ester.[3a]

Iodododecanoic acid **6** $I{-}CH_2\,(CH_2)_{10}COOH$ used in the cathodic electrografting experiment, is obtained in situ by reaction with **3** (0.1 M) in anhydrous CH_3CN with NaI (0.2 M) as supporting electrolyte and filtering. From a ^{1}H-NMR control experiment in CD_3CN it was found that the advancement of the substitution reaction between **3** and NaI is yield 65% after 24 h in 0.1 M solution: dH 3.43 (1.0 H, t, J 6.8, – CH_2Br), 3.25 (1.6 H, t, J 6.8, –CH_2I).

Quantitative solution fluorescence analysis of 7-amino-4-methylcoumarin A 10^{-4} M stock solution of 7-amino-4-methylcoumarin is prepared in DMF. From this stock solution, eight solutions at variable concentration in the $2\cdot10^{-8}$–10^{-7} M range are prepared by adding distilled water. The pH of all these solutions is adjusted to ca. 8 with 10^{-3} M Noah. The measured maximum emission intensities of these solutions ($\lambda_{ex} \sim 380$ nm, $\lambda_{em} \sim 440$ nm) show a linear dependence on coumarine concentration, as illustrated in **Fig.4.6**

Amide hydrolysis test in homogeneous aqueous solution - Among the three synthesised amides the most thermally stable compound **4a** amide was selected for the hydrolysis test in water. A 10^{-4} M stock solution of **4a** is prepared in DMF, because this compound is only sparingly soluble in neat water. This stock solution is diluted 1: 100 (v/v) with distilled water. To 3.5 cm^3 of the resulting solution 15 cm^3 of 0.1 M HCl is added. This solution is heated at 90 °C for 3 h. After cooling down to room temperature the pH is raised to ca. 8 with 0.1 M NaOH. The maximum emission of this solution, centred at 440 nm, is measured and compared with that of a standard aqueous solution of **5a** at the same concentration (ca. 10^{-7} M), same pH (ca. 8) and with the same proportions of DMF (0.1%) and NaCl (0.2% w/w). The resulting advancement of the hydrolysis reaction is ca. 90%.

Stability test of 7-amino-4-methylcoumarin ***5a*** *and 7-amino-4-trifluoromethyl coumarin* ***5b*** **-** A 10^{-6} M stock aqueous solution of **5a** at pH ca. 1 for HCl and containing 0.1% of DMF is prepared. A 15 cm^3 sample of this solution is alkalinised with 0.1 M NaOH till pH ca. 8 (solution A). An equivalent sample of the stock solution at pH ca. 1 is heated at 90 °C for 3 h. After cooling down to room temperature the pH of this solution is raised to ca. 8 with 0.1 M NaOH (solution B). The resulting maximum emission intensity, centred at 440 nm, of both A and B solutions is the same within the experimental error (6%). In contrast, the same test on **5b** indicates that it mostly decomposes under the hydrolysis reaction conditions.

4.2.2 Preparation of silicon surface

Silicon wafer samples with areas of ca. 2 cm^2 were first oxidised in 70% aqueous HNO_3 at 100 °C for 5 min, rinsed copiously with water and then etched with 50% aqueous HF for 5 min and rinsed with water again. After repeating this procedure for three times, the samples were dried under a stream of nitrogen and immediately used in the functionalization process.

Silicon functionalization -The samples were prepared following different routes. After functionalization the sample is cleaned by sonication in air four times with different solvents, for 5 min each (CH_2Cl_2, CH_3CN, H_2O, CH_3OH) and dried in a stream of nitrogen.

Thermal immobilisation. The silicon samples (p-Si) were functionalized in 0.08 M solution of the reactant to be anchored: with **1** or **2** in mesitylene at reflux (180 °C) for 2 h; with **4a** in mesitylene at reflux for 2 h or 4 h or in DMF at room temperature for 2 h, with **4b** in toluene at 100 °C for 1 h; with **8** in toluene at reflux (110 °C) for 2 h. The sample functionalized with **2** is subsequently hydrolyzed to the free acid form with *tert*-butoxide in DMSO,[8] before the amidation reaction.

Photoimmobilization. A freshly etched piece of silicon (p-Si(100) or n-Si(111)) is placed in a quartz tube, filled with N_2, containing neat **2** (~2 cm^3). The tube is stoppered and air-cooled while irradiated with the mercury lamp for 1 h at a power density of 95 mW cm^2. Before the coupling with **5**, the ester-terminated surface was converted to the corresponding carboxylic acid *via* hydrolysis, as described above.

Electrografting. The samples were prepared varying the reactant, with **1** or **3** or **6**, under a cathodic or anodic current through n-Si (111) and n-Si(100).

Condensation of 7-amino-4-methylcoumarin with the carboxylic acid terminated monolayer on silicon surfaces - The Si surface capped -COOH, is treated with isobutylchloroformiate and TEA in THF and **5a** in DMF under the same conditions as those adopted for the amide formation, in the homogeneous phase. Then, the sample is thoroughly cleaned by sonication with CH_2Cl_2 for 5 min and CH_3OH for a further 5 min.

Quantitative analysis of the monolayer anchored on Si substrate via amide hydrolysis - The Si sample, functionalized on the surface with the amide in one or two steps as described above, is treated with an aqueous solution of 0.1 M HCl (4 cm^3) containing 0.1% DMF at 90 °C for 3 h in a stoppered tube. After cooling down to room temperature, the sample is withdrawn and the pH of the solution is raised to ca. 8 with 0.5 M NaOH. The **5** amount in solution, resulting from the hydrolysis of the related amide, is determined by a fluorescence analysis. After making allowance for the solution volume and the sample area, the specific concentration of the monolayer is obtained. Resulting values of this quantity fall in the range $0.24–2.9 \cdot 10^{-10}$ mol cm^{-2} or $1.5–17.5 \cdot 10^{13}$ molecules cm^{-2}.

4.3 Results

Hydride terminated silicon surface (Si-H) - The Si-H surface was first characterized with AFM, XPS and static water contact angle measuments .

The AFM imaging show a low roughness **Fig.4.3**.

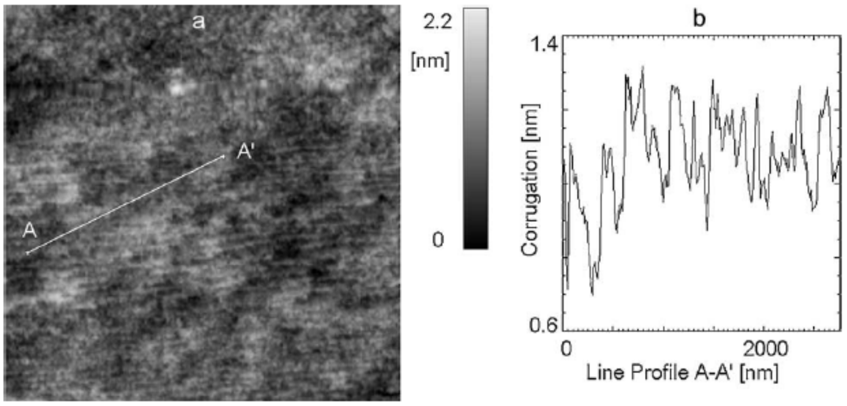

Fig.4.3 (a) AFM image (5 μm·x 5 μm) in a top-view representation, obtained in the constant force mode, on the Si-H substrate. The repulsive force applied to the sample was a few nanoNewtons from zero cantilever deflection. The grey scale varies from black for the deepest zones to white for the highest. (b) Corrugation along the AA' line.

As can be seen in **Fig.4.3a-b** the surface is very flat and homogeneous showing topographical variations of 0.3–0.4 nm

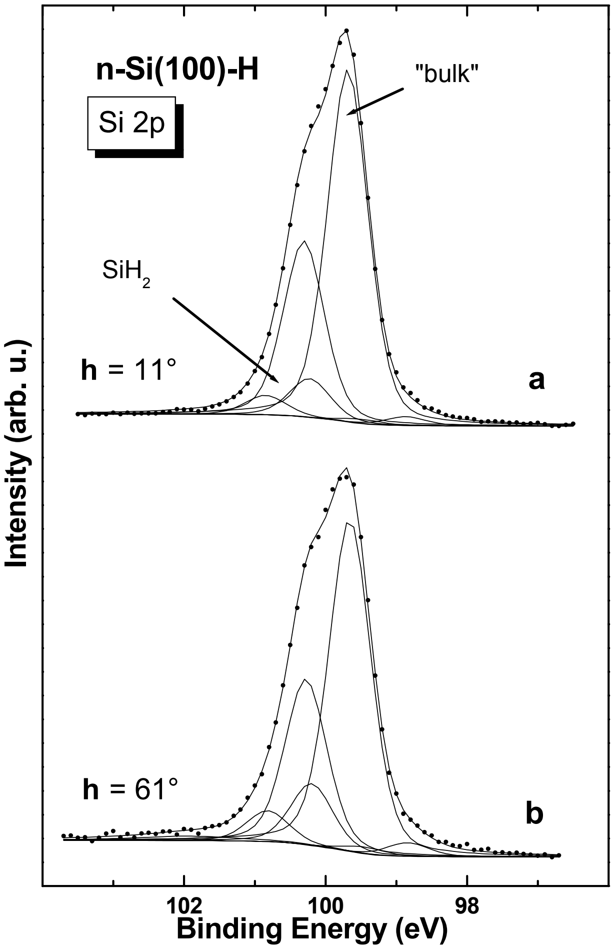

Fig.4.4 XPS spectra Si 2p (PE 10 eV) of Si(100)-H, at different take-off angle: (a) 11° and (b) 61°.

The XPS analysis shows the absence of silicon oxide. The bulk components and signals of surface bond are present. The literature reported that signal 2p of SiH_2 and SiH_3 have a chemical shift respectively at 0.2÷0.3 eV and 0.35÷0.6 eV higher binding energy (BE) than the signal of bulk. In the spectra there is a components at BE +0.55 eV respect to the component of bulk, that it has been assigned to SiH_2. It is important that the components of SiH_2 are more intens at higher *take-off* angle. (**Fig.4.4** compare a and b)

The water static contact angle values are reported in **Table 4.1**.

Surface	**Θ_{static}**
Si-H	78°±2°
Si/SiO_2	10°±2°

Table 4.1 Water Static Contact Angle values on Si-H and SiO_2 surfaces

In **Table 4.1** we show the water static contact angle of Si-H and that of oxidized silicon surface (Si/SiO_2). The latter surface was prepared and analysed expressly for comparison. The values reported are in accord with the literature data for a hydrophilic surface (Si/SiO_2, **17°)**[9] and for a clean hydrophobic surface (Si-H, 72°).[1]

Functionalization – Si-H surfaces have been further functionalized with carboxylic acid terminated monolayer. The concentration of the monolayers has been determined by the following stepwise procedure (**Fig.4.5**).

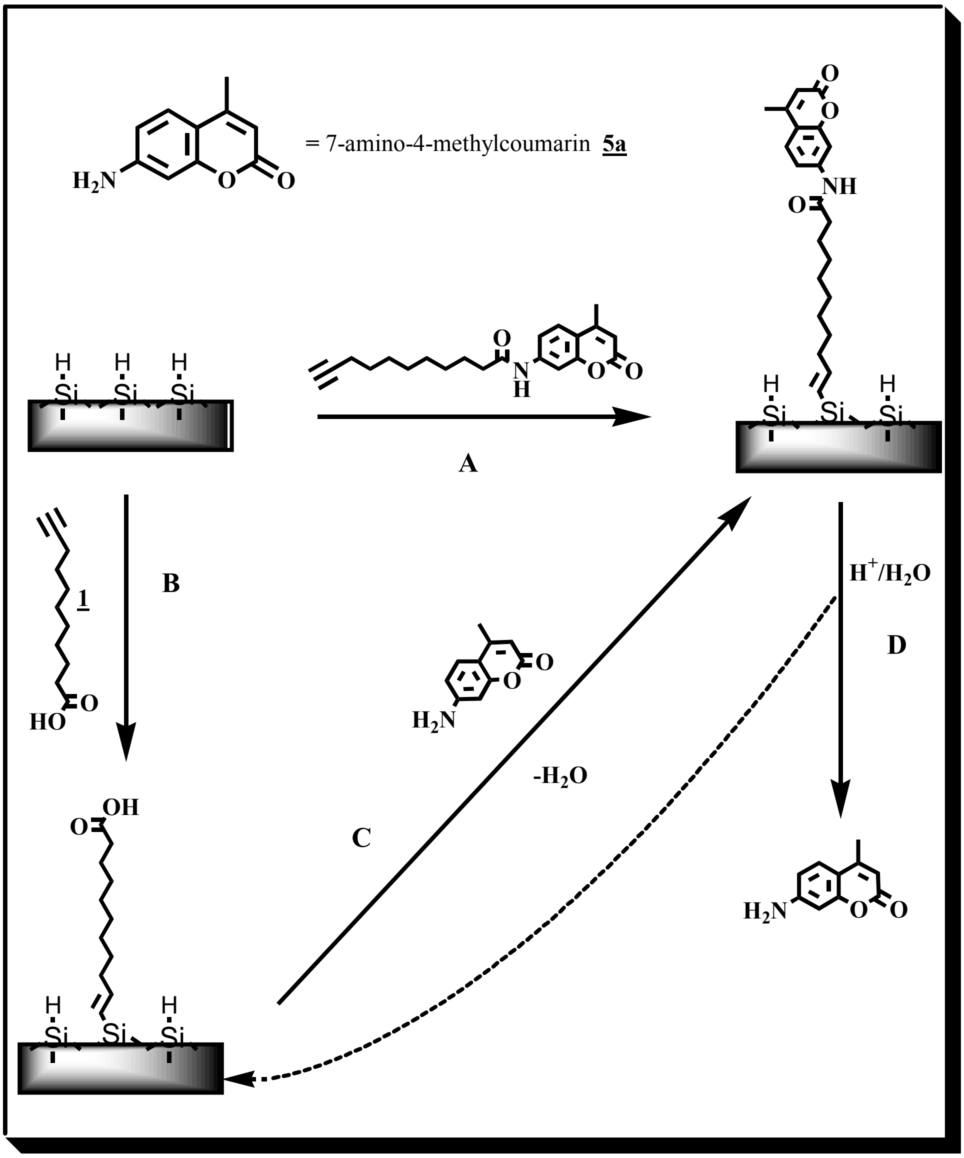

Fig.4.5 General procedure to anchor fluorescent probe to silicon surface

A fluorescent probe **5a** is covalently bonded to the –COOH terminated monolayer on the surface (step C), then the surface is intensely washed in order to remove any physisorbed species, finally the fluorophore is detached from the surface (step D) and determinated by a fluorescence analysis in solution. The efficiency of the surface washing treatment has been ascertained through several control experiments on various differently functionalized samples. As implied in this analytical procedure, also the yields of both the steps C and D had to be evaluated as reported below

Two amide-terminated monolayers on Si have been prepared (**Fig. 4.5**), *via* a thermal reaction by one-step (A) or two-step (B + C) procedure using **4** or **1**, respectively, as substrate. The resulting surface coverage concentrations are different in the two cases (entries 2 and 6 of **Table 4.2**) and the ratio of the corresponding values furnishes the yield of the amidation reaction in the heterogeneous phase (C): ~ 62%.

Fluorescence measurements - The fluorescence intensity of **5a** has been measured on several samples within the concentration range $2{\cdot}10^{-8} - 1{\cdot}10^{-7}$ M, where the **5a** concentration values of the current solutions, resulting from the hydrolysis of the surface amide terminated monolayers on Si fall. A simple linear relationship is observed when these measurement values are plotted against the fluorophore concentration.

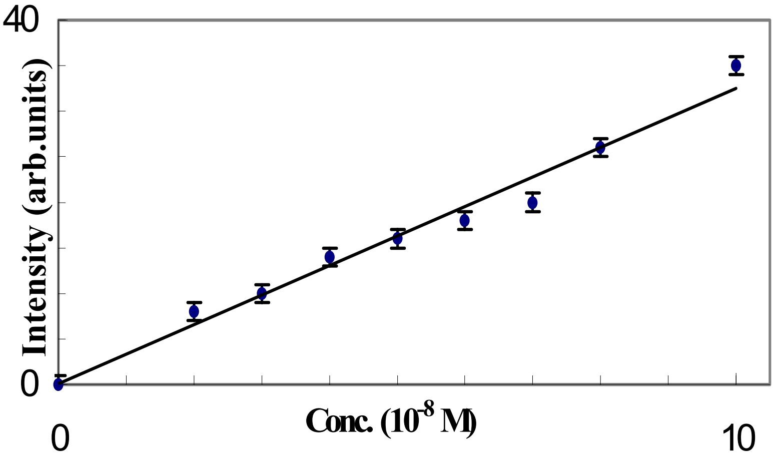

Fig.4.6 Dependence of the maximum intensity emission (λ_{em} 440 nm, λ_{exc} 380 nm) of AMC on its concentration in water with 0.1% DMF at pH 8. Volume of the sample cuvette 3 mL.

A least-squares fitting of the data, the origin included as an experimental point, produced a *y* intercept of 0.1154 and a correlation index of 0.9769 (**Fig. 4.6**). Using this calibration plot, the approximation on fluorophore determination is $\approx 0.6{\cdot}10^{-8}$ M and thus the limit of detection (LOD) of AMC in solution is $1.8{\cdot}10^{-8}$ M, equivalent to $5.5{\cdot}10^{-11}$ moles, taking into account the volume of the sample cuvette (3 mL). So, recalling that the maximum density of a monolayer (ML) formed by alkane-chain molecules on crystalline Si is $6.47{\cdot}10^{-10}$ moles cm^{-2},[10] for the amide-terminated monolayers anchored on a flat support a surface coverage concentrations lower than 0.1 ML may be detected with this method provided that the area of the support is larger than 1 cm^2 and the final solution after hydrolysis and pH adjustment has a total volume $\leq$3 mL.

Amide hydrolysis - The hydrolysis of the current amides can be easily followed in solution by monitoring the fluorescence of the resulting **5** given that these amides are much less fluorescent than **5** itself according to the literature.[11] So, the optimal experimental conditions were readily found in order to maximise the hydrolysis advancement (ca. 90%) without decomposing **5** (pH 1, 90 °C, 3 h). The same conditions were adopted in the heterogeneous hydrolysis reaction of the amide-terminated monolayers on Si (**Fig4.5**, step D). It is reasonable to assume that also in this case the hydrolysis is almost complete (ca. 90%) like in homogeneous solution, given that the amide bond to be hydrolysed is spaced enough from the surface by an alkane-chain molecule and neither the catalyst (H^+) nor the reactant (H_2O) are sterically demanding.[12]

Entry	Support	Reactant	Functionalization procedure	Concentration (10^{13} molecules/cm^2)
1	p-Si(100)	**4a**	RT x 1 h	2.50
2	p-Si(100)	**4a**	180 °C x 2h	5.54
3	p-Si(100)	**4a**	180 °C x 4h	12.64
4	n-Si(100)	**2**	UV, neat x 1h/hydrolysis/ amidation	4.31
5	p-Si(100)	**2**	UV, neat x 1h/hydrolysis/ amidation	2.27
6	p-Si(100)	**1**	180 °Cx 2h/ amidation	3.43
7	n-Si(111)	**3**	CEG/ amidation	4.28
8	n-S(111)	**6**	CEG/ amidation	10.23
9	n-Si (111)	**1**	CEG/ amidation	9.63
10	p-Si(100)	**1**	AEG/ amidation e	42.26
11	p-Si(100)	**8**	110 °C x 2 h	1.45
12	p-Si(100)	**2**	180 °C x 2h/hydrolysis/amidation	4.11
13	p-Si(100)	**4b**	100 °C x 1 h	---

Table 4.2 amide terminated monolayer concentration values x all the prepared samples

Functionalization of silicon surface

Thermal functionalization - The reactants **1**, **4a** and **8** were used in this functionalization process under the reaction conditions reported in the literature.[13] As expected, the surface coverage concentration depends on the time and temperature of the reaction. Accordingly, an increase of this quantity is observed increasing the temperature and/or the reaction time (see entries 1–3). The yield of the amide formation on the surface has been evaluated, carrying out the appropriate experiment (entry 6) and comparison (with entry 2): 3.43/5.54 ~ 62%. In addition, we ascertained whether it is convenient to protect the –COOH group in this functionalization process when using the reactant **1**, in order to prevent the silyl-ester formation after reaction with adventitious Si–OH groups on the silicon surface.[3] To this end, we carried out a control experiment using the acid-methyl ester **2**. On comparison of the result of this experiment (entry 12) with the analogous one using reactant **1** (entry 2), it is evident that this protection is not convenient. These findings are in accord with the conclusion from a recent report on the thermal functionalization of silicon surface with **1** where it is claimed that the acid terminal group is not affected by the thermal chemical process.[14] Finally, we ascertained the thermal functionalization with react **8** (entry 11) is little efficient as expected.

Photoimmobilization - This functionalization has been carried out with neat **2**, *i.e.* with an acid-methyl ester, liquid at room temperature, according to the observations by some authors who performed a similar experiment with ω-undecenoic acid as reactant.[15] Indeed, these authors converted the acid into the corresponding ethyl ester before the reaction with the silicon surface in order to avoid nucleophilic attack by –COOH groups on light-induced positively charged silicon sites on the surface creating Si-ester species. Then, after running the various heterogeneous reactions, the amide monolayer is measured (entries 4 and 5). It is particularly interesting to note that following this procedure n-Si (111) is functionalized to a larger extent than p-Si (100).

Electrochemical functionalization - As reported in the literature, the functionalization of a flat silicon surface, without damaging it, can be performed cathodically (CEG) with a terminal alkyne[16]or a halide[17] as reactant. Actually, we prepared four samples with the results summarised in **Table 4.2** (entries 7–10). Entry 10 is concerned with the anodic electrografting which inevitably damages the silicon surface. In fact, the resulting surface is rather rough so that it is not interesting for our pourposes. Moreover, doing the appropriate control experiment, we ascertained that in the CEG process, the carboxylic proton reduction, if any, does not lower the yield of the surface coverage.

XPS measurements - We used XPS for two distinct purposes. First, we aimed to determine the extent of surface oxidation of silicon on changing the surface functionalization method. The results of this investigation are reported in **Fig. 4.7**, where the Si 2p XPS peaks, after different sample preparations, are compared.

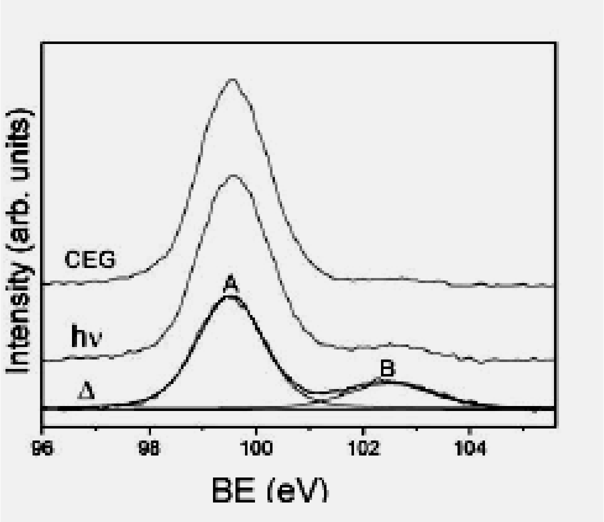

Fig.4.7 Comparison of Si 2p XP spectra of Si (100) surfaces, functionalised thermally with the acid **1** (Δ), photochemically with the ester **2** (hν) and electrochemically with the acid **1** (CEG).

The A band, centred at 99.5 eV, and B band, centred at 102.4 eV, are due to elemental silicon and oxidised silicon atoms on the surface, respectively. In this way, the relative amount of oxidised silicon present in the three differently functionalized samples can be evaluated: 20%, Δ; 7%, hν and 2.4%, CEG.

Secondly, we tried to investigate the surface coverage of the samples after their functionalization and hydrolysis independently of the method based on the attachment and detachment of a fluorescent probe. To this end, we sought to mark the substrate with a XPS sensitive label. For these reasons we prepared fluorine containing monolayers on Si surfaces using as reactant the trifluoromethyl derivative amides **4b**(entries 12). The F 1s XPS spectra of these monolayers, as prepared and after hydrolysis, have been measured (**Fig. 4.8**). The peak fitting showed that the F 1s spectra, as prepared (**Fig. 4.8**, spectra A), are composed of two components: fluorine in ionic bond at 685.9 eV, arising from HF contamination, and fluorine in covalent bond at 688.9 eV.[18] The component related to the ionic bond disappears after hydrolysis and it is not important for the discussion of this work. Concerning the covalent bond component, it is evident that hydrolysis is not complete (**Fig4.8**, spectra B), in qualitative agreement with the hydrolysis experiment of amide **4a** in bulk solution (see Experimental). More precisely, the fractional amount of fluorinated coumarin, removed from the support surface after hydrolysis, as evaluated from the F/Si atomic ratio, is 55% for Si.

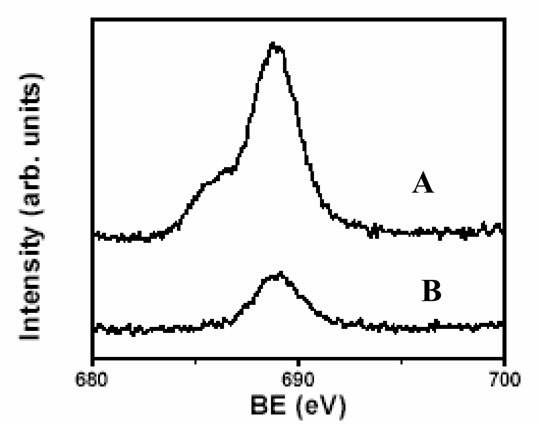

Fig.4.8 Fluorine (1s) XP spectra of Si(100) surfaces functionalized with **4b** as prepared (A) and after hydrolysis (B).

AFM investigations - Several Si samples, differently surface functionalized, were examined. **Fig. 4.9a** (5 μm by 5 μm) and **b** show, image and profile, after thermal functionalization with amide **4**.[19] The corrugation changes appreciably with respect to the bare substrate giving rise to topographical variations of 1–2 nm.

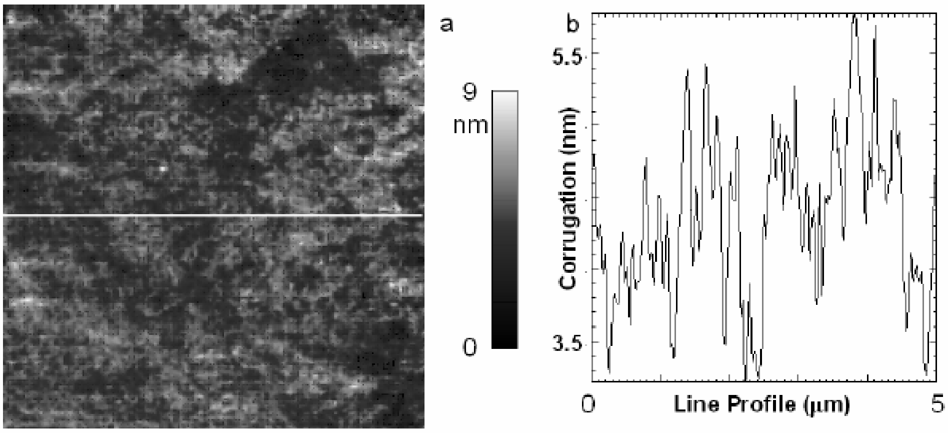

Fig.4.9 (a) AFM image (5 μm by 5 μm) in a top-view representation, obtained in the constant force mode, on the Si substrate, after thermal functionalization with amide **4a**. The corrugation of the white line trace is shown in (b)

From these images we can say that the deposited material, amide **4a**, on clean Si substrates is covering all the surface in a very homogeneous way.

Moreover, the silicon samples, functionalized with the carboxylic acid **1** or the methyl ester **3** by the three different current wet-chemistry methods, have been investigated. **Figs. 4.10–12** show AFM topography of these three samples.

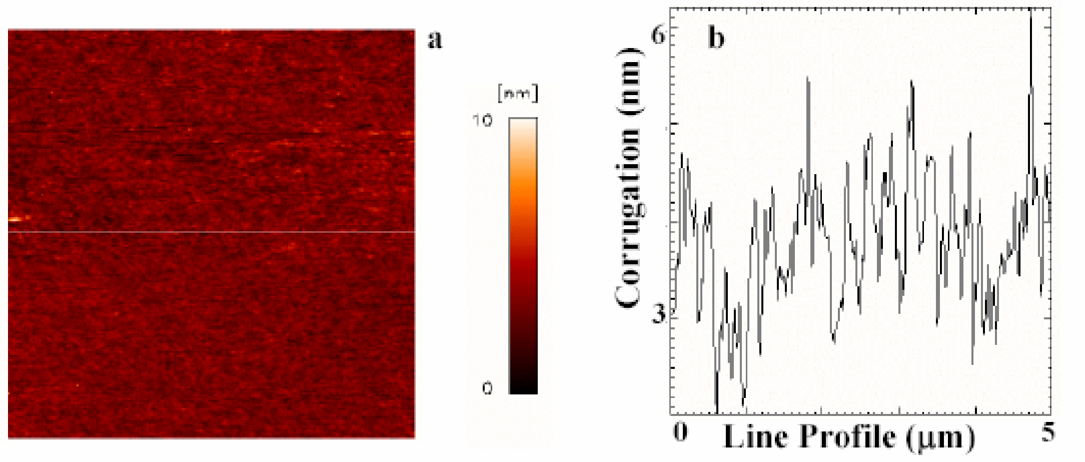

Fig.4.10 (a) AFM image (5 µm by 5 µm) on Si substrate functionalised electrochemically with the acid **1** using charge= 120 mc. The corrugation of the white line trace is shown in (b).

Cross sections, referring to the line drawn on the images, are reported as well, in order to describe the typical corrugation of the observed structures. In morphological terms, every sample was found to be quite homogeneous all over the observed areas in such a way that the reported images can be considered representative of the sample itself.

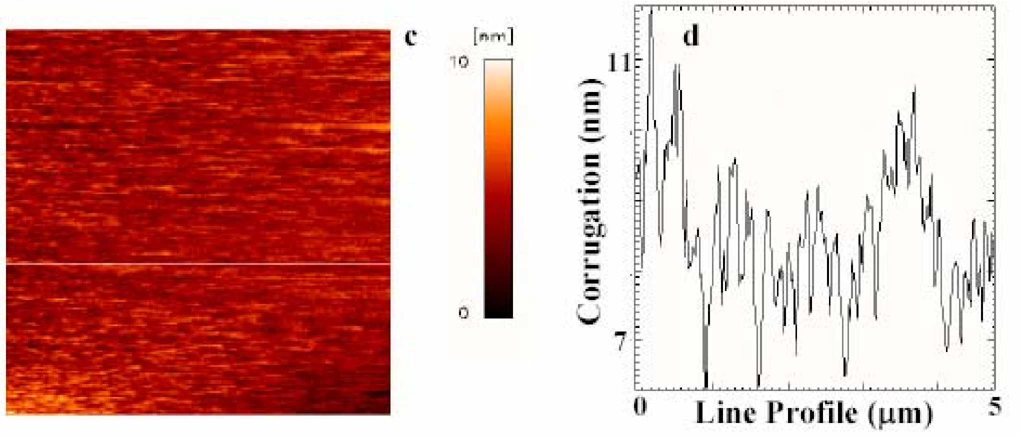

Fig.4.11 (a) AFM image (5 µm by 5 µm) on Si substrate functionalised thermally with the ester **2**. The corrugation of the white line trace is shown in (b).

The analysis of the AFM images, collected with a noise of a few angstrom in the three samples, revealed characteristic corrugations ranging between 1 and 2 nm.

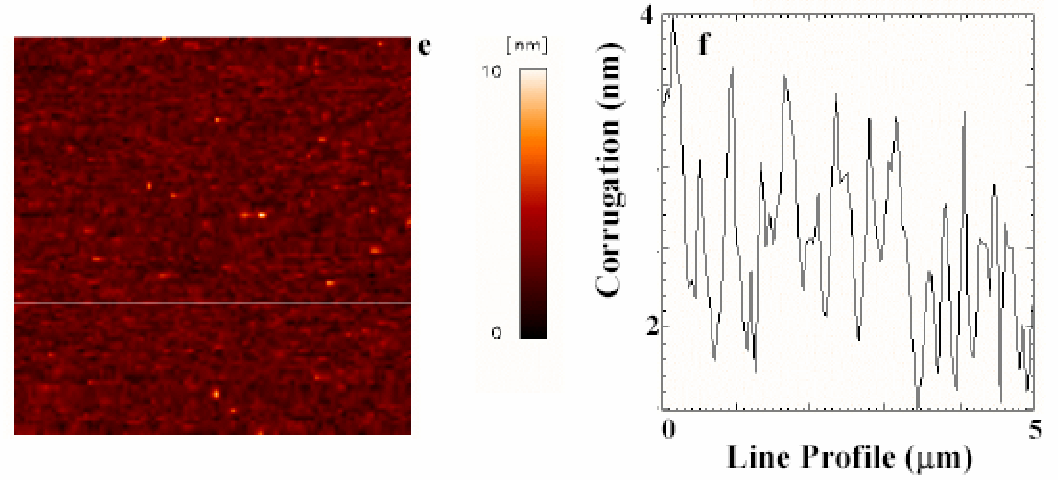

Fig.4.12 (a) AFM image (5 μm by 5 μm) on Si substrate functionalised photochemically with the ester **2**. The corrugation of the white line trace is shown in (b).

Such corrugation, well above the expected value on the bare silicon substrate, is consistent with the hypothesis of a single molecular monolayer covalently bonded to the substrate.

Surface	**Θ_{static}**
Si/SiO_2	10°±2°
Si-H	78°±2°
-COOH	58°±2°

Table 4.3 Water Static Contact angle measurements average of 5 readings

The static contact angle value is in accord with the literature[4] for the silicon surface functionalized with carboxylic acid. It is in between the corresponding values for oxidied and hydrogenated surface.

The monolayer concentration of the current samples, expressed as fractional monolayer [ML], is obtained after normalising the corresponding values reported in **Table 4.2** (molecules cm^{-2}) to the molecule number density for coverage of unity by alkane-chain molecules on a flat support: $\sim 4 \cdot 10^{14}$ molecules cm^{-2}.[10] Then, all the values are 11% increased taking into account the percentage of **5a** detachment from the surface after hydrolysis (ca. 90%). In the following, the amide- and carboxylic acid-terminated monolayers are examined separately.

Amide terminated monolayer concentration - These values are reported in **Fig.4.13**.

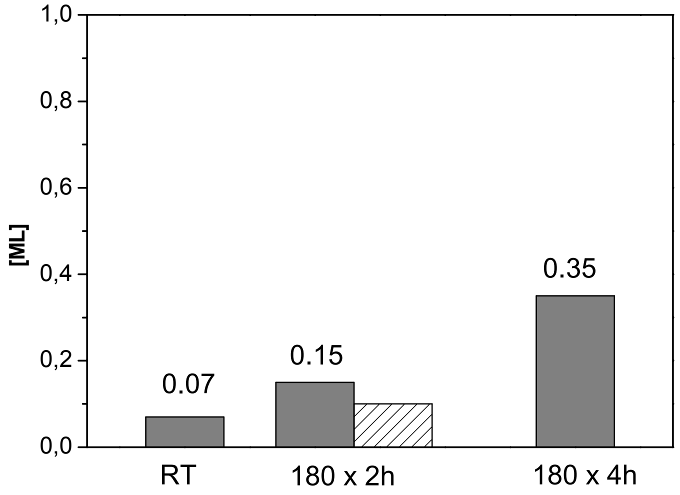

Fig.4.13 One-step (uniform bar) and two-step (patterned bar) amide terminated monolayer concentration, on silicon surfaces, expressed as monolayer fraction [ML]. The [ML] values from left to right are calculated (see text) from entries 1, 2, 6 and 3, respectively, of **Table 4.2**.

We note that submonolayers are formed in every case and, on Si, [ML] increases on increasing the time and/or the temperature of the functionalization reaction. In two cases, the same monolayer was formed through different routes: A and B + C (**Fig.4.6**), represented in **Fig.4.13** by uniform and patterned bars, respectively. The ratio of the corresponding values furnishes the yields of the amidation reactions in the heterogeneous phase (C), which is 62%. Unfortunately, it was not possible to dose the surface density of the fluorine-containing amide terminated monolayers with the method based on water solution fluorescence measurements, because the fluorinated coumarin **5b** is not stable on prolonged heating in water.

Carboxylic acid terminated monolayer concentration - The carboxylic acid terminated monolayer concentrations can be calculated from the related, two-step formed, amide-terminated monolayer values (**Table 4.2**) after correction (increasing) for the yield of amidation reaction in the heterogeneous phase. These values are reported in **Fig.4.14**. Interestingly, as apparent from these data, silicon is best functionalized via cathodic electro-grafting (CEG). Moreover, it is worth to recall that during CEG silicon is normally protected against oxide (SiO_2) growth, which is instead enhanced in photochemical and mostly in thermal processes, as shown by the above XPS data.

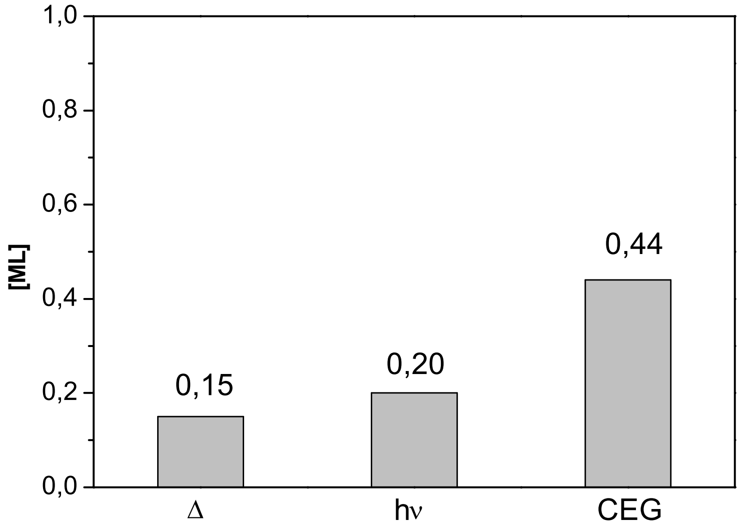

Fig.4.14 Carboxylic acid terminated monolayer concentration, on silicon surfaces, expressed as monolayer fraction [ML], for different functionalization methods: thermal (Δ), photochemical (hν), cathodic electrografting (CEG). The [ML] values from left to right are calculated (see text) from entries 6, 4 and 8, respectively, of **Table 4.2**.

---

[1] Z. Lin, T. Strother, W. Cai, X. Cao, L. M. Smith, R. J. Hamers, *Langmuir*, **2002**, *18*, 788.

[2] 4 R. Boukherroub D. D. M. Wayner, *J. Am. Chem. Soc.*, **1999**, *121*, 11513.

[3] (a) A. B. Sieval, A. L. Demirel, J. W. M. Nissink, M. R. Linford, J. H. van der Mass, W. H. de Jeu, H. Zuilhof E. J. R. Sudhölter, *Langmuir*, **1998**, *14*, 1759. (b) T. Strother, W. Cai, X. Zhao, R. J. Hamers L. M. Smith, *J. Am. Chem. Soc.*, **2000**, *122*, 1205.

[4] T. Strother, R. J. Hamers and L. M. Smith*, Nucleic Acids Res.*, **2000**, *28*, 3535.

[5] G. Binning, C. F. Quate C. H. Gerber, *Phys. Rev. Lett.*, **1986**, *56*, 930.

[6] (a) H. Y. Nie, T. Shimizu H. Tokumoto, *J. Vac. Sci. Technol. B*, **1994**, *12*, 1843. (b) S. M. Hues, C. F. Draper R. J. Colton, *J. Vac. Sci. Technol. B*, **1994**, *12*, 2211

[7] L. F. Fieser and M. Fieser, *Reagents for Organic Synthesis*, Wiley, New York, 1967, vol. 1, p. 364.

[8] P.G. Gassman, W.N. Schenk, *J. Org. Chem.*, **1977**, *42*, 918.

[9] Y. Ryu, K. Shin, E. Drockenmuller, C. J. Hawker, T. P. Russell, *Nature*, **2005**, *308*, 236

[10] M.R. Linford, P. Fenter, P.M. Eisenberger C.E.D. Chidsey, *J. Am. Chem. Soc.*, **1995**, *117*, 3145.

[11] Y. Kanaoka, T. Takahashi, H. Nakayama, T. Ueno, T. Sekine, *Chem. Pharm. Bull.*, **1982**, *30*, 1485.

[12] A. D. Pomogailo, *Catalysis by Polymer-immobilized Metal Complexes*, Gordon and Breach Science Publishers, Amsterdam, 1998, p. 18.

[13] (a) E. J. Bateman, R. D. Eagling, D. R. Worral, B. R. Horrocks,A. Houlton, *Angew. Chem.*, Int. Ed., **1998**, *37*, 2683; A. B. Sieval, R. Opitz, H. P. A. Maas, G. M. Schoeman, G. Meijer, F. J. Vergeldt, H. Zuilhof, E. J. R. Sudhölter, *Langmuir*, **2000**, *16*, 10359; (c) G. F. Cerofolini, C. Galati, S. Reina and L. Renna, *Mater. Sci. Eng. C*, **2003**, *23*, 253.

[14] R. Boukherroub, J. T. Wojtyk, D. D. M. Wayner D. J. Lockwood, *J. Electrochem. Soc*, **2002**, *149*, H59–H63.

---

[15] T. Strother, W. Cai, X. Zhao, R. J. Hamers, L. M. Smith, *J. Am. Chem. Soc.*, **2000**, *122*, 1205.

[16] E. G. Robin, M. P. Stewart, J. Buriak, *Chem. Commun.*, **1999**, 2479.

[17] C. Gurtner, A. W. Wun, M. J. Sailor, *Angew. Chem.*, Int. Ed., **1999**, *38*, 1966.

[18] C. D. Wagner, W. M. Riggs, J. F. Moulder, *Handbook of X-Ray Photoelectron Spectroscopy*, Eden Prairie, MN, 1995, p. 42.

[19] A. Cricenti, G. Longo, M. Luce, R. Generosi, P. Perfetti, D. Vobornik, G. Margaritondo, P. Thielen, J. S. Sanghera, I. D. Aggarwal, J. K. Miller, N. H. Tolk, D. W. Piston, F. Cattaruzza, A. Flamini, T. Prosperi, A. Mezzi, *Surf. Sci.*, **2003**, *544*, 51.

CHAPTER 5

CONTROLLED LOADING OF OLIGODEOXYRIBONUCLEOTIDE MONOLAYERS ONTO UNOXYDISED CRYSTALLINE SILICON

5.1 Introduction

In nanobiotechnology numerous materials, such as gold,[1,2,3,4] glass,[5,6] quartz,[7] metal oxides,[8] oxidized silicon,[9] organic polymers,[10] harbouring oligodeoxyribonucleotides (ODNs) as probes, have been much more considered for the preparation of biosensors. While related publications on unoxydised crystalline silicon are relatively few[11] and do not adequately address the following fundamental issues. First, the formation of the layer was performed through several steps in most reported cases,[11a-d,f] one step being an alkaline hydrolysis,[11b,d] which inevitably damages the silicon surface.[13a] Second, the quality of the cross-linking layer, spacing out the silicon surface and supporting the ODN, was controlled and optimised only in a few cases,[11c,f] although this feature critically influences reproducibility in using the resulting materials.[6a,7c,9a,10f] Third, the probe concentration on the surface was usually not quantified, even though it's well-known that this concentration should be kept below a limiting value: $2 \cdot 10^{12}$ strands/cm^2 according to some reports,[1b,3b,c,4c] or $4\text{-}6 \cdot 10^{12}$ strands/cm^2 according to other reports,[1a,2b,c] for attaining the maximum hybridisation efficiency and thus for attaining the maximum sensitivity and selectivity; in fact only the hybridised target-ODN concentration was commonly reported.[11a-c] Fourth, the accuracy of this latter determination, achieved by solid-state fluorescence microscopy[11a,b] and by electrochemistry with an external probe,[11c] was rather low that the authors themselves write of "approximate, rough values", without giving the corresponding estimated standard deviations (ESD).

In **Fig.5.1** is outlined our work, addressing the four points cited above: as reported in Chapter 4 we have functionalised unoxydised crystalline silicon with 10-undecynoic acid (Si ├COOH) with a single step procedure, obtaining a controlled monolayer of the acid. On this surface we have anchored a fluorescent-ssODN, verifying the loading upon digestion with a DNase. Alternatively, this anchored ODN was considered as a probe and hybridised with a complementary, fluorescent-ssODN, which, after repeated washings, was subsequently freed through denaturation and measured.

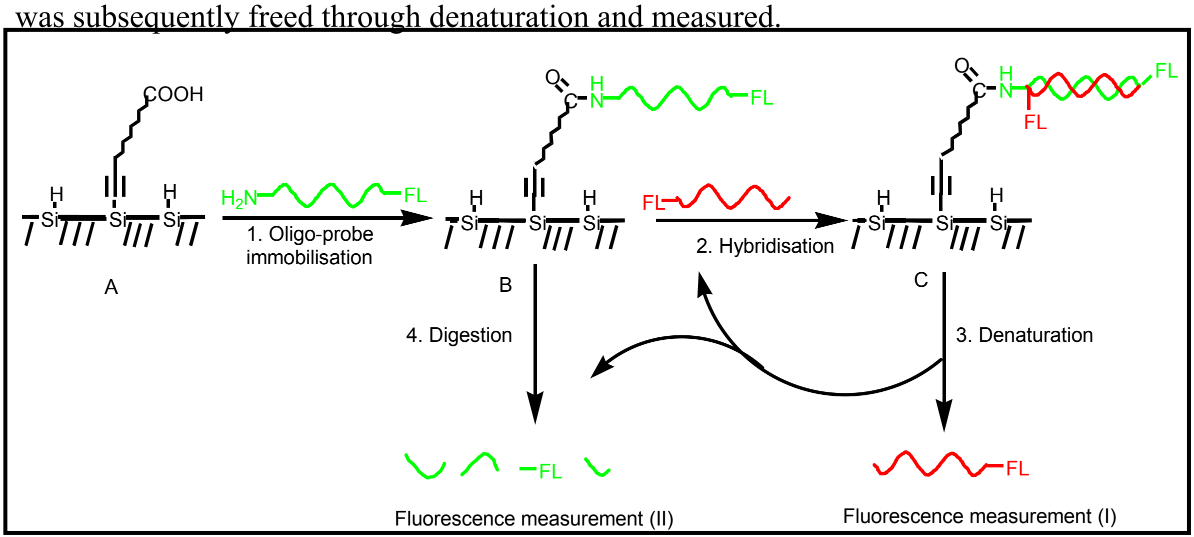
COOH
H
Si
A
H₂N
FL
1. Oligo-probe immobilisation
O
C
N
B
2. Hybridisation
C
3. Denaturation
4. Digestion
Fluorescence measurement (II)
Fluorescence measurement (I)

Fig.5. 1 Overall procedure.

The ODN linked on the surface has, then, been evaluated as before to, finally, estimate the hybridisation efficiency. The whole process was also monitored in parallel by Atomic Force Microscopy (AFM).

5.2 Experimental

5.2.1 Preparation of ODNs

The ODNs (**1-8**, **Table 5.1**) were prepared, at the 1 µmole scale and, having used Tac-protected dC (Proligo), were cleaved from the solid support by a mixture of ammonia and methylamine (AMA, Beckmann) in 10 min at r.t, then the solution was heated for 10 min at 55°C. After SpeedVac removal of AMA the samples were dissolved in triethylammonium acetate 0.1 M, pH 7.0 buffer (TEAA) and purified on an HPLC column Vydac C18, 300 Å, 5µ, 50 x 22 mm, eluted at a flow-rate of 6 mL/min with a linear gradient 3-45% MeCN in TEAA 0.1 M, pH 7.0, in 20 min. The ODNs were further purified by HPLC on a SAX Dionex Nucleopack100, 250 x 22 mm column, with a slightly concave gradient 10-30% of $NaClO_4$ 0.5 M in TrisHCl 25 mM buffer, pH 8, in 15 min, at a flow-rate 9.0 ml/min, then lyophilized and desalted on the Vydac column as above, but replacing TEAA with water. The ODNs were analysed on a SAX Dionex Nucleopack100, 250 x 4 mm column, with the same gradient as above, at a flow-rate 1.5 ml/min. The ssODNs were also analysed by PAGE on 15% polyacrylamide, 7 M urea gels (1 mm), containing 50 mM Tris-borate pH 8.0, 0.1 mM EDTA buffer (Sigma), staining with ethidium bromide. The dsODNs were analysed both by HPLC and PAGE under analogous conditions as above, but omitting urea in PAGE.

1	Fluorescein-5'-dA$_{20}$-3'-Hexyl-NH$_2$
2	Fluorescein-5'-dT$_{20}$-3'-Hexyl-NH$_2$
3	Fluorescein-5'-dA$_{20}$-3'
4	Fluorescein-5'-dT$_{20}$-3'
5	Fluorescein-5'-d(GCC TGG CTA GGT GAC GAG CT) -3'-Hexyl-NH$_2$
6	Fluorescein-5'-d(AGC TCG TCA CCT AGC CAG GC)-3'
7	Fluorescein-5'-d(GCA TCA TAC GAT ATC CAT GAC GAG TGA CCG TCG AGA GGT CAC ACG AGT CTG)-3'-Hexyl-NH$_2$
8	Fluorescein-5'-d(GTC ATG GAT ATC GTA TGA TGC)-3'

Table 5.1. List of oligodeoxynucleotides

Immobilization of ODNs - Unoxydised, crystalline silicon samples, pre-functionalised with undecynoic acid, were immersed in 4 ml phospate buffer (Na2HPO4/NaH2PO4, pH 6.84) containing variable amount of ODN (ca 30-0.5 μM), EDAC 0.026 M and NHS 0.0017 M and let react overnight at room temperature. Afterwards, the solution was removed and silicon was cleaned by sonicating two times for 20 min and two times for 20 min with NaH2PO4 20 mM, NaCl 300 mM, EDTA 2 mM, SDS 7 mM (SPPE), and then rinsed thoroughly with SPPE at 60 °C until the discarded solution was no longer fluorescent. The incubation time proved suitable to attain the thermodynamic equilibrium of the loading onto the Si├COOH substrate. Different surface loading values of ODN were obtained depending on the ODN concentration in solution (**Table 5.2**).

ODN concentration in solution (μM)	**ODN density on silicon surface (10^{12} strands/cm^2)**	**Hybridization efficiency[a] %**
27.135	8.10	40
13.567	9.44	73
2.714	6.54	92
0.543	5.64	100

Table 5.2. Density of the ODN-probe **2** immobilised on the silicon surface (1.5 cm^2 exposed area) as function of its concentration in solution. (Reaction conditions: 4 ml phosphate buffer plus EDAC 0.026 M and NHS 0.0017 M; overnight; room temperature).

[a] After hybridisation, denaturation and fluorescence measurements in solution (see text).

Fluorescence measurement calibration - Given the fact that the fluorescence quantum yield of fluorescein is dependent on the substrate to which it is bound,[12] then, for each fluorescein labelled ODN used in this study (1-8, **Table 5.1**), the corresponding fluorescence calibration plot was determined employing the same ODN as standard. In each case, the fluorescence intensity (λex = 492 nm, λem = 520 nm) was measured twice on five samples, from a 10-4 M stock solution prepared in the digestion buffer (TRIS-HCl) or 7 M urea solution, diluted up to 0.5 - 4.0·10-9 M, i. e. the solution composition and the expected range of measurement. Two typical, slightly different trends, namely of ODN 2 and 3, in TRIS-HCl buffer and 7 M urea respectively, are reported here (**Fig.5.2**).

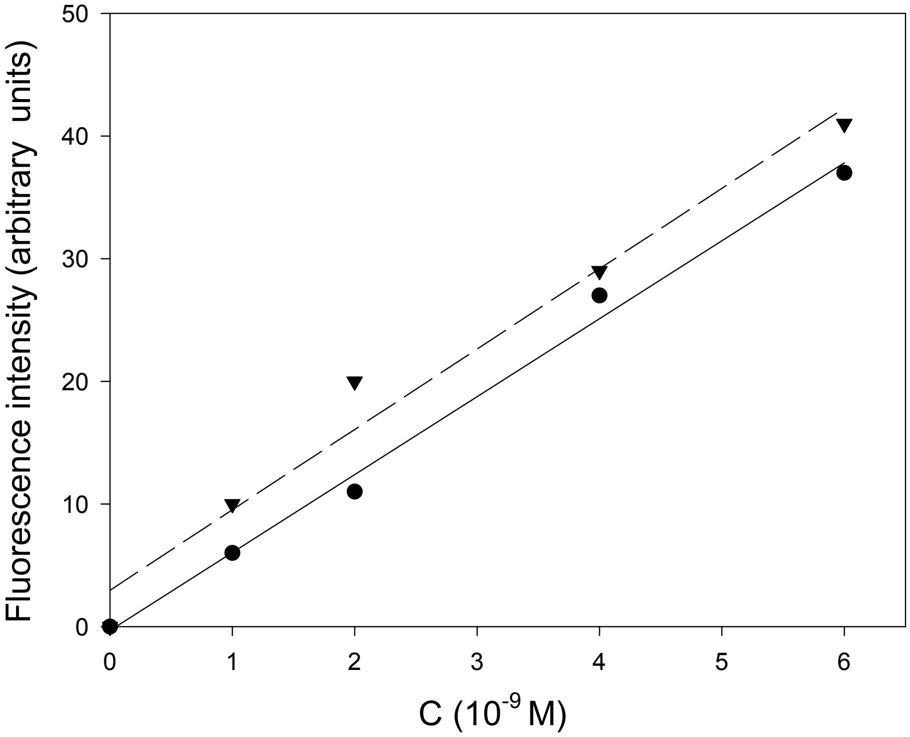

Fig.5.2 Dependence of the maximum intensity emission (λem = 520 nm, λex = 492 nm) of ODN Fluorescein-5'-dT20-3'-Hexyl-NH2 on its concentration in TRIS-HCl buffer (——, •) and of ODN Fluorescein-5'-dA20-3' in urea 7 M (----, ▼)

They are both linear, expressed by the equations -0.32+6.35(x) and 2.96+6.55(x), with associated correlation indexes 0.9744 and 0.9933, resulted by application of least-squares fitting, including the origin as an experimental point. Using these calibration plots, the approximation on fluorescein determination is ~$0.10 \cdot 10^{-9}$ M, and thus the limit of detection of fluorescein in solution is ~$0.30 \cdot 10^{-9}$ M, equivalent to $1.2 \cdot 10^{-12}$ moles, for a measurement volume of 4 ml. By considering that such two-dimensional ODN-monolayers, fully covering the planar support, have a density of $6 \cdot 10^{-11}$ moles/cm^2,[13] this method allows to detect a submonolayer lower than 2.0%, provided that the area of the functionalised silicon surface is ≥ 1.0 cm^2 and the volume of the solution is ≤ 4 ml.

Evaluation of the anchored ODNs - The enzymatic degradation of the probe-ODNs present on the silicon surface was accomplished by immersing the sample in 4 ml of KH_2PO_4 10 mM, 10 mM $MgCl_2$-$6H_2O$, pH 7.0, adding 4 mU of Phosphodiesterase I, leaving for 6-24 h at 40 °C, following digestion kinetics up to apparent completion through fluorescence measurements. The results are reported in **Fig.5.7**

Tm measurements - The ability to hybridise of the free, modified complementary ssODNs (**1**+**4**, **2**+**3**, **5**+**6** and **7**+**8**) was monitored by heating the appropriate mixtures (µM) in NaH_2PO_4 10mM, NaCl 100 mM, EDTA 0.1 mM, pH 7.2, at 95 °C for 2 min and allowing them to reach slowly r.t. Thermal denaturation curves were then obtained by monitoring the absorbance of the pre-hybridised ODNs at 260 nm as a function of temperature with a Perkin-Elmer 330 spectrometer, equipped with a Peltier temperature control accessory, in a stoppered 1 cm path length couvette. A ramp rate of 1 °C/min with a hold time of 1 min was used over the range 25-85 °C. T_m values of 44.6 °C (see **Fig.5.3**)for both **1**+**4** and **2**+**3**, and 66.9 °C for **6**+**7** were estimated from the inflection points of the curves obtained by plotting the collected data of absorbance versus temperature. The hybrid **8**+**9** did not show any definite inflection point, although producing a continuous increase of absorbance upon heating.

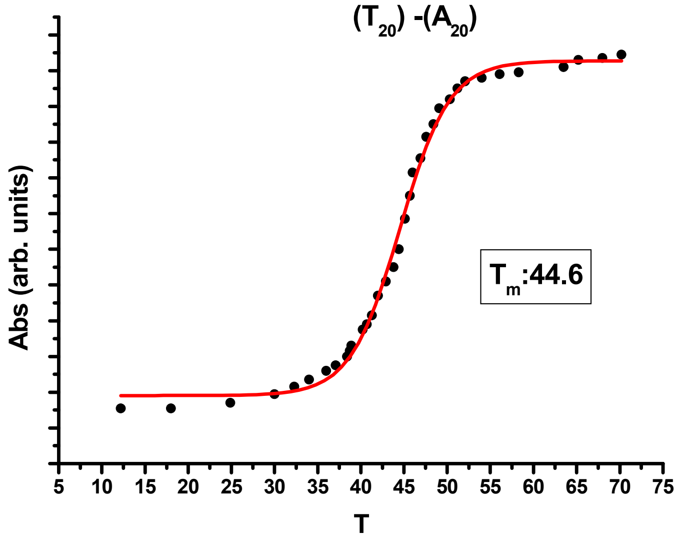

Fig.5.3 Thermal denaturation curves T_{20}- A_{20}

Evaluation of on-surface hybridisation - The surface, derivatized with either 1, 2, 5 or 7 ODN, was immersed into 4 ml of hybridisation solution of 4 (16.281 μM), 3 (9.369 μM), 6 (13.716 μM), or 9 (12.282 μM) respectively. The system was then heated at 90 °C for 5 min, slowly let cool down to room temperature, and left for 1 h at 5 °C. Afterwards the solution was removed, the surface was repeatedly soaked into a solution of hybridisation buffer and then two times for 5 min in SPPE at room temperature, until the discarded solution was no longer fluorescent, in order to remove all non-specifically adsorbed ODN. Afterwards, denaturation of the hybrid was accomplished by immersing the sample in 4 ml of urea 7 M at 90 °C for 5 min. The solution was removed while still hot, cooled down to room temperature and analysed through fluorescence measurements. The repetition of the procedure produced no additional fluorescence. The sample was then addressed to the evaluation of ODN loading. Furthermore, the minimum amount of ODN-target in solution, which can be detected within the dynamic range accessible with this method, was determined. To this end, six samples with immobilized ODN-probe 2 at almost the same surface density (5.64 - 5.87·1012 strands/cm2) were prepared and hybridized with the ODN-target 3 at a variable solution concentration (9.369-0.312 μM). The obtained results are reported in **Table 5.3**.

ODN concentration in solution (μM)	**ODN density on silicon surface (10^{12} strands/cm^2)**
9.369	5.63
3.123	2.39
1.874	2.82
1.615	2.17
0.625	2.39
0.312	1.95

Table 5.3. Density of the ODN-target **3** hybridized [a] with the ODN-probe **2** immobilized on the silicon surface of 1.5 cm^2 exposed area, [b] as function of its concentration in solution.

[a] Reaction conditions: 4 ml hybridization buffer, at 90 °C for 5 min and then at 5 °C for 1 h (see Experimental). [b]ODN-probe **2** density on silicon surface for the various samples is nearly constant: 5.64 - 5.87·10^{12} strands/cm^2.

5.2.2 AFM imaging

AFM images were taken in different areas of every sample in order to characterize the quality of each step of the procedure, either in the contact or tapping mode. Unlike the conventional optical or electronic microscopes, AFM allows high resolution imaging while requiring almost no sample preparation. The measurements were performed in air, at room temperature and constant 30% relative humidity. No noise filter was applied to the raw data which were treated by only a background subtraction and, when necessary, a plane alignment. In the contact mode, the microscope works in the weak repulsive regime (interaction between tip and sample <1 nN) allowing high-resolution imaging. The images of the 10-undecynoic acid layers were taken in this way (**Fig.5.4**).

The lateral scanning motion of the tip in the contact mode causes shear forces that can deform or even destroy the surface of soft samples, especially biological systems. These shear forces can scratch molecules from the samples and these particles can stick to the tip, thus damaging the samples and reducing the resolution of the measurement. Since ODNs are very soft molecules, they can be deformed or damaged by the shear forces typical of a contact-mode AFM and can stick to any probe-tip that comes to a too high interaction with the sample.[14] Thus the ideal work regime for the analysis of the ODN covered samples is the intermittent contact mode AFM (Tapping mode AFM[15]) In this modality, the tip oscillates on the sample with a mean interaction during a complete oscillation in the order of tens of pN, while the maximum interaction (still below 1 nN) is present only for a very small fraction of the time per oscillation and the lateral forces are strongly decreased. This allows a weak interaction with the sample, while maintaining a good lateral resolution, that depends on the choice of the tip in use.

In this work we have selected two kind of tips: standard tips with an apical radius of less than 30 nm, which have been used for most AFM contact and tapping mode images, and “super-tips” with an apical radius of less than 2 nm, which were used to determine the influence of the tip apical radius in the determination of the lateral dimensions of the imaged ODN molecules. These ultra-small tips have the advantage of delivering a high resolution imaging but introduce a larger deformation on the sample: the same force applied on a smaller area produces a higher pressure.

5.3 Results and Discussion

To produce a good DNA biosensor, it is necessary that the sensor material evidences two specific relevant properties: (i) the crosslinking layer between the surface and the ODN (the undecynoic acid layer on silicon in our case) should be deposited as a uniform monolayer and (ii) the surface density of the immobilized ODN should be so high as to ensure the highest sensitivity in the molecular recognition event without causing, at the same time, any risk of steric hindrance in the formation of double strands on the surface. With regard to the first point, taking advantage of our previous studies (CHAPTER 4), we attained the object modulating the faradaic charge during the CEG of the acid and controlling with AFM the resulting surfaces. Several samples were prepared varying the charge from 1200 to 12 mC. With 1200 mC the acid deposited as multilayer (**Fig.5.4A**).

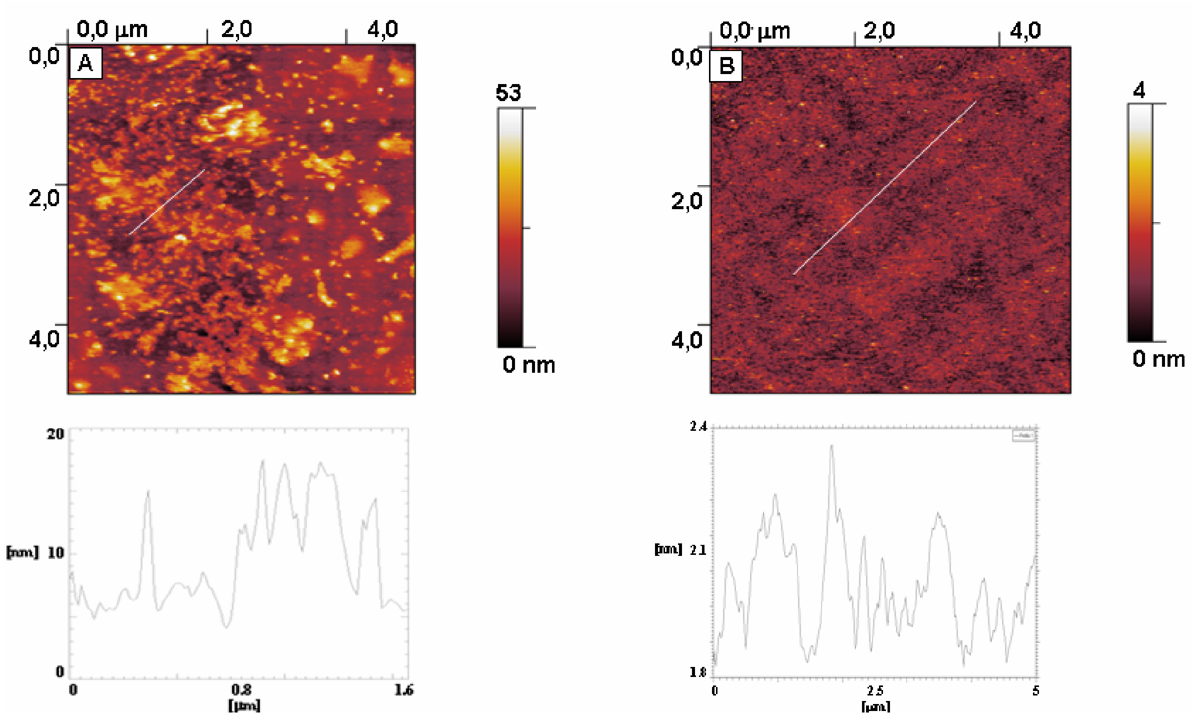

Fig.5.4 A) AFM topographic image (5 x 5 µm) acquired in contact mode showing dishomogeneity and aggregation in the 10-undecynoic acid deposition due to CEG performed with high cathodic charge. B) AFM topographic image (5 x 5µm) acquired in contact mode, showing an the homogeneous surface deriving from a low cathodic charge functionalization with the undecynoic acid.

With a tenfold lower charge (120 mC), a uniform homogeneous monolayer was formed, as we reported previously (CHAPTER 4). Then, lower charges (36 and 12 mC) were tested in order to check whether can be avoided exposing the silicon surface to the passage of an unnecessary large charge, which can damage the surface. With 36 mC a homogeneous monolayer was obtained (**Fig.5.4B**), practically undistinguishable from that obtained with 120 mC, while with 12 mC the silicon surface resulted only partially functionalized (**Fig.5.5**).

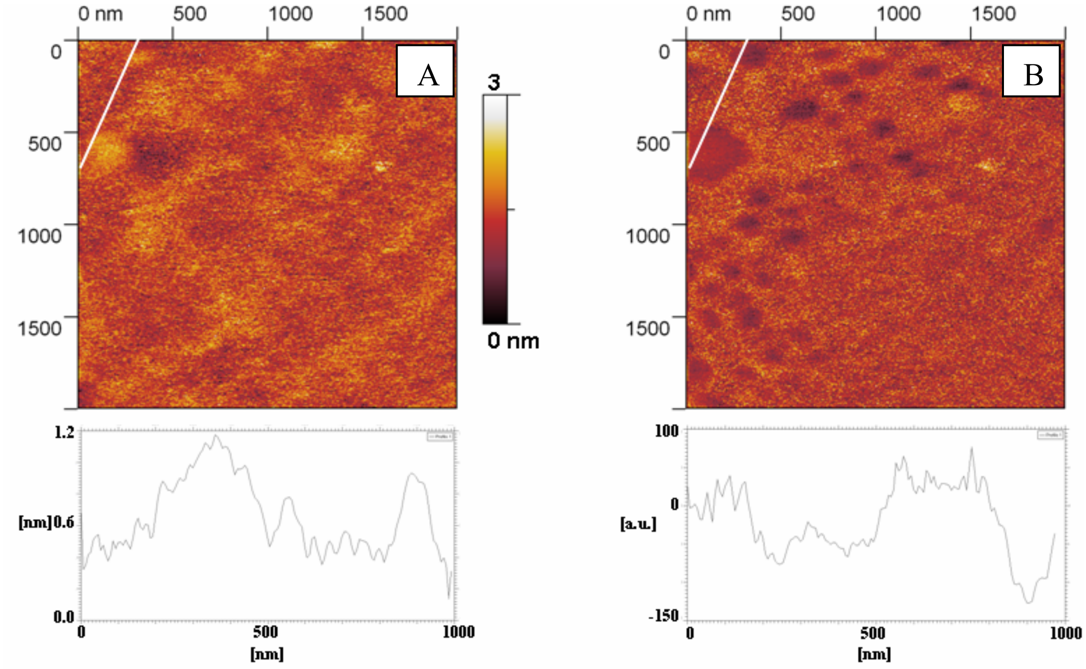

Fig.5. 5 Contact mode topography (left) and friction force (right) images of samples functionalized with CEG with 12 mC/cm^2 cathodic charge. The surface appears rougher than the well-covered monolayer cases. Interesting round forms appear in the friction image. As the cross sections confirm, these “friction holes” match the higher areas in the topography

In fact, **Fig.5.4A** shows the topography of a multilayer deposition obtained at Q=1200 mC/cm^2, characterized by the presence of protrusions as high as 8-15 nm; **Fig.5.4B** shows the contact AFM image of a uniform monolayer deposition (ca. 0.4 nm local corrugation) obtained at Q=36 mC/cm^2; **Fig.5.5A** shows a non uniform functionalization with a mean corrugation of 0.9 nm resulting after the passage of Q= 12 mC/cm^2. In **Fig.5.5B** the same area has been analyzed with the friction force modality, showing the formation on the surface of round patches that correspond (cfr. the cross sections) to well functionalized zones. It is to be noted that in any case the used charge is in large excess with respect to the theoretical catalytic amount needed. In fact, the overall reaction ($\equiv$Si-H + HC$\equiv$CR $\rightarrow$ $\equiv$Si-C$\equiv$CR + H_2) is catalyzed by the application of just a cathodic bias to the silicon surface, then a surface silyl anion is generated, which initiates a chain reaction.[16] Evidently, in the applied reaction conditions the current efficiency of this electrocatalyzed process is very low.

In order to evaluate the actual thickness of the 10-undecynoic monolayer, a tapping mode image of a very low density ODN sample, evidencing well distinguished functionalised and non-functionalised areas is shown in **Fig.5.6**.

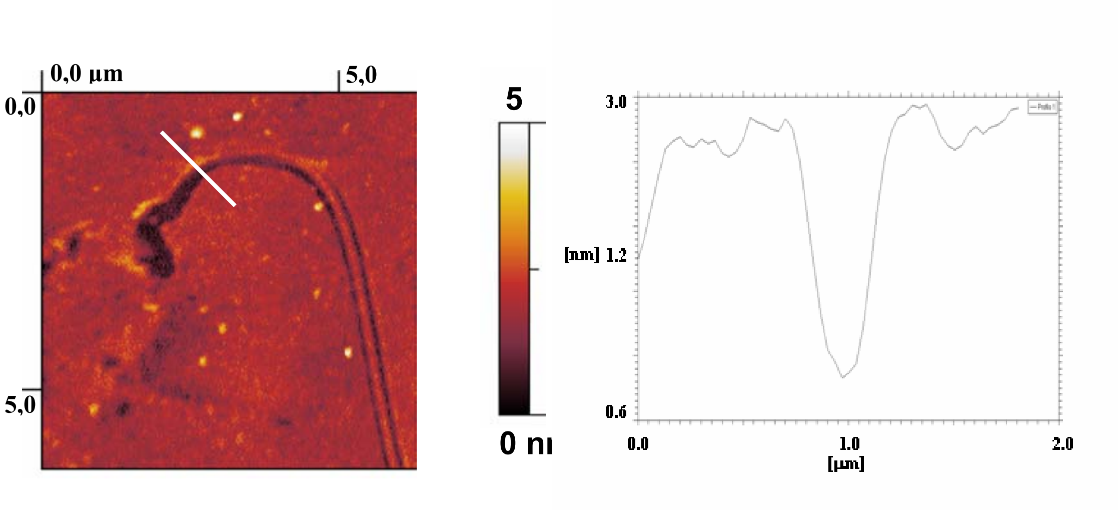

Fig.5.6 Image (6 x 6 µm) of a sample functionalised with 10-undecynoic acid performed at low cathodic current and covered with a very low concentration of ssODN. The non-functionalised area allows to define as ~1.5 nm the height of the acid layer on the surface. The ODN molecules are represented as small round structures.

As described later, the ODN molecules appear as sparse round structures present on the uniformly functionalized surface, which remains non-modified by the ODN immobilization process. The non-functionalised scratch-like area has probably been caused by some debris present on the silicon surface during the functionalization, that were removed by the cleaning procedure performed after the CEG, leaving a clean non-functionalised area. In fact, a thorough analysis of the two zones show that the surface has a mean corrugation of 1 nm outside the scratch and only 0.3 nm inside the scratch. This confirms the different nature of the two areas. The depth of the scratch is around 1.5 nm, thus compatible with the dimension of a single layer of 10-undecynoic acid molecules, as found by Matteschi *et al.*, who reported, from an analogous AFM experiment concerning the 10-undecenoate ester grafted on Si(100) surface that depth of the scratch is 1.1 nm.[17]

Subsequently, ODN-probes were immobilized on these substrates, prepared by CEG at Q =36 mC/cm^2, starting with ODN **2**. They were anchored onto the Si├COOH surfaces under near equilibrium conditions, using carbodiimide-mediated amidation, as described in the literature.[11d,e,g] The concentration of the immobilized ODN was then evaluated through enzymatic digestion with a DNase. To our best knowledge, this procedure was never applied before for a similar purpose. The only related reports[1d,e] deal with the enzymatic removal of fluorescent ODNs, deposited as millimetre sized spots on gold surfaces, and detected by fluorescence microscopy. It is claimed that, the digestion is complete in 3 hours, at room temperature, with 20 units of enzyme. We used a lower enzyme amount and verified the completeness of the digestion by measuring the fluorescence of the solution over time. Fluorescence increased asymptotically towards a limiting value (**Fig.5.7**) and the digestion was apparently almost complete in 6 hours.

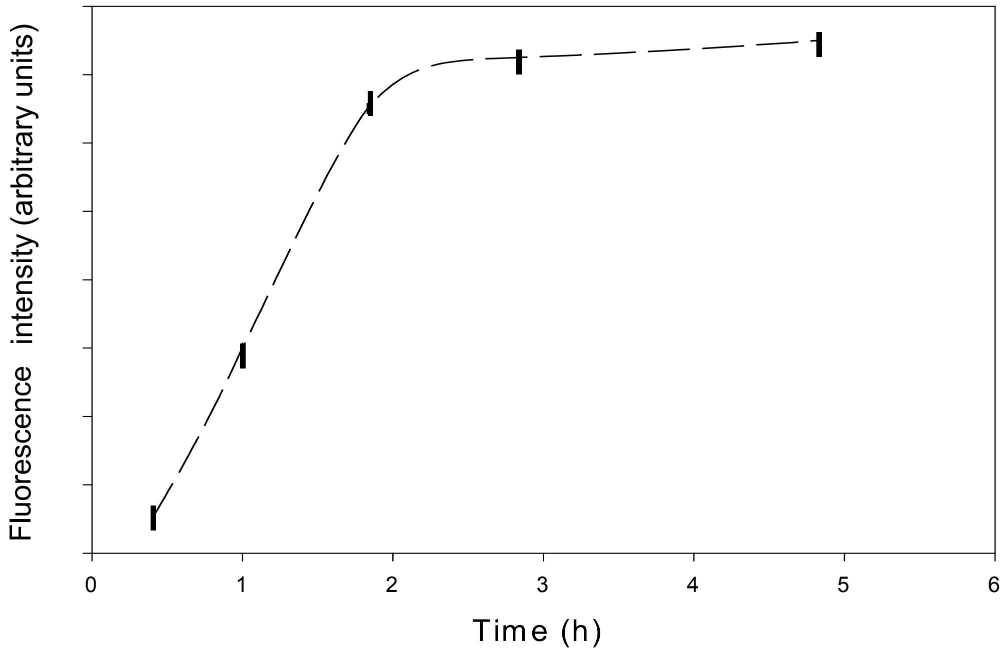

Fig.5.7 Solution fluorescence intensity vs time, during the enzymatic digestion of an amino-terminated oligonucleotide immobilized on the silicon surface.

Then, other samples were prepared lowering the concentration of the ODN-probe in solution. Furthermore, all these samples were evaluated in their hybridisation efficiency. As shown in **Table 5.2**, the optimal ODN-probe density is $5.6 \cdot 10^{12}$ strands/cm^2, resulting after the reaction with an ODN at low concentration in solution (0.543 μM for **2**); the minimal ODN-target concentration, required for a 100% hybridisation yield on this substrate, in solution was 9.369 μM (**Table 5.3**). For completeness, several other experiments were carried out, changing the ODN-probe (**1**, **3**, **5**, **7**) and/or the support (-COOH or H-terminated unoxidized silicon and HO-terminated oxidized silicon). In every experiments, the ODN solution concentration (0.441-0.175 μM) was even lower than that already established for ODN **2**, (0.543 μM) for obtaining the optimal probe density on the surface. The overall results are reported in **Table 5.4**.

Support	ODN	C (µM)	Reactant	Surface ODN conc.[a] (10^{12} strands/cm^2)	Surface hybridised ODN conc.[b] (10^{12} strands/cm^2)
Si├COOH	**1**	0.312	EDAC/NHS	5.63±0.15	7.56±0.28
Si/SiO$_2$├OH	**2**	0.543	EDAC/NHS	0	
Si├H	**1**	0.312	EDAC/NHS	0	
Si├COOH	**1**	0.312	-	0	
Si├COOH	**3**	0.312	EDAC/NHS	1.19±0.15	0
Si├COOH	**5**	0.441	EDAC/NHS	5.93±0.34	7.43±0.80
Si├COOH	**7**	0.175	EDAC/NHS	1.97±0.16	2.78±0.15

Table 5.4. Experimental results obtained with ODNs immobilised on the silicon surface

[a] After enzymatic digestion and fluorescence measurement in solution. [b]After denaturation and fluorescence measurement in solution.

In details, four different probe-ODNs were anchored: Fluorescein-5'-dA$_{20}$–3'-Hexyl-NH$_2$ (**1**), Fluorescein-5'-T$_{20}$–3'-Hexyl-NH$_2$ (**2**), and mixed ODNs Fluorescein-5'-dX$_{20}$–3'-Hexyl-NH$_2$ (**5**) and Fluorescein-5'-dX$_{51}$–3'-Hexyl-NH$_2$ (**7**) (**Table 5.1**). After immobilization on identical supports (type A in **Fig.5.1**), the surface concentrations of the 20-mer ODN **1** and **5** resulted (±ESD from three determinations) similar to each other and close to the optimal value: 5.63±0.15 and 5.93±0.34·10^{12} molecules/cm^2, respectively; a lower concentration resulted (1.97±0.34·10^{12}) for the longer 51-mer **7**, although it proved still able to hybridise efficiently. Furthermore, we performed several control experiments to confirm that the overall procedure is robust and takes place mainly in the specific way outlined in Scheme 1. To this end, in order to check whether immobilisation can occur through simple adsorption, or through reaction of the exocyclic amino groups, or through the formation of ester bonds, we tested: (a) **3** and **4** according to the standard, complete procedures; (b) HO-terminated oxidized silicon (Si/SiO$_2$├OH) and **2** in the presence of EDAC/NHS; (c) hydrogenated silicon (Si├H) and Fluorescein-5'-dA$_{20}$–3'-Hexyl-NH$_2$ (**1**) in the presence of EDAC/NHS; (d) Si├COOH and **1** without EDAC/NHS. A small amount of ODN **3** proved able to anchor on the surface too, likely through the formation of amido bonds with its exocyclic amino groups, as found by other authors on glass supports,[18] however it proved totally unable to hybridise. No control experiments other than (a) for **3** gave any detectable fluorescence signal.

To characterize the above preparations we performed tapping mode AFM imaging of ODN covered samples (namely **1**), which displayed a homogeneous distribution of round structures, with lateral dimensions of ca. 16 nm and vertical heights of ca. 3 nm with some sparse higher and larger structures probably due to apparent aggregation (**Fig.5.8**).

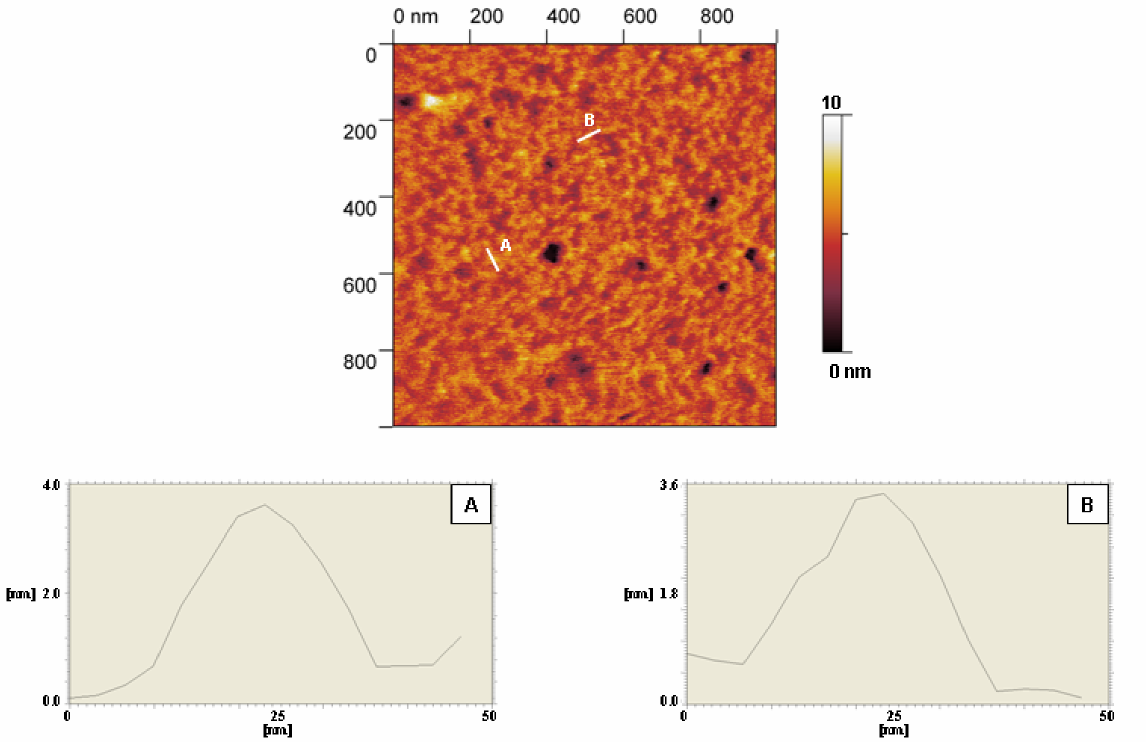

Fig.5.8 1 x 1 micron image of a ssODN covered sample. The cross sections A and B show typical structures ~18 nm wide and ~3 nm high, compatible with the dimension of a 20-mer ODN **1** linked on the surface.

Since the expected height of a 20-mer ODN is slightly less than 7 nm,[19] to understand the vertical dimensions of these structures we must take into account the mechanism of AFM imaging. The tip-sample interaction always produces a deformation of the sample. Ultra-soft molecules like ssODN can be considered as elastic rods,[20] thus due to the probe-induced compression, their measured heights are lower than the actual molecule vertical dimensions. This effect is probably coupled with a non-vertical protrusion of the molecules over the surface. The angular tilting of immobilized oligonucleotides was recently investigated (4) and could partially justify the low height values we have measured.

Regarding the lateral dimensions, the structures appear wider than the estimated width of a ssODN, ca. 2 nm as theoretically calculated,[21] however the measured widths are comparable or better than most of those recently reported, regarding similar specimen analyzed in analogous conditions.[22] In fact, the AFM technique intrinsically produces images in which the structures appear as the convolution with the tip form and this effect is particularly evident if the probe has an apical radius larger than the lateral dimensions of the structures under analysis. These anomalously large dimensions can be attributed to the image broadening effect due to the tip-sample convolution.[23]

To better assess this effect, we acquired some images using high resolution tips. These "super-tips" have an apical radius of ca. 2 nm, thus the convolution has a much weaker impact in the lateral dimensions of the ODNs.[24] As shown in **Fig.5.9**, the molecules appear as round structures with width of ca. 8 nm, and height of ca. 1.7 nm.

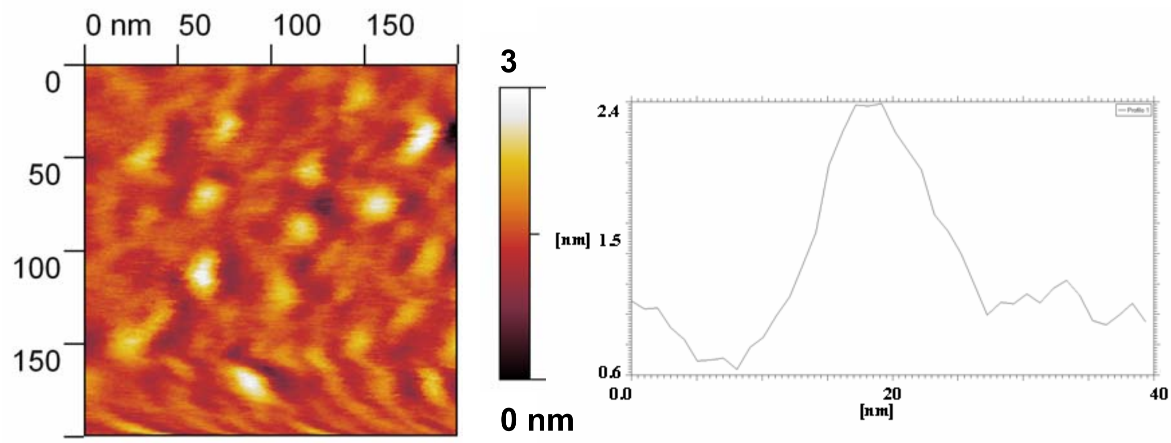

Fig.5.9 250 x 250 nm image of a ssODN (**1**) covered sample imaged with the use of the supertips. The cross section shows a typical structure ~8 nm wide and ~1.8 nm high. The different lateral dimensions of these structures compared with the samples analyzed with the normal tips illustrates the importance of the apical radius and form. The different vertical dimensions are probably the effect of the greater tip pressure due to the much smaller contact area.

The different vertical dimensions are explainable considering that an unchanged probe force generates an higher pressure if applied on a smaller interaction area, thus producing a larger deformation and probably enhancing the angular tilt of the molecules on the surface. The much smaller lateral dimensions confirm the effect of the apical radius and tip form of in an AFM measurement. In both low and high resolution images, the surface between each structure is uniform and has a corrugation comparable with a clean silicon surface functionalised with 10-undecynoic acid. The different measured vertical dimensions confirm the larger deformation induced by the measurement process on the sample, due to the increase in pressure caused by the small contact area of the supertips.

Hybridisation trials were then carried out in triple on four different substrates (type B in Scheme 1), containing the probe-ODNs: Fluorescein-5'-dA$_{20}$-3'-Hexyl-NH$_2$ (**1**) or

Fluorescein-5'-dT$_{20}$-3'-Hexyl-NH$_2$ (**2**), Fluorescein-5'-dX$_{20}$-3'-Hexyl-NH$_2$ (**5**), or Fluorescein-5'-dX$_{51}$-3'-Hexyl-NH$_2$ (**7**). In all four cases, high hybridisation efficiency was obtained upon interaction with the corresponding complementary ODNs: Fluorescein-5'-dT$_{20}$ (**4**), Fluorescein-5'-dA$_{20}$ (**3**), Fluorescein-5'-dX$_{20}$ (**6**) and Fluoresceine-5'-dX$_{24}$ (**8**) respectively, followed by denaturation of the hybrids, and the results are reported in **Tables 5.2** and **5.4**. The anchored ODNs **1**, **2**, **5** and **7** were then finally digested with the DNase and their amounts were compared with those of the hybridised **3**, **4**, **6** and **8**, resulting practically equivalent within the ESD (**Table 5.2** for ODN **2** and **Table 5.4** for ODNs **1**, **5** and **7**).

Similarly as above, Figure 7 shows the tapping mode AFM image of a typical ODN sample after hybridisation (namely **1**+**4**) using standard tips.

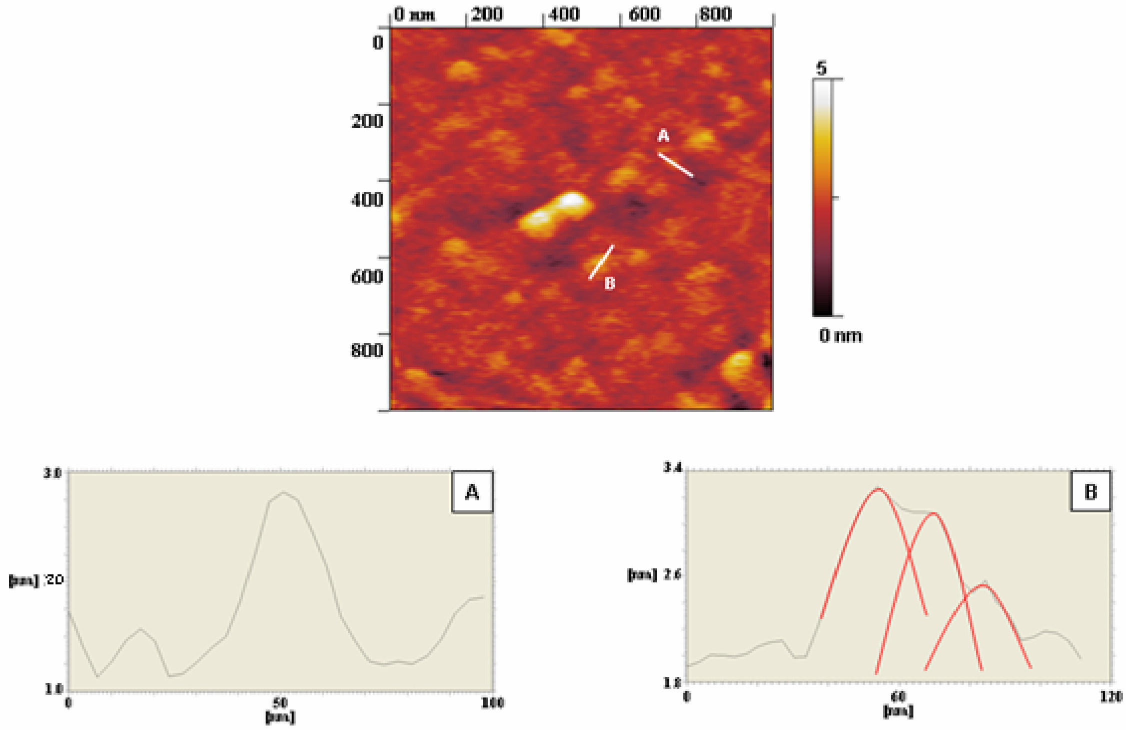

Fig.5.10 1 x 1 micron image of a dsODN (**1**+**4**) covered sample. The molecules appear as rod-like structures. The cross section A shows a typical structure ~20 nm wide and ~1.5 nm high. The different height compared to the single strand images is probably due to a different orientation of the molecules on the surface. The cross section B, taken on a large agglomerate, can be deconstructed in three smaller structures with dimensions, shown by the fit curves, comparable with the dimensions of the single molecules. The formation of large agglomerates is a side-effect of the hybridization process.

The sample appears covered with small rod-like structures and some larger aggregates. The formation of these larger structures is an effect already reported by others in similar samples .[9d]

The dsODNs on the surface appear as structures with lateral dimensions of ca. 25 nm and vertical dimensions of ca. 2 nm. A confirmation that the wider structures are in fact aggregates of smaller dsODNs is shown in the cross section (**Fig.5.10B**) where a ~80 nm wide structure has been fitted as the aggregation of three smaller ~20 nm formations, whose dimensions are compatible with the single rod-like structures. The different vertical dimensions of the structures can be interpreted as consequence of a different angle formed by the dsODN with respect to the surface. This is also confirmed by the greater mean lateral dimensions of the structures.

---

[1] (a) Herne,T.M., Tarlov,M.J. *J. Am. Chem. Soc.*, **1997**, *119*, 8916. (b) Peterlinz,K.A., Georgiadis,R.M. *J. Am. Chem. Soc.*, **1997**, *119*, 3401. (c) Jordan,C.E., Frutos,A.G., Thiel, A.J., Corn,R.M. *Anal. Chem.*, **1997**, *69*, 4939. (d) Frutos,A.G., Liu,Q., Thiel,A.J., Sanner, A.M.W., Condon,A.E., Smith,L.M., Corn,R.M. *Nucleic Acids Res.*, **1997**, *25*, 4748. (e) Frutos,A.G., Smith,L.M., Corn,R.M. *J. Am. Chem. Soc.*, **1998**, *120*, 10277.

[2] (a) Yang,M., Yau,H.C.M., Chan,H.L. *Langmuir*, **1998**, *14*, 6121. (b) Steel,A.B., Herne,T.M., Tarlov,M.J. *Anal. Chem.*, **1998**, *70*, 4670. (c) Levicky,R., Herne,T.M., Tarlov,M.J., Satija,S.K. *J. Am. Chem. Soc.*, **1998**, *120*, 9787. (d) Brockman,J.M., Frutos, A.G., Corn,R.M. *J. Am. Chem. Soc.*, **1999**, *121*, 8044. (e) Demers,L.M., Mirkin,C.A., Mucic,R.C., Reynolds,R.A., Letsinger,R.L., Elghanian,R., Viswanadham,G. *Anal. Chem.*, **2000**, *72*, 5535. (f) Smith,E.A., Wanat,M.J. Cheng,Y. Barreira,S.V.P. Frutos,A.G., Corn, R.M. *Langmuir*, **2001**, *17*, 2502.

[3] (a) Weizmann,Y., Patolsky,F., Willner,I. *Analyst*, **2001**, *126*, 1502. (b) Peterson,A.W., Heaton,R.J., Georgiadis,R.M. *Nucleic Acids Res.*, **2001**, *29*, 5163. (c) Peterson,A.W., Wolf,L.K., Georgiadis,R.M. *J. Am. Chem. Soc.*, **2002**, *124*, 14601. (d)Yu,H.Z., Luo,C.Y., Sankar,C.G., Sen,D. *Anal. Chem.*, **2003**, *75*, 3902. (e) Wirtz,R., Wälti,C., Germishuizen, W.A., Pepper,M., Middelberg,A.P.J., Davies,A.G. *Nanotechnology*, **2003**, *14*, 7.

[4] (a) Shumaker-Parry,J.S., Zareie,M.H., Aebersold,R., Campbell,C.T. *Anal. Chem.*, **2004**, *76*, 918. (b) Guiducci,C., Stagni,C., Zuccheri,G., Bogliolo,A., Benini,L., Samorì,B., Riccò,B. *Biosensors and Bioelectronics*, **2004**, *19*, 781. (c) Yu,F., Yao,D., Knoll,W. *Nucleic Acids Res.*, **2004**, *32*, e75

[5] (a) Maskos,U., Southern,E.M. *Nucleic Acids Res.*, **1992**, *7*, 1679. (b) Guo,Z., Guifoyle, R.A., Thiel,A.J., Wang,R., Smith,L.M. *Nucleic Acids Res.*, **1994**, *22*, 5456. (c) Vo-Dinh, T., Alarie,J.P., Isola,N., Landis,D., Wintenberg,A.L., Ericson,M.N. *Anal. Chem.*, **1999**, *71*, 358. (d) Zammatteo,N., Jeanmart,L., Hamels,S., Courtois,S., Louette,P., Hevesi,L., Remacle,R. *Analytical Biochemistry*, **2000**, *280*, 143. (e) Podyminogin,M.A., Lukhtanov, E.A., Reed,M.W. *Nucleic Acids Res.*, **2001**, 29, 5090.

[6] (a) Oh,S.J., Cho,S.J., Kim,C.O., Park,J.W. *Langmuir*, **2002**, *18*, 1764. (b) Cerrina,F., Blattner,F., Huang,W., Hue,Y., Green,R., Singh-Gasson,S., Sussman,M. *Microelectronic*

Engineering, **2002**, *61-62*, 33. (c) J.Albert,T.J., J.Norton,J., M.Ott,M., T.Richmond,T., K.Nuwaysir,K., E.F.Nuwaysir,E.F., K.P.Stengele,K.P.,Green,R.D. *Nucleic Acids Res.*, **2003**, *31*, e35. (d) Kumar,P., Choithani,J., Gupta,K.C. *Nucleic Acids Res.* **2004**, *32*, e80. (e) Pirri,G., Damin,F., Chiari,M., Bontempi,E., Depero,L.E. *Anal. Chem.* **2004**, *76*, 1352.

[7] (a) Lamture,J.B., Beattie,K.L., Burke,B.E., Eggers,M.D., Ehrlich,D.J., Fowler,R., Hollis, M.A., Kosicki,B.B., Reich,R.K., Smith,S.R., Varma,R.S. Hoga,M.E. *Nucleic Acids Res.* **1994**, *22*, 2121. (b) Lee,G.U., Chrisey,L.A., Colton,R.J. *Science* 1994, *266*, 771. (c) Jin,L., Horgan,A., Levicky,R. *Langmuir*, **2003**, *19*, 6968. (d) Shen,G., Anand,M.F.G., Levicky,R. *Nucleic Acids Res.* **2004**, *32*, 5973.

[8] Xu,J., Zhu,J.J., Huang,Q., Chen,H.Y. *Electrochemistry Comm.* **2001**, *3*, 665.

[9] (a) Gray,D.E., Case-Green,S.C., Fell,T.S., Dobson,P.J. Southern,E.M. *Langmuir* **1997**, *13*, 2833. (b) O'Donnell,M.J., Tang,K., Köster,H., Smith,C.L., Cantor,C.R. *Anal. Chem.* **1997**, *69*, 2438. (c) Berney,H., West,J., Haefele,E., Alderman,J., Lane,W., J.K.Collins,J.K. *Sensors and Actuators B*, **2000**, *68*, 100. (d) Lenigk,R., Carles,M., Ip,N.Y., Sucher,N.J. *Langmuir* **2001**, *17*, 2497. (e) Cavic,B.A., McGovern,M.E., Nisman,R., Thompson,M. *Analyst* **2001**, *126*, 485. (f) Li,Z., Chen,Y., Li,X., Kamins,T.I., Nauka,K.,Williams,R.S. *Nano Lett.* **2004**, *4*, 245. (g) Macanovic,A., Marquette,C., Polychronakos,C.,Lawrence, M.F. *Nucleic Acids Res.* **2004**, *32*, e20.

[10] (a) Meinkoth,J., Wahl,G. A*nal. Biochem.* **1984**, *138*, 267. (b) T.R.Gingeras,T.R., D.Y.Kwoh,D.Y., G.R.Davis,G.R. *Nucleic Acids Res.* **1987**, *15*, 5373., (c) Lund,V., Schmid,R., Rickwood,D., Hornes,E. *Nucleic Acids Res.* **1988**, *16*, 10861. (d) Saiki,R.K., Walsh,P.S., Levenson,C.H., Erlich,H.A. *Proc. Natl. Acad. Sci., USA*, **1989**, *86*, 6230. (e) Rasmussen,S.R., Larsen,M.R., Rasmussen,S.E. *Anal. Biochem.* **1991**, *198*, 138. (f) Zhang, Y., Coyne,M.Y., Will,S.G., Levenson,C.H., Kawasaki,E.S. *Nucleic Acids Res.* **1991**, *19*, 3929.

[11] (a) Strother,T., Hamers,R.J., Smith,L.M. *Nucleic Acids Res.* **2000**, *28*, 3535. (b) Strother,T., Cai,W., Zhao,X., Hamers,R.J., Smith,L.M. *J. Am. Chem. Soc.* **2000**, *122*, 1205. (c) Patole,S.N., Pike,A.R., Connolly,B.A., Horrocks,B.J., Houlton,A. *Langmuir* **2003**, *19*, 5457. (d) Wei,F., Sun,B., Guo,Y., Zhao,X.S. *Biosensors and Bioelectronics* **2003**, *18*, 1157. (e) Voicu,R., Boukherroub,R., Bartzoka,V., Ward,T., Wojtyk,J.T.C., Wayner,D.D.M. *Langmuir* **2004**, *20*, 11713. (f) Cai,W., Peck,J.R., van der Weide,D.W., Hamers,R.J. *Biosensors and Bioelectronics* **2004**, *19*, 1013-1019. (g) Yin, H.B., Brown,T., Greef,R., Wilkinson,J.S., J.Melvin,J. *Microelectronic Engineering*, **2004**, *73-74*, 830.

[12] Wang,L., Gaigalas,A.K., Blasic,J., Holden,M.J. *Spectrochimica Acta, Part A* **2004**, *60*, 2741.

[13] Kelley,S.O., Jackson,N.M., Hill,M.G., Barton,J.K. *Angew. Chem. Int. Ed. Engl.* **1999**, *38*, 941.

[14] A. Rosa-Zeiser, E. Weilandt, S. Hild, O. Marti; *Meas.Sci. Technol.* **1997**, *8*, 1333.

[15] Q. Zhong, D. Inniss, K. Kjoller, V. B. Elings; *Surf. Sci.* **1993**, *290*, L688-92.

[16] Robins,E.G., Stewart,M.P., Buriak,J.M *Chem. Comm.* **1999**, 2479.

[17] G. Condorelli, A. Motta, I. L. Fragalà,F. Giannazzo, V. Raineri, A. Caneschi, D. Gatteschi; *Angew. Chem.* **2004**, *116*, 4173.

[18] Adessi,C., Matton,G., Ayala,G., Turcatti,G., Mermod,J.J., Mayer,P., Kawashima,E. *Nuclei Acid Res.* **2000**, *28*, e87

[19] Sinder, R, *DNA structure and function*, 1994, Academic Press, INC. Chapter 1, Page 23

[20] T. Morii, R. Mizuno, H. Haruta, T. Okada; *Thin Solid Films* **2004**, *464-465*, 456.

---

[21] A. L. Lenninger, D. L.Nelson, M. M. Cox; *Principles of Bioche*mistry; Worth Publishers, New York, 1993

[22] (a) E. Huang, F. Zhou, L. Deng; *Langmuir*; **2000**,*16*, 3272. (b) X. Yang, L. A. Wenzler, J. Qi, X. Li, N. C. Seeman; *J. Am. Chem. Soc.*; **1998**, *120*, 9779. (c) M. H. Rouillat, V. Dugas, J. R. Martin, M. Phaner-Goutorbe; *Appl. Surf. Sci*; In press.

[23] S. O. Kelley, J. K. Barton, N.M. Jackson, L.D. McPherson, A. B. Porter, E. M. Spain, M. J. Allen, M. G. Hill; *Langmuir*, **1998**, *14*, 6781.

[24] C. Bustamante, J. Vesenka, C. L. Tang, W. Rees, M. Guthold, R. Keller; *Biochemistry*, **1992**, *31*, 22.

CHAPTER 6

MAGNETITE NANOPARTICLES ANCHORED TO CRYSTALLINE SILICON SURFACE

6.1 Introduction

Given our expertise on silicon surface handling, we sought it would be possible to anchor magnetic nanoparticles on it.[1] Unoxidized crystalline silicon, because has a remarkably uniform and homogeneous surface at nanometer scale, is considered almost the ideal substrate,[2] for the construction of magnetic nanostructured material.[3] Generally, the attachment of nanoparticles to a surface needs a cross linker, *e.g.* an α, ω-heterobifunctional molecule, which acts as bridge between the surface and the nanoparticles. As shown below, in the case of silicon we investigated whether 10-undecynoic acid **1** could be a right cross-linker to this end. It could bind to silicon surfaces through a covalent Si-C bond after the hydrosilylation reaction, while the free carboxylic end group could[4] bind the nanoparticles. Among the most important magnetic species to be considered in this context are magnetite nanoparticles, that, to the best of our knowledge, have not yet been anchored to unoxidized silicon surfaces in spite of some special physical properties, due to half metallic character of magnetite, which makes it a very interesting candidate to be exploited in spin electronics applications.

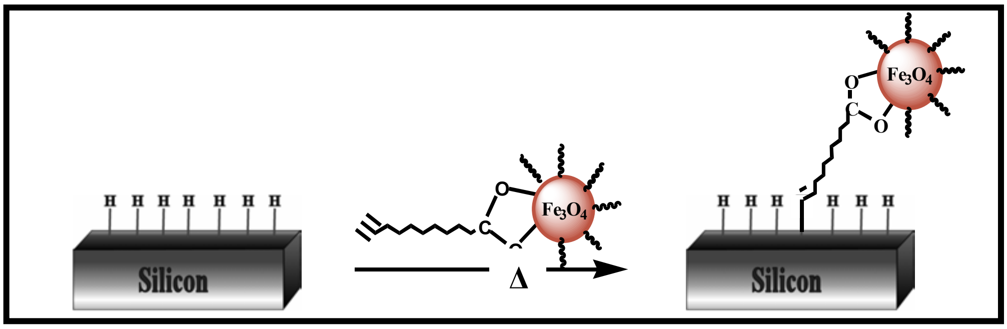

Fig.6.1 General procedure for anchoring magnetite nanoparticles on silicon surface

To carry out this, we have followed a multistep procedure (**Fig.6.1**). Magnetite nanoparticles, covered by **1** were first prepared, and then these were anchored to the silicon surface after thermal hydrosilylation (Δ).

6.2 Experimental

6.2.1 Preparation and characterization of magnetite nanoparticles

$Fe(acac)_2$ (2 mmol), 1,2–hexadecanediol (10 mmol), oleic acid (6 mmol), oleylamine (6 mmol) and benzyl ether (20 mL) were mixed and magnetically stirred under nitrogen. The reaction flask was immersed in an oil bath at 200 °C for 30 min, the oil bath temperature was then raised to 220 °C and the reaction flask heated for another 30 min. The black-brown mixture was cooled to room temperature by removing the heat source. Ethanol (40 mL) was added to the mixture. A black precipitate was separated via centrifugation. The product was then dissolved in 50 mL hexane containing oleic acid (0.05 mL) and oleylamine (0.05 mL). Centrifugation (8000 rpm, 10 min) was used to remove any undispersed residue. Ethanol was then added to the dispersion, the resulting mixture centrifuged, and the solid product dispersed again in hexane. This procedure was repeated twice in order to remove any excess oleic acid. The coupling of **1** to the nanoparticles was then attained after an exchange reaction in a colloidal solution, as follows. The product of the previous step, dispersed in 40 mL hexane containing **1** (550 mg, 3 mmol) was heated under nitrogen at 60 °C and mechanically stirred, overnight. It was cooled to room temperature and, after addition of 40 mL of ethanol, centrifuged. The black product was dispersed in hexane and centrifuged to remove any undispersed residue. Ethanol was added to the dispersion, the mixture centrifuged and the solid product dispersed again in hexane. This procedure was repeated twice in order to remove any excess undecynoic acid. Finally the product was dried overnight under vacuum and collected. Analysis - Found: C, 14.18; H, 2.01%. Calc. for $(Fe_3O_4)3.2(C_{11}H_{20}O_2)$: C, 14.19; H, 2.16%. By assuming this formula, the yield of the isolated product was 48%, based on $Fe(acac)_2$. IR: 3296 (w, H-CC), 2921 and 2857 (m, H-C), 2117 (w, HC≡C), 1533 and 1432 (s, COO-). Differential thermal analyses (DTA) in air show an exothermic peak at 250°C. This product was further characterized by X-ray diffraction (XRD) analysis with results reported in the next section.

6.2.2 Anchoring of magnetite nanoparticles on silicon surfaces.

The magnetite nanoparticles, covered with **1** (158 mg) were dissolved under N_2 in mesitylene (10 mL) forming a dark brown solution. A freshly etched silicon wafer (see

CHAPTER 4) was immersed in this solution. The mixture was heated at 180°C for 2 h in a stoppered glass container filled with N_2. The silicon sample was cleaned by sonication in air three times with different solvents for 5 min each (mesitylene, acetonitrile, methanol) and dried in a stream of N_2. The amount of iron present on the silicon surface of the final samples was determined by atomic absorption spectroscopy as follows. Three silicon wafers, equivalent to an active surface area 30.62 cm^2, were functionalised with magnetite nanoparticles as described above. Then, the silicon wafers were treated with concentrated HNO_3 (4 mL) at reflux for 3 h. After this treatment, the nanoparticles were completely detached from the surface as revealed by iron XPS (*see infra*). This solution was transferred to a 10 mL volumetric flask to which water was added (Carlo Erba "Water Plus", 3 x 2 mL). Standard water iron solutions, in the concentration range 0-2 ppm were prepared and measured. The resulting calibration plot was linear ($y = 0.11192\ x$) with an associated correlation index equal to 0.9996. By using this plot, the above 10 mL solution was measured and the iron concentration determined, *i.e.* 1.64 ± 0.15 ppm/mL, equivalent to 9.5 ngram-atoms/cm^2. Further characterization has been performed with X-ray photoelectron spectroscopy (XPS), scanning probe microscopies and magnetic measurements with results reported below.

6.3 Results

The magnetite nanoparticles have been anchored to the silicon surface with the intervening **1** as crosslinker between the particles and the surface. In particular, they are anchored through a coordination bond to the carboxylate group of the acid that, in turn, is attached to the surface via a covalent C-Si bond. To accomplish this, we followed a multistep procedure, consisting of (i) the preparation of magnetite nanoparticles covered by oleic acid, (ii) the exchange between oleic acid and undecynoic acid on the surface of the nanoparticles, and finally, (iii) the anchoring these particles, covered by **1**, to the silicon surface.

Preparation of the samples - Magnetite nanoparticles, covered by oleic acid, were prepared applying a modified method of literature.[5] Modifications introduced consisted of starting from $Fe(acac)_2$ instead of $Fe(acac)_3$, to hinder as much as possible the growth of the oxidized phase maghemite (γ-Fe_2O_3) during the formation of magnetite, and using a 50 degree lower reaction temperature to slightly increase the particle size. Then, oleic acid was exchanged with **1**. A complete exchange occurred on the surface of the magnetite particles. In fact, CHN elemental analyses of magnetite nanoparticles covered by **1** showed it to be a nitrogen-free product, in agreement with the formula $(Fe_3O_4)_{3.2}(C_{11}H_{20}O_2)$. It should be noted that the measured H/C atomic ratio is 1.69, which compares well with the theoretical value of 1.64 for **1**, whereas the theoretical value for oleic acid is 1.89. IR spectra show the absorption bands characteristic of ionised **1**. The XRD pattern (**Fig. 6.2**) provides additional structural information on the sample.

The positions of all diffraction peaks match those of magnetite.[6] The peak broadening can be attributed mainly to the small crystallite size of the powder, which is directly related to the decrease in the particle size. The peaks, after a correction for the instrumental broadening, were fitted with a pseudo-Voigt profile shape function. The full width at half maximum (FWHM) and the mixing parameter (η) values, resulting from the fitting procedure, were used as input for the program BREADTH,[7] to determine the volume weighted mean crystallite size and its distribution function, according to the 'double-Voigt' method.[8] An average crystallite size of 5.3 ± 1.2 nm was estimated.

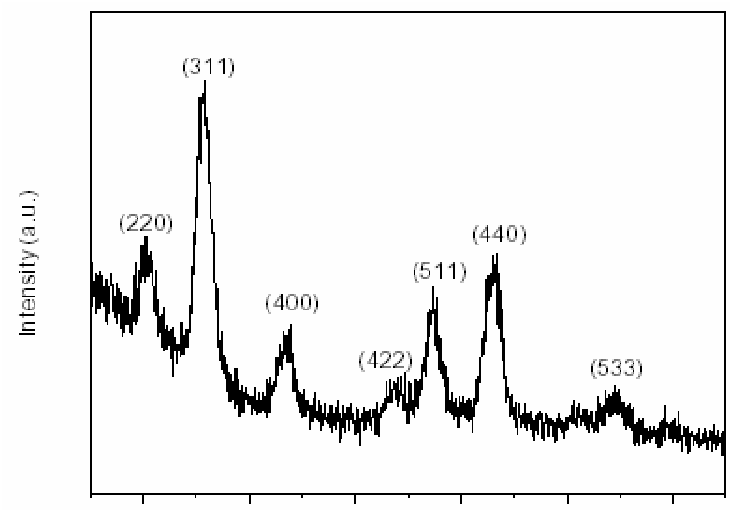

Fig.6.2 X-ray diffraction pattern of magnetite (Fe_3O_4) powder.

Furthermore, DTA analysis shows a peak attributable to the expected oxidation phase change from magnetite (Fe_3O_4) to maghemite (γ-Fe_2O_3).[9]

In the final step, the magnetite nanoparticles coated with undecynoic acid were anchored to the silicon surface through a stable covalent C-Si bond via the well-known hydrosilylation reaction as reported in the literature for the silicon thermal functionalization with terminal alkynes in organic solutions.[10] During the reaction workup, particular attention was paid to the washing procedure to remove any physisorbed species. To this end, stringent rinsing in ultrasonic baths of various solvents was applied.

The surface chemical composition of the sample was studied by means of XPS, and a typical Fe2p spectrum is shown in **Fig. 6.3a**. The identification of iron oxidic species can be derived from the binding energy (BE) of the Fe2p3/2 component and from the satellite 'shake-up' structure accompanying the (3/2;1/2) spin-orbit split Fe2p spectrum. We conclude that our sample consists of a Fe_3O_4-like phase since the relevant Fe2p3/2 component lies at BE= 710.9 eV, and no sizable satellite structure is observed.[11] (A satellite signal lying ~ 6 or ~8 eV to the high-BE side of each main component would be observed, had FeO or Fe_2O_3 been present, respectively.)

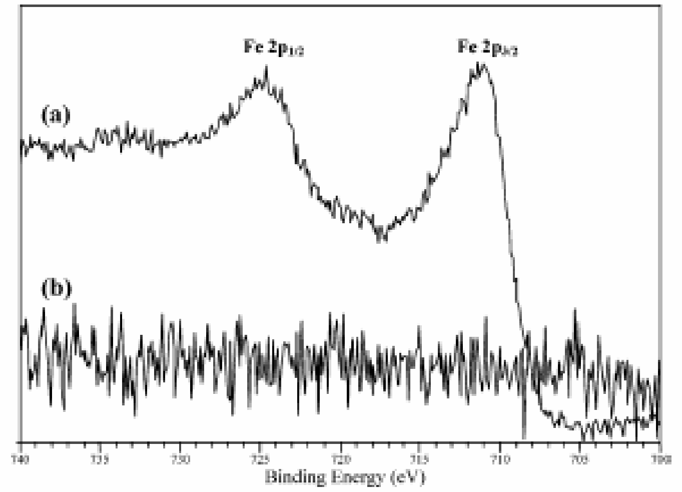

Fig.6.3. Fe 2p region XPS spectra of the Si (100) surfaces covered with magnetite nanoparticles: before (a) and after (b) the removal of the nanoparticles

In addition, the iron content in the sample (a) was determined by atomic absorption in water solution after completely removing the nanoparticles from the silicon sample with concentrated HNO_3 at reflux. The effectiveness of this treatment was ascertained, again, by XPS analysis (**Fig.6.3b**). The resulting iron value, 0.54 ± 0.05 μg /cm^2, corresponds to a densely packed magnetite particle monolayer covering approximately 50% of the silicon substrate, assuming a mean particle diameter of 5 nm. These results were consistent with our earlier findings, (CHAPTER 4) and with those of other authors,[12,30] which indicated that thermal hydrosilylation reactions in solution on silicon surface are not complete.

Morphology characterization - The morphology of the sample was studied by field emission-scanning (FE-SEM), scanning-tunnelling (STM) and atomic force-microscopies (AFM).

FE-SEM investigations show well distributed almost spherical particles (**Fig.6.4** and **Fig.6.5**).

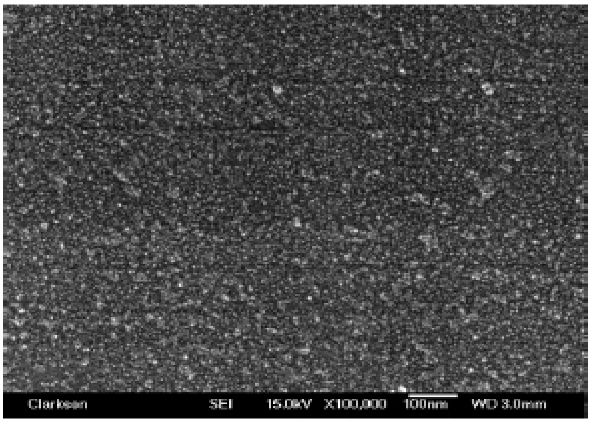

Fig.6.4 FE-SEM micrograph of a Si (100) crystalline surface (1.2 x 0.87 μm) covered with magnetite particles.

The size distribution obtained measuring 195 particles in **Fig.6.5** is fitted to a log normal function centred at 5 ± 1 nm.

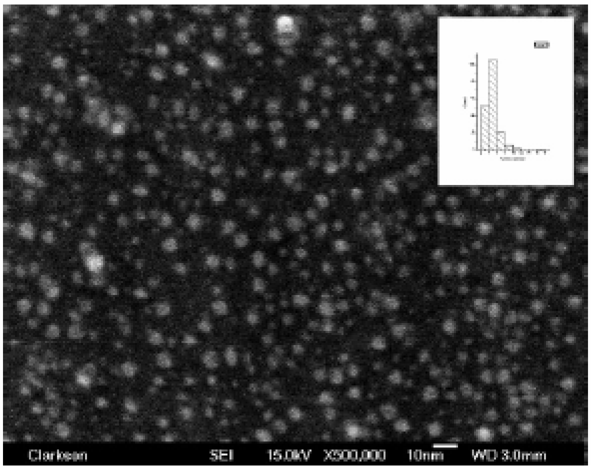

Fig.6.5 FE-SEM micrograph of a Si(100) crystalline surface (120 x 87 nm) covered with magnetite particles. The inset shows the size distribution histogram obtained measuring all the particles of the image.

Fig.6.6 shows a comparison between the size distribution obtained by FE-SEM measurements on the magnetite particles attached to the silicon surface and the log-normal distribution calculated from XRD data on the pristine particles.

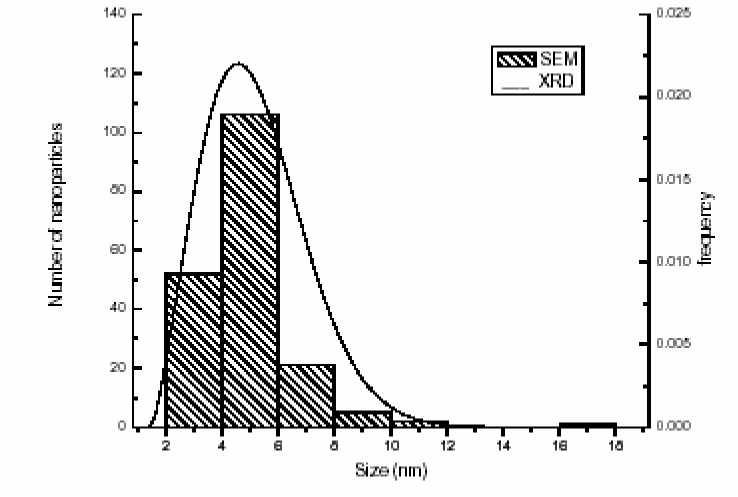

Fig.6.6 Comparison between the histogram of nanoparticle size distribution as obtained from SEM measurements and the log-normal distribution size inferred from XRD data analysis.

Noticeably, similar particle size and size distribution were obtained. We conclude, then, that the thermal anchoring of the nanoparticles to the surface does not alter their morphology.

STM images (**Fig.6.7**) show a homogeneous distribution of almost spherical particles with typical dimensions 4-6 nm. The particle close packing indicates that the organic molecules covering the nanoparticles are efficient ligands for them. Moreover, areas in which nanoparticles form a second layer on top of the first one are also visualized; the different grey tones of the images indicate that the grains are distributed on the surface at two different heights with respect to the silicon substrate.

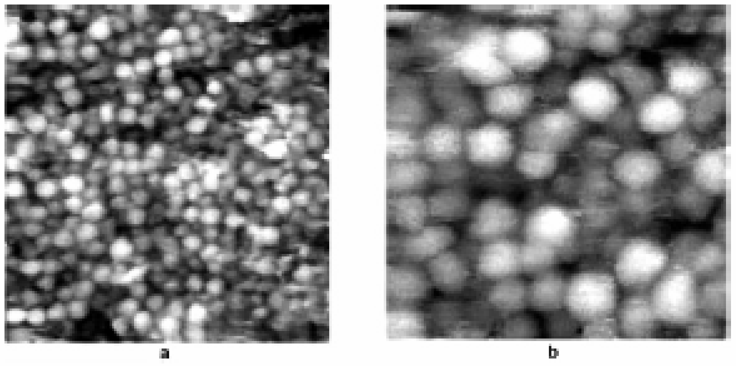

Fig.6.7 STM images of the magnetite nanoparticles attached to Si(100) surface at different scales. (X,Y range = 100nm, 45 nm for a), b), respectively).

To account for this, a reliable route leading to the formation of the double layer, interconnected by covalent bonds has been proposed and is depicted in **Fig.5.8**.

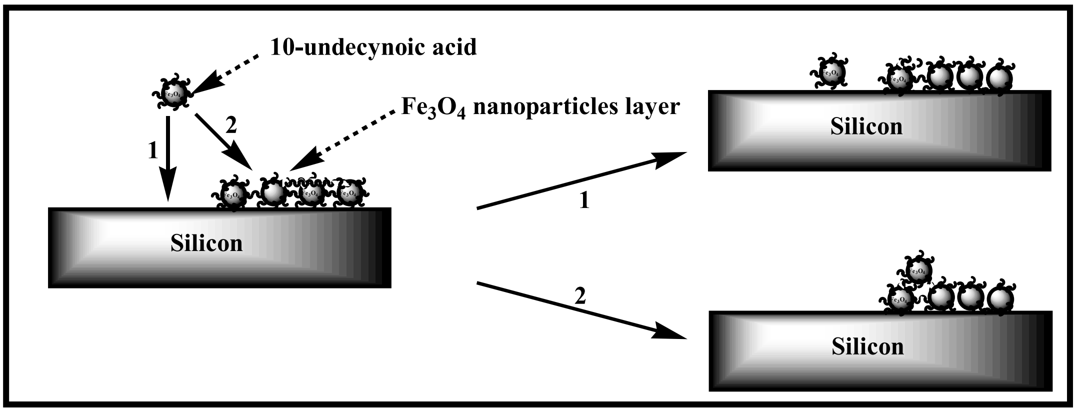

Fig.6.8 Scheme of formation second layer

Excluding any non-specific interactions and given the stringent washing conditions during the preparation of the samples as pointed out above, we reason that during the thermal functionalization of the silicon surface and after the growth of the monolayer to some extent, a magnetite nanoparticle in solution, capped by **1**, might react either with hydrogenated silicon contributing to the monolayer (1) or with other nanoparticles, already cast in the monolayer, so forming a double layer (2). In the latter case, the reaction type at work could be the terminal alkyne dimerization, occurring between two acid **1** surfactant molecules, belonging to two different nanoparticles, one bonded to silicon (*e.g.* Y-C≡CH) and the other one dispersed in solution (*e.g.* Z- HC≡C). This is a well known reaction in alkyne chemistry, which yields vinylacetylenes: Y-C≡CH + HC≡C-Z → Y-C≡C-CH=CH-Z.[13]

AFM images also indicate a particle lay-out analogous to that observed by STM.

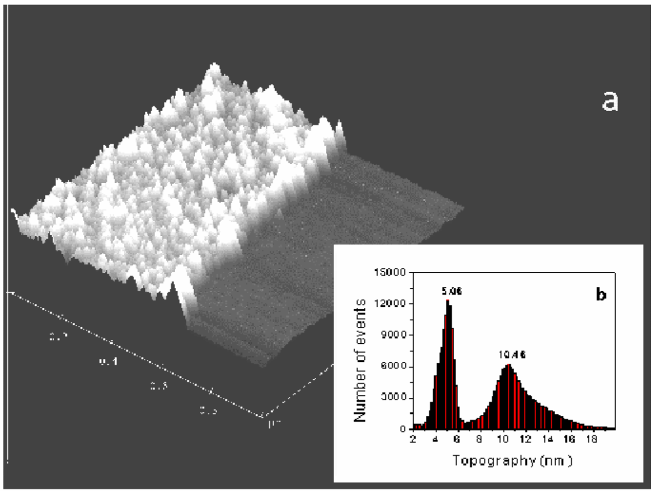

Fig.6.9 a) AFM 3d view of the sample, 1μm x 1μm; b) Statistical height histogram of AFM

Interestingly, during this investigation, some particle-free silicon gaps, adjacent to the nanoparticle double layers, came into focus, displaying the line of demarcation along which the two areas meet (**Fig.6.9a**). So, we had the opportunity to measure the individual layer thickness at the boundary line between the bare Si substrate and the layer of deposited nanoparticles. The height distribution evaluated from statistical analysis of the AFM image on **Fig.6.9a** clearly shows two maximum peaks (**Fig.6.9b**). The first peak centred at 5.0 nm is related to one layer of silicon attached nanoparticles, while the second peak centred at 10.5 nm is related to nanoparticles deposited on the first layer. Because the peak amplitude ratio is 2, as shown in **Fig.6.9b**, the surface covered by the nanoparticle monolayer is two times larger than the double layer covering the silicon surface.

Magnetic measurements - The temperature dependence of the magnetization measured by means of a commercial SQUID magnetometer is shown in **Fig.5.10** for particles anchored to the Si surface.

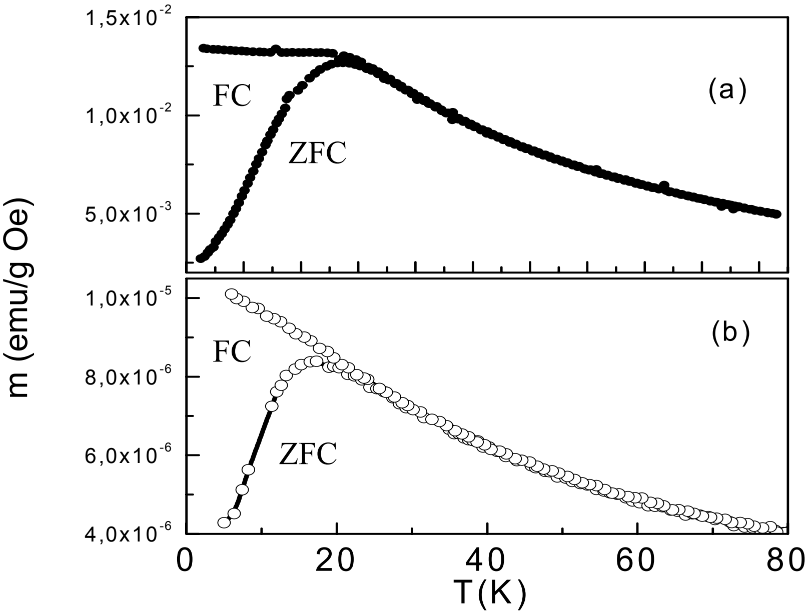

Fig.6.10 Magnetization as a function of temperature: (a) pristine Fe_3O_4 powder, H_a = 20 Oe (solid line); (b) Fe_3O_4 particles attached to silicon, H_a = 100 Oe (symbols).

The curve marked as ZFC (zero field cooled) was obtained by first cooling the system in zero magnetic field from 300 K to 5K; the magnetic field was then applied and the magnetization measured on increasing the temperature. The curve marked as FC (field cooled) was obtained by measuring the magnetization while the temperature was decreased in the same magnetic field. Both curves exhibit the main features of super-paramagnetic systems. Namely, the ZFC curve shows a rounded maximum at T_{max} ~20K whereas the FC branch continues to increase with decreasing temperature; moreover the ZFC and FC branches of magnetization curve overlap at a temperature slightly larger than T_{max}, with a temperature dependence of a Curie-Weiss type. The temperature behavior of the FC branch should reflect the non (or very weakly) interacting character of the particle assembly.[14]

In such a case, the Neel-Brown law for the relaxation time of the particle moment $K_a = 25kT_b/V$[15] can be used. T_b is the blocking temperature, defined as the temperature at which the relaxation time of the particle moment is on the order of the experimental time window (*ca* 100s for macroscopic magnetic measurements), V is the particle volume and K_a can be deduced from the Arrhenius law replacing V with the mean particle volume <V> and T_b with the mean blocking temperature $<T_b>$. Due to the log-normal particle size distribution, $<T_b> = T_{max}/c$, where c= 1.5.[16] It turns out then that $K_a = 6\ 10^5$ erg/cm^3. By contrast, for pristine nanoparticles in a powder form (**Fig.6.11**), the ZFC curve of the magnetization vs temperature shows a rounded maximum at T_{max} ca 55 K and the FC curve displays a flattening as the temperature decreases. The higher T_{max} value (reflecting an increase of the effective anisotropy energy barrier) and the behavior of the FC magnetization is usually ascribed to the presence of interparticle interactions[15] to which the associated energy is much higher than the single particle anisotropy energy, unlike for Fe_3O_4 particles attached to the Si surface. In a control experiment, an intermediate behavior (T_{max} = 26K; tendency to flattening of the FC magnetization below T_{max}), revealing the existence of non negligible interparticle interactions, was observed for particles deposited on Si, weakly bonded to the surface. The magnetization cycle at 5 K on silicon attached nanoparticles is shown in **Fig.6.11**.

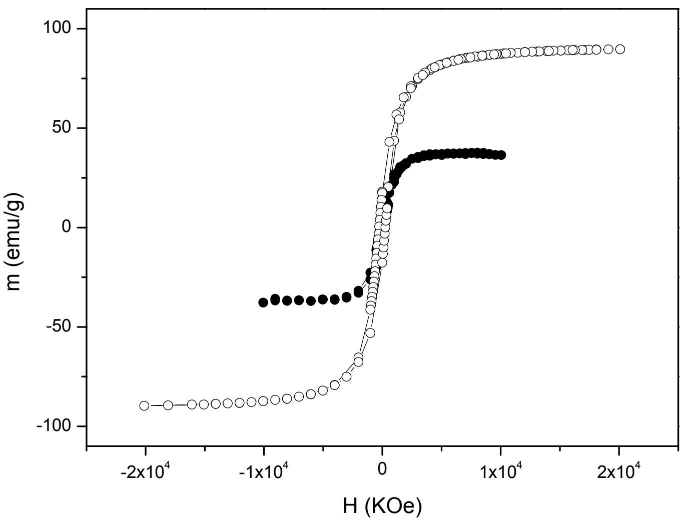

Fig.6. 11 Magnetization *vs* applied magnetic field at 5K and silicon attached particles (solid line); pristine particle powder (open symbols)

The magnetization saturation value is 40 emu/g, much lower than the magnetite bulk value (92 emu/g).[17] Spin canting and disorder at the particle surface, associated with the breaking of crystal symmetry, could be responsible for such a reduction. The low field region of the magnetization cycles for silicon attached and pristine particles is shown in **Fig.6.12**.

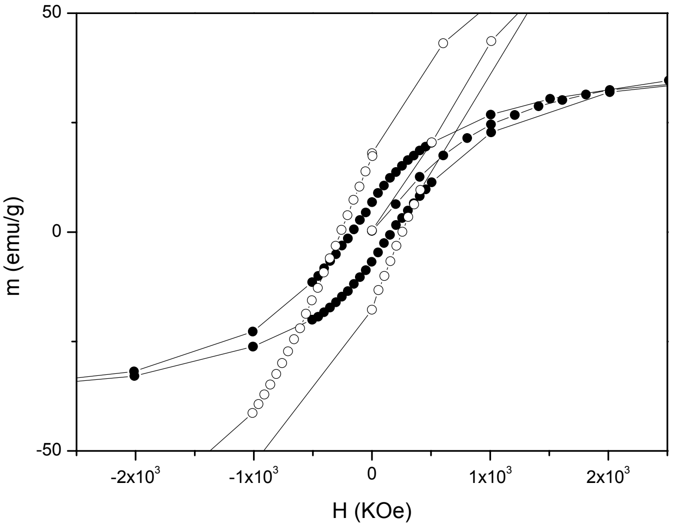

Fig.6 12 magnification of the field range –1 kOe/+ 1kOe: silicon attached particles (solid line); pristine particle powder (open symbols)

The difference in coercivity between the two samples (260 Oe for the pristine sample; 160 Oe for the silicon attached particles) should be mainly due to the different surface state of the particles, due to covalent bonds with Si substrate depending on the actual roughness profile of the sample (incomplete particle double layering).

---

[1] (a) Thiaville, A.; Miltat, J. *Science* **1999**, *284*, 1939. (b) Cornia, A.; Fabretti, A. C.; Pacchioni, M.; Zobbi, L.; Bonacchi, D.; Caneschi, A.; Gatteschi, D.; Biagi, R.; Del Pennino, U.; De Renzi, V.; Gurevich, L.; Van der Zant, H. S. J. *Angew. Chem.* **2003**, *115*, 1683.

[2] (a) Hersam, M. C.; Guisinger, N. P.; Lyding, J. W. *Nanotechnology* **2000**, *11*, 70. (b) Yin, H. B.; Brown, T.; Greef, R.; Wilkinson, J. S.; Melvin, T. *Microelectronic Engineering* **2004**, *73-74*, 830.

[3] Palacin, S.; Hidber, P. C.; Bourgoin, J. P.; Miramond, C.; Fermon, C.; Whitesides, G. M. *Chem. Mater.* **1996**, *8*, 1316. Zhong, Z.; Gates, B.; Xia, Y. *Langmuir* **2000**, *16*, 10369.

[4] (a) Sieval, A. B.; Demirel, A. L.; Nissink, J. W. M.; Linford, M. R.; van der Mass, J. H.; de Jeu, W. H.; Zuilhof, H.; Sudhölter, E. J. R. *Langmuir* **1998**, *14*, 1759. (b) Boukherroub, R.; Wayner, D. D. M. *J. Am. Chem. Soc.* **1999**, *121*, 11513. (c) Strother, T.; Cai, W.; Zhao, X.; Hamers, R. J.; Smith, L. M. *J. Am. Chem. Soc.* **2000**, *122*, 1205. (d) Wei, F.; Sun, B.; Guo, Y.; Zhao, X. S. *Biosensors and Bioelectronics* **2003**, *18*, 1157.

[5] Sun, S.; Zeng, H.; Robinson, D. B.; Raoux, S.; Rice, P. M.; Wang, S. X.; Li, G. *J. Am. Chem. Soc.* **2004**, *125*, 273.

[6] (JPCDS 19-0629). It is to note that, due to the proximity of the peaks of the oxidized phase (maghemite, γ-Fe_2O_3), the presence of maghemite cannot be, on the basis of only XRD data, completely excluded.

[7] http://www.boulder.nist.gov/div853/balzar/breadth.htm.

[8] Balzar, D.; Ledbetter, H. *J. Appl. Cryst.* **1993**, *26*, 97.

[9] Cornell, R. M.; Schwertmann, U. Ed. *The Iron Oxides*; Wiley-VCH: Weinheim, 1996.

[10] (a) Bateman, E. J.; Eagling, R. D.; Worral, D. L.; Horrocks, B. R.; Houlton, A. *Angew. Chem., Int. Ed. Engl.* **1998**, *37*, 2683. (b) Sieval, A. B.; Opitz, R.; Maas, H. P. A.; Schoeman, G. M.; Meijer, G.; Vergeldt, F. J.; Zuilhof, H.; Sudhölter, E. J. R. *Langmuir* **2000**, *16*, 10359.

[11] (a) Brundle, C. R.; Chuang, T. J.; Wandelt, K. *Surf. Sci*. **1977**, *68*, 459. (b) McIntyre, N. S.; Zetaruk, D. G. *Anal. Chem.* **1977**, 49, 1521. (c) McIntyre, N. S.; Chan, T.C. in: *Practical Surface Analysis*, vol. 1, Editors D. Briggs, M.P. Seah, J. Wiley & Sons, Chichester, UK, **1990**.

[12] Cerofolini, G. F.; Galati, C.; Reina, S.; Renna, L. *Mater. Sci. Eng. C* **2003**, *23*, 253.

[13] Smith, M. B.; March, J. Ed., *March's Advanced Organic Chemistry*, Wiley Interscience, **2001,** 1020**.**

[14] Dormann, J. L.; Fiorani, D.; Tronc, E. *Adv Chem-Phys* **1997**, *98*, 283-294.

[15] (a) Neel, L. *Ann. Geophys.* **1949**, *5*, 99. (b) Brown, W. F. *Phys.Rev.* **1963,** *130*, 1677.

[16] Pankhurst, Q. A.; Ucko, D. H.; Fernandez Barquin, L.; Garcia Calderon, R. *J. Magn. Magn.Mat.* **2003,** *266*, 131.

[17] Popplewell J.; Sakhnini, L . *J. Magn. Magn.Mat.* **1995**, *149*, 72.

APPENDIX

General information

Physical Techniques

DTA analysis was performed in air with a Du Pont 950 apparatus. The Shimadzu AA-6300IR instrument was used for atomic absorption iron analysis.

IR measurements were performed with a Perkin-Elmer 16F PC FT spectrometer on KBr pellets (0.75% w/w); the stretching frequencies (ν/cm^{-1}) of the absorption maximum of the most significant bands are given.

FE-SEM (Field Emission Scanning Electron Microscope) images were obtained with a JEOL 7400F. Scanning tunnelling microscopy (STM) characterization was carried out with a commercial STM-UHV system (WA tech). The typical tunnelling parameters are: tip-sample voltage = 2-3V, tunnelling current=0.05-0.08 nA.

XRD measurements were performed on a Seifert XRD 3000 powder diffractometer in the 2θ range 25° to 85°, using Cu Kα radiation (λ = 1.5418 Å).

Magnetic measurements were performed by a commercial SQUID magnetometer operating between 2 K and 400 K, with a maximum magnetic field of 55 kOe.

The XPS studies were performed in an ESCALAB MkII (VG Scientific, UK) instrument, using the Al Kα line as a source (h**ν** = 1486.6 eV) and a 5-channeltron as a detection system. Photoelectrons were probed at a take-off angle of 90°, while the analyser was opened with a constant pass energy of 20 eV. The pressure from residual gases never exceeded 1x10^{-8} mbar in the analysis chamber during the measuring time. The linearity of the binding energy (BE) scale was calibrated according to the procedures proposed by Seah and Smith.[1] Following this calibration, both the accuracy and reproducibility of measurements were found to be within ± 0.1 eV. To compensate for charging phenomena, measured BEs were referenced to that of C 1s peak (resulting from carbonaceous contamination adventitiously adsorbed onto the surface), taken as lying at 285.0 ± 0.1 eV.

The AFM measurements were performed in air (at room temperature), with the microscope working in the weak repulsive regime of contact mode with a force of less than 1 nN from zero cantilever deflection. Gold coated Si_3N_4 (Park Scientific Instruments; Sunnyville, California, USA) microlevers with a spring constant of 0.023 N m^{-1} and an expected statistical apical radius of 5–30 nm were used. The raw data were treated only using background subtraction and the reproducibility of data (including the absence of sample damage) was successfully tested. In all AFM images a grey map was superimposed which varies from black for the deepest zones to white for the highest.

Sessile drop water contact angle measurements were obtained with a Face Contact Anglemeter model CA-A under ambient conditions with an error±2°. A micropipetor was used to dispense 12 μL drops of H_2O at multiple point across the substrate surface.

Reflectance spectra were recorded on a Cary 5.

Fluorescence spectra were recorded on a Perkin-Elmer MPF-44B spectrometer, in a 3 mL quartz cuvette.

The mp's were determined with a Büchi SMP-20 model melting point apparatus. Elemental analyses were by Servizio Microanalisi of CNR, Area della Ricerca di Roma.

IR measurements were performed with a Perkin-Elmer 16F PC FT spectrometer on KBr pellets (0.75% w/w); the stretching frequencies (ν/cm^{-1}) of the absorption maximum of the most significant bands are given.

The ^{1}H-NMR spectra were obtained in $CDCl_3$ and CD_3CN solution with a Bruker AMX-250 spectrometer. The chemical shifts (δ/ppm) were referred to the residual $CHCl_3$ proton (singlet, 7.26 ppm) of $CDCl_3$ or the CHD_2CN proton (quintet, 1.97 ppm) of CD_3CN. The J-values are given in Hz.

The functionalization experiments on the surface activated samples were carried out in an N_2(g)-purged Dry-Box (Braun) or using standard preparative Schlenk line procedures.

An AMEL system (model 472 polarograph, model 721 integrator, model 550 potentiostat) was used for the electrochemical experiments.

Silicon

Silicon wafers of 250 mm thickness, p-Si (boron doped, double side polished, 0.01 Ω cm resistivity, (100) orientation) and n-Si (phosphorus doped, single side polished, 0.005 Ω cm resistivity, (111) orientation) were purchased from Siltronix.

Chatodhic Electrografting

In detail, CEG process was carried out at constant intensity current (0.6 mA) in a two compartment polyethylene cell. The working electrode was the silicon wafer with 1.5 cm^2 exposed area, in a CH_3CN solution (3.5 ml) of 10-undecynoic acid 0.1 M and tetrabutylammonium perchlorate (TEAP) 0.1 M as the supporting electrolyte. An ohmic contact on the rear side of the silicon was established after scratching the surface, rubbing it with Ga-In eutectic and attaching a copper contact to it. The electrode set-up was obtained by pressing the silicon wafer against an O-ring sealing a calibrated hole in the bottom of the cell. The counter electrode was a Pt-coil in a 3ml solution of TEAP 0.1 M in CH_3CN, filling a glass tube separated from the working compartment by a glass sintered disc (porosity 3). Several samples were prepared varying the total amount of faradaic charge (Q), passed during CEG.

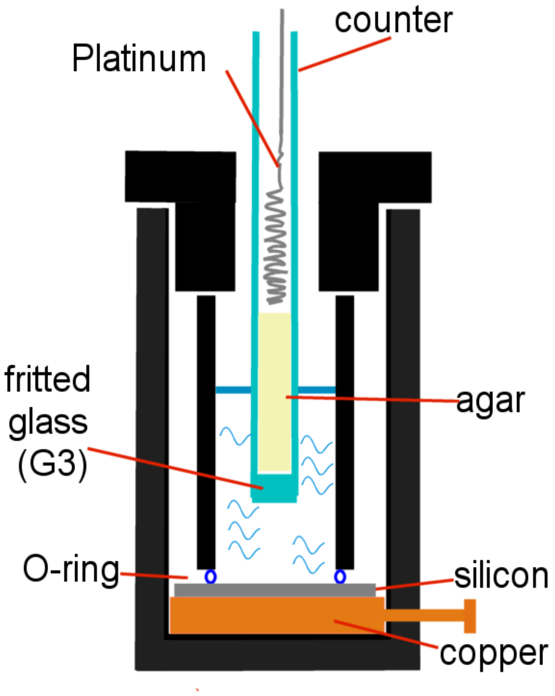

Scheme of electrochemical cell

Materials

Chapter 4 - Commercial 10-undecynoic acid, 12-bromododecanoic acid, 6-heptynoic acid, 7-amino-4-methylcoumarin, 7-amino-4-trifluoromethylcoumarin, isobutylchloroformiate, NaI and tetraethylammonium perchlorate (TEAP) were used as received from Fluka. The reaction solvents, tetrahydrofuran (THF), N, N-dimethylformamide (DMF) and acetonitrile (CH_3CN) were carefully dried and freshly distilled before use. In particular, THF and CH_3CN were refluxed and then distilled at atmospheric pressure under dinitrogen over sodium-benzophenone ketyl and CaH_2, respectively, while DMF first was dried by azeotropic distillation with benzene and by shaking the remaining liquid with Linde type 4 Å molecular sieves and then distilled under reduced pressure (15–20 mbar).

Chapter 5 - 1-(3-Dimethylaminopropyl)-3-ethylcarbodiimide hydrochloride (EDAC) and N-hydroxy succinimide (NHS) were from Fluka and used as received. All reagents used for preparing buffer solutions and Phosphodiesterase I from *Crotalus adamanteus* were from Sigma. Standard commercial reagents required for ODNs synthesis, including 3’-Amino-ON CPG columns, 5’-Aminolinker-phosphoramidite and 5’-(6-FAM)-Fluorescein phosphoramidite were from Proligo Biochemie and Link Technologies. All ODNs were prepared on a Perseptive Biosystems Expedite 8909 automated DNA synthesizer, using standard phosphoramidite chemistry. High-performance liquid chromatography (HPLC) was performed using a Perkin-Elmer Series 410 Bio LC pump system equipped with a Perkin-Elmer 235C Diode Array. The adsorption spectra of ODNs were recorded with a Perkin-Elmer Lambda Bio 40 spectrophotometer. The concentration of the ODNs is conventionally expressed as OD AUFS 260 nm, assuming that 1 OD is equivalent to 33 μg/ml.

Chapter 6 - Absolute ethanol, hexane, mesitylene, benzyl ether (99%), 1,2–hexadecanediol (97%), oleic acid (90%), oleylamine (>70%), iron(II)-acetylacetonate, 10-undecynoic acid (95%), were purchased from Aldrich Chemical Co. and used as received. Mesitylene was refluxed and then distilled at atmospheric pressure under dinitrogen over sodium lumps and stored in the Dry-Box.

---

[1] Seah, M.P. and Smith, G.C., in: *Practical Surface Analysis*, vol. 1, editors D. Briggs, M.P. Seah, J. Wiley & Sons, Chichester, UK, 1990, 531.